A dissertation submitted in partial fulfillment of the requirements for the degree of Doctor of Philosophy at Dublin City University

NONLINEAR DYNAMICS OF DC-DC CONVERTERS

Brendan Hayes B.Eng.

Supervisor: Dr. Marissa Condon

School of Electronic Engineering

Dublin City University

August 2016

Declaration

I hereby certify that this material, which I now submit for assessment on the programme of study leading to the award of Doctor of Philosophy is entirely my own work, and that I have exercised reasonable care to ensure that the work is original, and does not to the best of my knowledge breach any law of copyright, and has not been taken from the work of others save and to the extent that such work has been cited and acknowledged within the text of my work.

Signed:

ID No: 59366784

Date:

Contents

List of Tables

List of Figures

Glossary

A/D	Analog to digital
CCM	Continuous conduction mode
CMC	Current mode control
D/A	Digital to analog
DCM	Discontinuous conduction mode
DPWM	Digital pulse width modulator
ESL	Equivalent series inductance
ESR	Equivalent series resistance
FIR	Finite impulse response
IIR	Infinite impulse response
P	Proportional
PI	Proportional integral
PID	Proportional integral derivative
VMC	Voltage mode control
ZOH	Zero order hold

Abstract

Power electronic converters are time-varying, nonlinear dynamical systems. They exhibit a wide range of steady-state responses. The desired behaviour is a stable periodic motion around a predefined value with a frequency that is equal to that of the external clock. However, as parameters vary the operation can lose stability and go from one regime to another. Such phenomena are termed bifurcations and can degrade the output performance of the converter. Hence, it is of practical importance to know the conditions that cause such bifurcations to occur and to design the system so that it operates in the desired region.

In the past, engineers have typically analysed the stability of power electronic systems by linearising the model about a fixed point. This captures the low-frequency properties while ignoring the detailed dynamics occurring at frequencies higher than the external clock. However, the demand for better functionality, reliability and performance means an in-depth analysis into the complex behaviour exhibited by dc-dc converters is required.

Traditionally, dc-dc converters are employed with analog controllers whose function is to regulate the circuit. With advances in technology, digital control has become a potentially advantageous alternative to analog control. One of the main advantages of digital control is the ability to design more sophisticated design strategies to enable high performance dc-dc converters e.g. digital state-feedback control. Unfortunately, little work exists in the area of the effect of noise on digital control. This is a field that requires intensive study as to completely understand the nonlinear dynamics so as to enable accurate and economic designs.

The aim of this thesis is to address these issues through the application of advanced nonlinear mathematics. The stability of power electronic systems is assessed with a view to developing design guidelines in order to ensure stable operation over a wide operating region.

1 Introduction

1.1 Introduction

Power electronics is concerned with the processing and control of electrical power using electronic devices. These devices convert voltages and currents from one form to another form. The possibility for such high-efficiency devices comes through the continuous development of high-power semiconductor devices. DC-DC converters are one branch of power converters which steer energy around the circuit by employing switching components, such as transistors and diodes, and reactive components, such as inductors and capacitors, which act as energy stores.

They exhibit a wide range of steady-state responses including subharmonics, bifurcations and chaos. The desired behaviour is a stable periodic motion around a predefined value with a frequency equal to that of the external clock. The stability of this periodic mode of operation may, however, be lost due to the variation of parameters such as the input voltage or load resistance, resulting in undesired operation. When a dc-dc converter operates in one regime, loses stability and moves to another operating regime, such phenomena are termed bifurcations and can degrade the output performance of the converter. It is normal practice to specify a range of external parameters within which the converter will operate reliably in steady-state. Thus, even in well-designed converters, if some parameter is varied, the system could fail to operate as expected. Due to the demand from commercial sectors, better functionality, reliability and performance are required in power electronics systems. It becomes imperative to identify when these bifurcations will occur and thus, extend the range over which reliable operation can be expected.

With advances in technology, digital control has become a potentially advantageous alternative to analog control. Some of the potential advantages include low power, immunity to analog component variations, compatibility with digital systems and a faster design process [1]. One of the main advantages of digital control is the ability to design more sophisticated control strategies to enable high performance dc-dc converters to be designed. Previous works on the topic of digital control have assumed ideal operating conditions. In practical applications, this cannot be guaranteed. The effect of spurious signals in dc-dc converters employed with digital controllers requires investigation in order to derive design guidelines to ensure stable

operation and reliable and economic design. One particular system of interest is digital state-feedback controllers. Digital state-feedback controllers are frequently used in dc-dc converters when high/optimal performance is required. However, little work has been carried out into the analysis of the nonlinear behaviour exhibited by such systems.

Since these power electronic systems are nonlinear dynamical systems, they are difficult to study. One common technique used by power electronic engineers to study these systems is to linearise the model about a fixed point. This method enjoys mathematical simplicity and allows the application of familiar frequency-domain techniques. However, this method retains the low-frequency properties while ignoring the detailed dynamics within the switching period. Thus, new methods are required in order to analyse these systems so that the entire range of dynamical behaviour is captured. Only then can design guidelines be developed in order to ensure stable operation.

The aim of this research is to address these issues, that is, to apply nonlinear advanced mathematical tools to capture the detailed dynamics exhibited by these systems, characterise the types of behaviour observed and to develop control techniques to ensure that the systems operate with the desired period-1 orbit.

1.2 Overview of thesis

This thesis is organised as follows:

Chapter 2 presents a general introduction to the area of nonlinear dynamics. The chapter discusses the different types of bifurcations and modes of operation that are common in power electronic converters and the mathematical tools employed to analyse them that are used later in the thesis. A detailed derivation of the Filippov method is presented; a key approach for analysis performed in this research.

In Chapter 3, the area of dc-dc converters in power electronics is discussed. The buck converter is introduced as it forms the basis for the majority of the work in this thesis. Methods for controlling dc-dc converters are discussed as well as the various modeling techniques used in previous works. A survey of previous works concerned with nonlinear analysis of converters is presented, as well as techniques for controlling the nonlinear behaviours which occur in these circuits.

In Chapter 4, a buck converter operating with a PID controller is considered. The behaviour of the circuit is characterised and a model of the system is derived. The types of steady-state behaviours exhibited by the converter as various parameters are varied are observed. Using the Filippov method, analytical conditions that determine when these bifurcations occur are derived which leads to the development of an adaptive PID controller.

As discussed above, digital control has many potential advantages over analog control. One such system of particular interest is digital state-feedback control. Digital state-feedback control is often used in systems where high performance is required. However, little work exists on the nonlinear behaviour of such systems. While, the work of Chapter 4 assumes ideal operating conditions and ideal sources, in practical applications, noise sources can affect the input voltage of a buck converter. Chapter 5 investigates the steady-state behaviours observed when a digital state-feedback controller is employed with a buck converter where the input voltage is being perturbed by a sinusoidal noise signal. It is shown that the presence of noise, whose frequency is comparable to the switching frequency of the converter or its integer multiples, manifests itself through Hopf bifurcations in intermittent periods. However, for irrational frequency ratios, quasi-periodic operation is observed. The Filippov method is then used to assess the stability of the system and to derive conditions for the prediction of this intermittent operation. This enables the development of an adaptive controller to avoid this undesirable behaviour.

In Chapter 6, a buck converter operating with a digital PID controller is considered. Its behaviour is characterised and the types of steady-state operation exhibited are observed. It is seen that quantization in the digital controller can lead to limit cycles on the output. As a result, both a notch and a comb filter are considered as a method to remove these unwanted limit cycles. The effectiveness of both filters are compared.

In Chapter 7, a review of the work reported in the thesis and the major contributions are presented. This chapter also presents the future work that can be carried out in this field.

Each chapter includes a survey of relevant prior work.

2 Nonlinear Dynamics

2.1 Introduction

The dynamical behaviour of systems can be understood by studying their mathematical descriptions. The field of dynamics is concerned with describing these systems and how they evolve over time. The theory of linear systems is a mature topic and a powerful tool in describing dynamical systems. However, most real-world systems are nonlinear. Finding solutions to nonlinear systems can be mathematically complex and in some cases, impossible. Instead of addressing the problem directly, engineers typically linearise the mathematical model. This enables the application of the theory of linear systems. Unfortunately, this method cannot capture all of the behaviours. In order to describe these, a new approach is required. Hence, the field of nonlinear dynamics was developed.

Nonlinear effects are known to occur across a wide variety of disciplines. One of the first papers to characterise these nonlinear effects was by Lorenz in 1963 [2]. In studying a highly simplified model of convecting fluids, Lorenz was able to study the dynamics of a weather system. Using a deterministic model, one where the output of the system can be determined if the initial conditions of the system are known, Lorenz found that the system exhibited a sensitive dependence to initial conditions. This rendered the long-term predictability of the system impossible. This work was published in the Journal of Atmospheric Sciences, little read by mathematicians, and remained unnoticed until the 1970's. The next significant contribution was from May in 1976 [3]. May considered a deterministic iterated map to describe the growth of biological populations. The article describes the complex behaviour exhibited. Specifically, he highlights the period-doubling route to chaos. Similar phenomena have since been discovered in many areas of science and engineering [4].

This chapter is laid out as follows; firstly, the types of behaviour exhibited by linear systems and the techniques used to analyse them are discussed. The work then proceeds to investigate nonlinear systems and the types of attractors and forms of instabilities found. The theory of chaos and the different possible routes to chaos are presented. Finally, a full derivation of the Filippov method is performed. The Filippov method is used to analyse the stability of systems that switch between two or more topologies.

2.2 Dynamical systems

A dynamical system, in general terms, consists of a state vector, $\boldsymbol{x}$, and a function which relates the rate of change of the state vector to its current value and any inputs to the system. The state vector contains a set of independent variables which completely describe the system. The following form describes a dynamical system:

$$x(k+1) = f(x(k), u, k) \tag{2.1}$$

where u is the input vector and k is an integer. An autonomous system is one where n does not appear in f, while in a non-autonomous system k is present in f. While most real-life systems are nonlinear, the theory of linear systems is often applied to nonlinear systems by linearising the model about a fixed point. For this reason, a brief overview of the theory of linear systems is presented before discussing nonlinear system theory.

2.2.1 Linear systems

A linear system is one that satisfies the principle of superposition and is homogeneous of degree 1. For a function f operating with inputs x and y, the principle of superposition states

$$f(x, y) = f(x) + f(y) \tag{2.2}$$

The system is homogeneous of degree 1 if the following holds true:

$$f(\alpha x) = \alpha f(x) \tag{2.3}$$

for $\alpha \, \epsilon \, \mathbb{R}$. A linear system takes the form:

$$x(k+1) = Ax(k) \tag{2.4}$$

This is an autonomous system. This type of system forms the basis for the majority of this thesis. The equilibrium point of (2.4) is found by setting $x(k+1) = x(k)$ which gives the equilibrium point at $x = 0$. The equilibrium point can be stable, unstable or marginally stable depending on the following [5]:

1. The system is said to be asymptotically stable if the natural response approaches zero as n approaches infinity.

2. The system is said to be unstable if the natural response grows without bound as n approaches infinity.

3. The system is said to be marginally stable if the natural response neither grows nor decays but remains constant or oscillates as n approaches infinity.

A more conceptual view is shown in Figure 2.1 which shows a state-space plot. A state-space plot is one where each axis corresponds to one of the state variables. In (a), a stable plot is shown as the trajectory (marked with arrows) moves towards the fixed point. In (b), the plot is unstable as the trajectory moves away from the fixed point.

The stability of an equilibrium point can be determined by assessing the eigenvalues of the $\boldsymbol{A}$ matrix. These can be found by solving the equation $(\lambda I - A) = 0$. If the real part of λ is less than 0, the system is stable i.e. if the eigenvalues lie in the left half plane. If the real part is greater than 0, the equilibrium point is unstable.

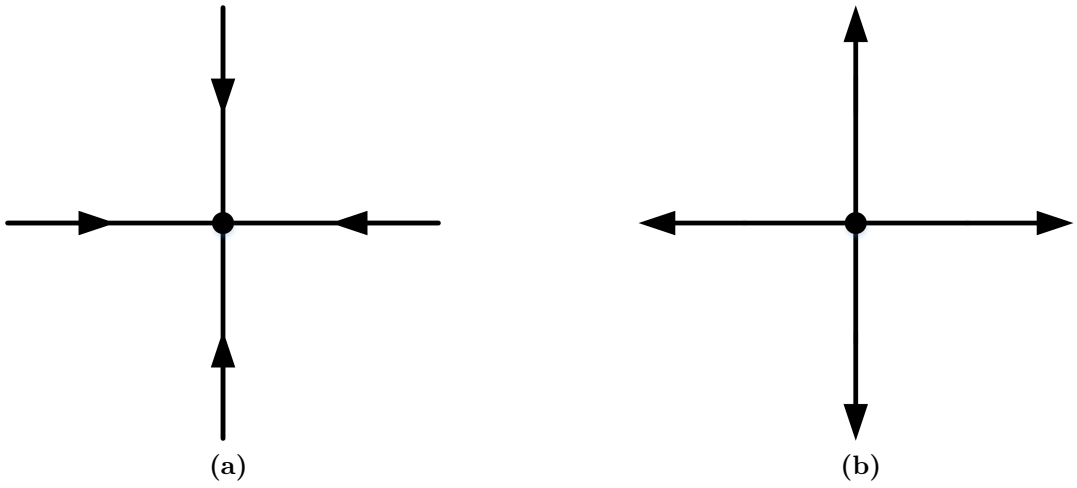

Figure 2.1: State-space plot for (a) stable system and (b) unstable system. The arrows represent the direction of the trajectory of the system described in (2.4).

An affine autonomous system is one which is closely related to a linear autonomous system but instead has an input vector. This type of system is described by:

$$\dot{x} = Ax + Bu \tag{2.5}$$

Again, the equilibrium point is found by setting $\dot{x} = 0$, which yields $Ax + Bu = 0$. Note that while the equilibrium point is no longer at $x = 0$, the inclusion of the Bu term merely shifts the equilibrium point. The stability of this point is determined in the same manner as (2.4), by evaluating the eigenvalues of the A matrix.

2.2.2 Nonlinear dynamical systems

A nonlinear dynamical system is one where the function f in (2.1) does not satisfy one or both of conditions (2.2) or (2.3).

$$x(k+1) = f(x(k), u, k) \tag{2.6}$$

If the function f is independent of k, then the system is autonomous. When the mapping function, f, is nonlinear, then the system in (2.6) is a nonlinear discrete-time dynamical system. If a continuous system has some regular forcing frequency associated with it, then sampling the system at the forcing frequency can yield an explicit map of the form (2.6). This is a useful tool in the analysis of nonlinear systems. A map generated from sampling a system at a constant frequency is termed a stroboscopic map. This is an example of a Poincaré mapping.

Poincaré mapping looks at how a given trajectory intersects a hyper-plane; a subspace of one dimension less than its ambient space. Each time the trajectory intersects the plane (in a given direction), it corresponds to a point [4]. This has the effect of reducing the order of the system, which can give insights into the system and its behaviour as well as making the system easier to analyse. Figure 2.2 shows a three dimensional state-space intersecting a two dimensional hyper-plane, termed a Poincaré section. Describing how one point on the Poincaré section relates to the next is termed a Poincaré map.

The Poincaré map can be used to qualitatively assess the type of attractor present in the system. The next section discusses the different types of attractors typically found in dc-dc converters.

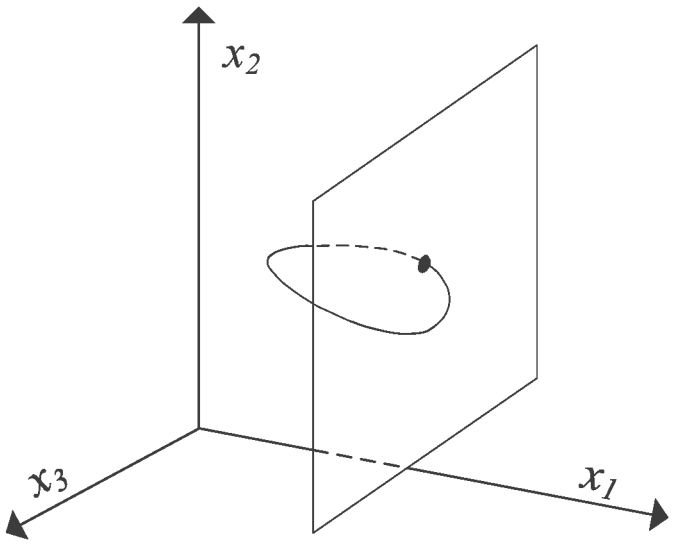

Figure 2.2: Three dimensional state-space with a two-dimensional Poincaré section.

2.3 Attractors

An attractor is a closed set A to which all neighbouring trajectories converge. A has the following properties:

1. A is an invariant set; any trajectory that starts in A stays in A for all time.
2. A attracts an open set of initial conditions; there is an open set U containing A such that if the initial condition $x(0)$ is contained in U, the distance between the trajectory $x(t)$ and A tends to zero as t approaches infinity i.e. A attracts all trajectories sufficiently close to it. The largest such U is termed the basin of attractors.
3. A is minimal i.e. A contains no subset that satisfies conditions 1 and 2.

In general, attractors can be classified into the following categories:

1. **Fixed point:** the solution to the dynamical system is a single point in the state space. This shows a single point on a Poincaré section as shown in Figure 2.3 (a).
2. **Limit cycle (periodic orbit):** The trajectory moves along a closed path in the state space. The motion is associated with a finite number of frequencies that are related to one another by a rational multiple. The motion is periodic. On a Poincaré section, this appears as a series of discrete points in a closed loop as illustrated in Figure 2.3 (b).
3. **Quasi-periodic orbit:** The trajectory moves along the surface of a torus[1]. The motion is associated with a finite number of frequencies that are related to one another by irrational multiples. The motion appears to be "almost periodic", but is not periodic. This appears as a closed loop where the trajectory passes through every point on the Poincaré section as shown in Figure 2.3 (c).
4. **Chaotic attractor:** The trajectory appears to move randomly in the state space. The motion is non-periodic and the trajectory is bounded. This is discussed in more detail in section 2.5. The Poincaré section for a chaotic trajectory is shown in Figure 2.3 (d). There appears to be no relationship between one point and the next.

Since fixed points are the desired attractors for the application in this thesis, the next section deals with determining their stability.

[1] A torus is similar to the surface of a doughnut-like object. A quasi-periodic orbit moves along the surface of a doughnut similar to an inductor coil winding about a ferrite core. If a cross section of the doughnut is taken, the trajectory is seen to go through every point along the cross section.

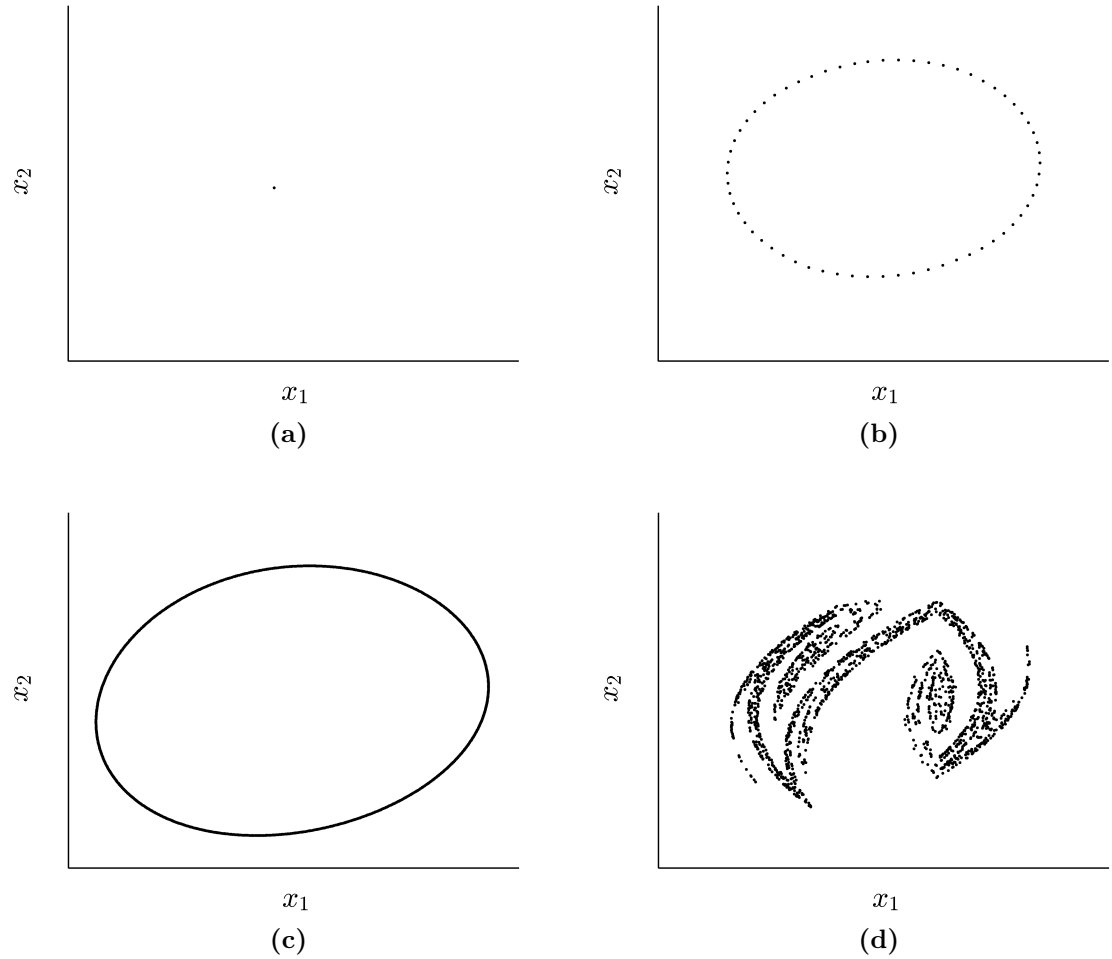

Figure 2.3: Poincaré section of different types of attractors (a) fixed point (b) limit cycle (c) quasi-periodic orbit and (d) chaotic attractor.

2.3.1 Stability of a fixed point

The simplest type of orbit for the system presented in (2.6) is a fixed point. Assuming an autonomous system and neglecting u so that the mapping function f is only a function of x, a fixed point is any point, x^*,that satisfies the following condition

$$x^* = f(x^*) \tag{2.7}$$

A fixed point is an equilibrium point of a system. Any trajectory that starts at a fixed point will stay there unless it is perturbed by some external force. A fixed point can either be stable or unstable depending on whether trajectories close to it are attracted or repelled. Fixed points that attract nearby trajectories are asymptotically stable. Fixed points that repel nearby trajectories are unstable. Cases where the fixed point neither attracts nor repels nearby trajectories are termed marginally stable.

To determine the stability of a system, small perturbations away from $x^*$are con-

sidered and how they behave as the systems trajectory evolves is examined. If the perturbation decays over time, the system is asymptotically stable. If the perturbation grows over time, the system is unstable. This information may be gathered by linearising about the fixed point. Given an initial point $x(1)$, close to x^*, consider how the distance between the fixed point at the next iteration $x(2)$ changes:

$$x(2) - x^* = f(x(1)) - x^* \tag{2.8}$$

Using the Taylor-series expansion for f about x^*:

$$x(2) - x^* = f(x^*) + f'(x^*)(x(1) - x^*) + ... - x^* \tag{2.9}$$

Only considering the linear terms, the distance between the second point in the trajectory and the fixed point is:

$$x(2) - x^* = f'(x^*)(x(1) - x^*) \tag{2.10}$$

Letting $\eta_k = x(k) - x^*$, (2.10) can be rewritten as a linear map:

$$\eta_{k+1} = f'(x^*)(\eta_k) \tag{2.11}$$

with eigenvalues $\lambda = f^{'}(x^*)$. The solution to this map can be found by writing the first few terms: $\eta_1 = \lambda\eta_0$, $\eta_2 = \lambda\eta_1 = \lambda^2\eta_0$. Thus, the general solution is:

$$\eta_{k+1} = \lambda^{k+1}\eta_0 \tag{2.12}$$

It is clear from (2.12) that if all of the eigenvalues of $f^{'}(x^*)$, which is termed the Jacobian matrix J, lie inside the unit circle, then the distance between the trajectory and the fixed point decreases with time and the system is asymptotically stable. If one or more of the eigenvalues of J lie outside the unit circle, the system is unstable. There are many different types of instability possible in systems. The next section discusses the most commonly observed instabilities in dc-dc converters.

2.4 Types of instability

A sudden change in the qualitative behaviour of a system is termed a bifurcation. Successive bifurcations lead to instability in power electronic converters. The type of bifurcation is classed by the qualitative change that takes place when a parameter is varied. How far a system is from instability is termed the stability margin. There are two metrics to consider; the phase margin and the gain margin. The

phase margin is the amount of phase that must be added to the system to cause it to be marginally stable. The gain margin is the amount of gain that must be added to the system to cause it to be marginally stable. Bifurcations that occur in power electronic converters are typically classed as standard (smooth) bifurcations or non-standard (non-smooth) bifurcations. Smooth bifurcations do not involve any structural change associated with the loss in stability. In continuous time systems, they occur when the real part of one, or more, of the eigenvalues of the system is greater than zero. In discrete-time systems, they occur when the magnitude of the eigenvalue is greater than 1.

Typically, for power electronic converters, smooth bifurcations can be classified into two categories; slow-scale bifurcations and fast-scale bifurcations which lead to slow-scale instability and fast-scale instability. Typical types of bifurcations that occur in power electronic converters are Hopf bifurcations and period-doubling bifurcations.

Non-smooth bifurcations do cause a structural change and are characterised by a sudden jump of the operating point. They occur due to interactions between system trajectories and state-space boundaries where the system switches from one configuration to another. Border collision bifurcations and grazing bifurcations are types exhibited by power electronic converters.

The following is a brief summary of some of the common types of bifurcations that take place in power electronic converters and Figure 2.4 illustrates the instabilities with solid lines representing stable points and dashed lines representing unstable points.

1. **Saddle-node bifurcation:** corresponds to the creation and destruction of fixed points. As a parameter varies, μ, two fixed points move towards each other, collide and mutually annihilate. The normal form is given by

$$\dot{x} = \mu + x^2$$

   From Figure 2.4 (a), it is clear there is a bifurcation at $\mu = 0$. The Jacobian matrix, J, is given by $2x$. For $\mu < 0$ there are two fixed points at $x = \pm\sqrt{-\mu}$. The equilibrium point at $x = -\sqrt{-\mu}$ is stable i.e. solutions starting close to it converge to $-\sqrt{-\mu}$. While the equilibrium point at $x = \sqrt{-\mu}$ is unstable. At $\mu = 0$, there is a single fixed point and initial conditions that are negative converge to 0 while positive initial conditions give solutions that increase without bound. Finally, for $\mu > 0$ there are no fixed points. Any initial condition will increase without bound.

2. **Transcritical bifurcation:** the exchange of the stability status of two fixed points of a system. The normal form is given by:

$$\dot{x} = \mu x + x^2$$

In this case, there is either one ($\mu = 0$) or two ($\mu \neq 0$) fixed points. When $\mu = 0$, the only fixed point is at $x = 0$ which is marginally stable. Positive initial conditions are stable, while negative initial conditions are unstable. When $\mu \neq 0$, there are two fixed points at $x = 0$ and $x = \mu$. For $\mu < 0$, the nonzero fixed point is stable and the zero fixed point is unstable. However, as μ crosses zero, the two fixed points exchange stability status i.e. the nonzero fixed point is unstable and the stable fixed point became unstable and vice versa. An example is illustrated in Figure 2.4 (b).

3. **Pitchfork bifurcation:** occur in systems where there is an overall parity symmetry i.e. if we replace the state variable, x, with its negative,$-x$, it yields the same set of equations. Pitchfork bifurcations can be classified into two categories:

   a) **Supercritical:** the normal form of a supercritical pitchfork bifurcation is:

   $$\dot{x} = \mu x - x^3$$

   Figure 2.4 (c) shows the resulting bifurcation diagram as μ is varied. When $\mu < 0$, the origin is the only fixed point in the system and it is stable. When $\mu = 0$, the origin remains stable but solutions no longer decay exponentially. This slow-down in the rate of decay is termed a critical slowing down. When $\mu > 0$, two new stable fixed points are created at $x = \pm\sqrt{\mu}$ and the fixed point at the origin remains but is now unstable. Hence, a supercritical pitchfork bifurcation occurs when, as a parameter varies, one stable fixed point expands to two stable fixed points and one unstable fixed point.

   b) **Subcritical:** the normal form of a subcritical pitchfork bifurcation is:

   $$\dot{x} = \mu x + x^3$$

   Note, the normal form is similar to the supercritical case but the cubic term has a destabilising effect on the system. Figure 2.4 (d) shows the bifurcation diagram which is the inverted version of the supercritical bifurcation diagram; the nonzero fixed points at $x = \pm\sqrt{-\mu}$ are unstable and exist before the bifurcation point i.e. $\mu < 0$. The origin is stable for $\mu < 0$, as in the supercritical case, and unstable for $\mu > 0$. However, the instability for $\mu > 0$ is no longer suppressed by the cubic term. This effect leads to a blow-up; starting at any initial condition $x_0 \neq 0$, the resulting trajectory $x(t) \to \infty$.

4. **Hopf bifurcation:** refers to the local birth or death of a periodic solution as a parameter, μ, crosses a critical value i.e. the birth of a stable limit cycle.

For a discrete system to be stable, all the eigenvalues must lie inside the unit circle. For a Hopf bifurcation to occur, one or more of the eigenvalues must leave the unit circle [4]. Hopf bifurcations can occur in phase-spaces of any dimension $n \geq 2$. A Hopf bifurcation can be modelled using the following normal form equations:

$$\begin{aligned} \dot{x} &= -y + x(\mu - x^2 - y^2) \\ \dot{y} &= x + y(\mu - x^2 - y^2) \end{aligned} \tag{2.13}$$

Converting from Cartesian to polar coordinates is clearer. Thus, the normal form is rewritten as:

$$\begin{aligned} \dot{r} &= r(\mu - r) \quad (a) \\ \dot{\Theta} &= 1 \qquad\quad (b) \end{aligned} \tag{2.14}$$

where $r = \sqrt{x^2 + y^2}$ and $\tan\Theta = y/x$. The solution to (2.14) (b) is $\Theta(t) = \Theta + t$, the angle continues to increase with time as the trajectory spirals around the origin. Figure 2.4 (e) shows the bifurcation diagram for a Hopf bifurcation. For $\mu < 0$, there is a single fixed point at $r = 0$. Finding the derivative of (2.14) (a) at $r = 0$ shows that the characteristic value is equal to μ. Thus, for negative values of μ, the fixed point at $r = 0$ is stable. For $\mu > 0$, the fixed point is unstable. Trajectories starting close to it will move away. However, there is a second fixed point at $r = \mu$. This fixed point corresponds to a limit cycle with a period of 2π in the time-domain. Looking at Figure 2.4 (d), at $\mu = 0$, a Hopf bifurcation takes place which gives birth to a limit cycle.

Similar to the pitchfork bifurcation, the Hopf bifurcation can be classified into subcritical and supercritical. If the resulting limit cycle is unstable, a subcritical Hopf bifurcation has taken place. While for a supercritical bifurcation, the critical point at the origin gives rise to a stable limit cycle.

5. **Period-doubling bifurcation:** a sudden doubling of a stable periodic orbit or limit cycle. Since the bifurcated orbit flips between two points, it is sometimes referred to as a flip bifurcation. There are two points such that applying the mapping function to the first point will yield the second point and vice-versa. For a discrete system, quantitatively speaking, this type of bifurcation is characterised by one of the eigenvalues passing through -1. An example is illustrated in Figure 2.4 (f).

6. **Border collision bifurcation:** these occur when two or more structurally different systems operate for different parameter ranges. When a parameter is varied across a critical value, the system exhibits an abrupt change in behaviour. The manner of the abrupt change is dependent on the system.

7. **Grazing bifurcation:** these occur when a system parameter or signal touches

an operational boundary e.g. when the control voltage touches the ramp tangentially. The system exhibits an abrupt change in behaviour.

2.5 Chaos

Chaos occurs in nonlinear systems and results in the seemingly random movement of trajectories within a bounded state-space. A chaotic trajectory is unpredictable in the long term; knowing the trajectory now does not guarantee knowing where the trajectory will end up. This contradicts the definition of a deterministic system. However, deterministic systems can exhibit chaotic behaviour. The key property of chaos is the sensitivity of nonlinear systems to initial conditions. Even a small error in specifying the initial conditions to a system can result in large differences in the output as time evolves. Hence, the long term predictability of a chaotic system is unpredictable in a practical sense. Consider the logistic map given by [3]:

$$x_{k+1} = rx_k(1 - x_k) \tag{2.15}$$

where x_k is a number between 0 and 1 representing the ratio of the existing population to the maximum possible population and r is the growth rate. Figure 2.5 (a) illustrates the chaotic behaviour of the deterministic logistic map presented in (2.15) with $r = 3.8$ and two nearby starting points at $x_0 = 0.01$ and $\bar{x}_0 = 0.010001$ which is 0.01% away. Figure 2.5 (b) shows the distance between the two trajectories, $x_0 - \bar{x}_0$, as k increases. The graph illustrates how the trajectories initially stay close for the first 20 iterations. When $k > 23$ the trajectories quickly move apart. With a 0.01% difference in the initial conditions, the trajectories still diverge along two different paths. In other words, the trajectory is unpredictable in the long term because there is a limit to the accuracy of the measurement of the initial conditions.

The characteristics of chaos are thus as follow [4]:

1. The output is bounded: this restriction is imposed for cases where the orbits go to infinity. In this case, it is relatively simple for their distances to diverge exponentially.
2. The output never repeats.
3. The output generates a fractal pattern on the Poincaré map.
4. The system exhibits a sensitivity to initial conditions. Two trajectories with similar initial conditions diverge along two different paths.

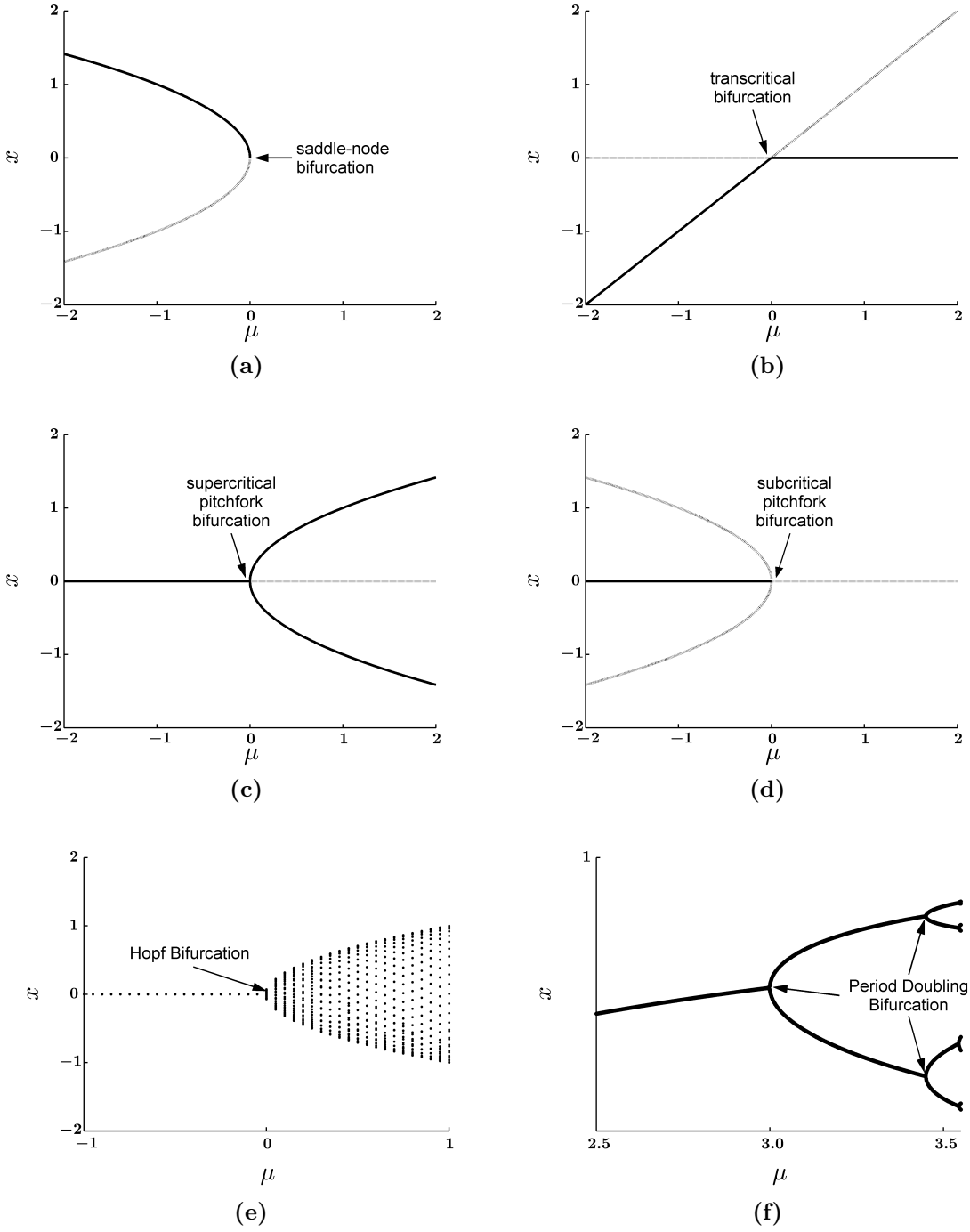

Figure 2.4: (a) Saddle-node bifurcation. (b) Transcritical bifurcation. (c) Supercritical bifurcation. (d) Subcritical bifurcation. (e) Hopf bifurcation. (f) Period-doubling bifurcation.

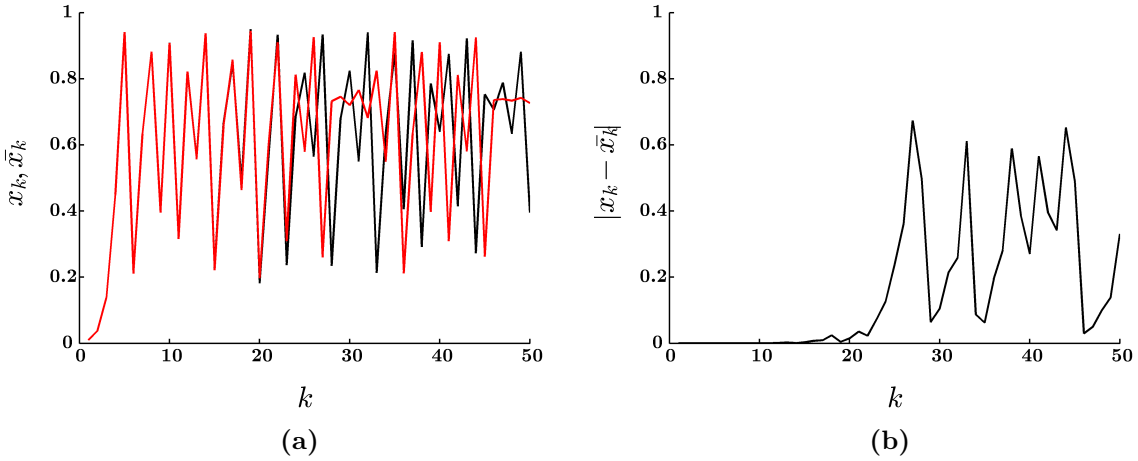

Figure 2.5: (a) Steady state behaviour of the logistic map with $r = 3.8$ with initial conditions $x_0 = 0.01$ (black) and $\bar{x}_0 = 0.010001$ (red) (b) Difference between steady-state responses with differing initial conditions.

2.5.1 Routes to chaos

A nonlinear dynamical system can exhibit a wide variety of behaviours with chaos being just one of these and these systems can undergo bifurcations whereby qualitative changes in the system take place. The series of bifurcations that a non-chaotic system goes through before developing into a chaotic system is termed the route to chaos [6]. The following outlines some possible routes to chaos:

1. **Period doubling route:** As a certain parameter is varied in one direction, a system may undergo a period-doubling bifurcation. As the parameter continues to vary, more period-doubling bifurcations may take place until the output of the system is chaotic.

2. **Quasi-periodic route:** Some nonlinear systems can undergo a Hopf bifurcation giving rise to a limit cycle as a parameter is varied. As the parameter continues to vary, another periodicity may develop which is not a rational multiple of the limit cycle. This results in quasi-periodic behaviour. As the parameter is further varied, the system may develop into a chaotic system.

3. **Intermittency route:** Some systems can be qualitatively described by distributed periods of irregular motion such as bursts of unstable/chaotic operation separated by long periods of stable operation. It occurs when a crucial parameter is being modulated by some external driving force, where the frequency of the driving force is different from the system's frequency. As the crucial parameter increases, the period of unstable/chaotic operation increases until the system develops into a chaotic system.

2.6 The Filippov Method

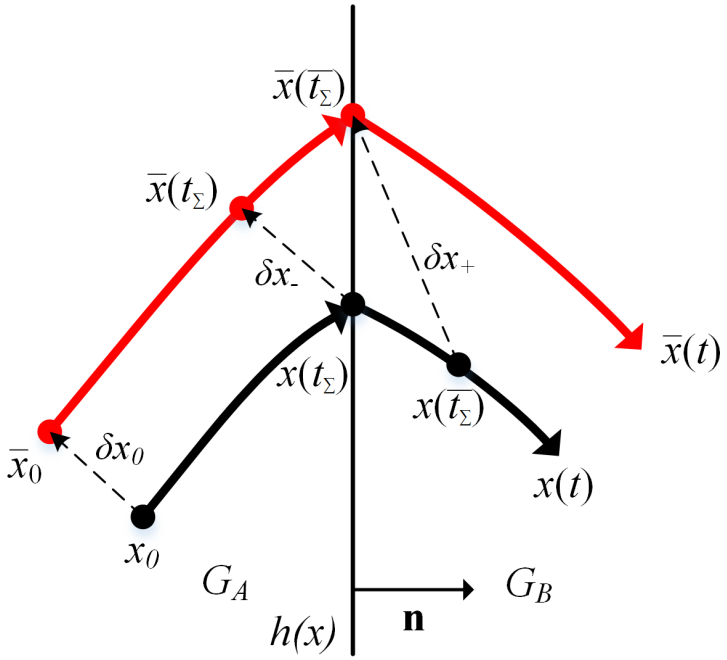

Figure 2.6: Orbit of interest.

The work of this thesis focuses on dc-dc converters which switch between two or more topologies in one switching period thus, assessing the stability of said systems is more complex compared to linear systems. The Filippov method is based on monitoring the evolution of a perturbed orbit [7]. The stability of a general orbit, say *x(t)*, is assessed by placing a small perturbation at $t = t_0$ and monitoring the evolution of the perturbation $\Delta x(t)$. The evolution is related to the initial perturbation by the fundamental solution matrix $\Phi(t, t_0)$ and when the vector field that governs the original orbit is linear time invariant, the fundamental solution matrix is given by the exponential matrix:

$$\Delta x(t) = \Phi(t, t_0)\Delta x(t_0) = e^{A(t-t_0)}\Delta x(t_0) \tag{2.16}$$

where $\Phi(t, t_0)$ is termed the state transition matrix. If the orbit is periodic, then the stability can be quantitatively determined by the eigenvalues of the fundamental solution matrix evaluated at $t = t_0 + T$, where T is the period of the orbit under study. The fundamental solution matrix obtained at $t = t_0 + T$ is termed the Monodromy matrix whose eigenvalues are called Floquet Multipliers. If the Floquet Multipliers lie inside the unit circle, the orbit is stable.

DC-DC converters switch between two or more topologies. It is important to note that the term *topology* in this work refers to the set of differential equations used to describe each operating mode of a dc-dc converter e.g. when the switch is open

or closed in the buck converter. It does not refer to the different types of dc-dc converters e.g. buck, boost etc. Each topology is described by a linear vector field:

$$\dot{x} = A_j x + B_j x_{in} \tag{2.17}$$

where j denotes the different topologies of the dc-dc converter. Mathematically, this switching action is described by a smooth scalar function *h(x,t)* called the switching manifold, which splits the state space into two areas. When the switching manifold crosses a border, the system changes between topologies. Due to the switching action, the stability of (2.16) cannot be assessed directly.

Assume that the orbit whose stability is to be tested is *x(t)* and starts at $t = t_0$ from the point x_0 in G_A and then hits the border and goes into G_B as in Figure 2.6. The perturbed trajectory $\bar{x}(t)$ also starts in G_A but from $\bar{x}_0$ and hence, the perturbations are given by the following:

$$\begin{cases} \delta x_- = \bar{x}(t_\Sigma) - x(t_\Sigma) \quad x \epsilon G_A \quad (a) \\ \delta x_+ = \bar{x}(\bar{t_\Sigma}) - x(\bar{t_\Sigma}) \quad x \epsilon G_B \quad (b) \end{cases} \tag{2.18}$$

where $\bar{t_\Sigma}$ is the instant where the perturbed orbit hits the switching manifold. Using a Taylor series expansion, it can be deduced that:

$$x(\bar{t_\Sigma}) = x(t_\Sigma) + f_+(x(t_\Sigma), t_\Sigma)\delta t \tag{2.19}$$

$$\bar{x}(\bar{t_\Sigma}) = \bar{x}(t_\Sigma) + f_-(\bar{x}(t_\Sigma), t_\Sigma)\delta t \tag{2.20}$$

where $\delta t = \bar{t_\Sigma} - t_\Sigma$ and $f_-$and f_+ are the right hand side of (2.17) before and after switching. Using (2.18) (b):

$$\begin{aligned} \delta x_+ &= \bar{x}(t_\Sigma) - x(t_\Sigma) + (f_-(\bar{x}(t_\Sigma), t_\Sigma) - f_+(x(t_\Sigma), t_\Sigma))\delta t \\ \delta x_+ &= \delta x_- + (f_-(\bar{x}(t_\Sigma), t_\Sigma) - f_+(x(t_\Sigma), t_\Sigma))\delta t \end{aligned} \tag{2.21}$$

From (2.18) (a) and (2.20), we have the following:

$$\bar{x}(\bar{t_\Sigma}) = x(t_\Sigma) + \delta x_- + f_-(\bar{x}(t_\Sigma), t_\Sigma)\delta t$$

As $t \to \bar{t_\Sigma}$ with $t \epsilon [t_0, t_\Sigma]$, $h_A\left(\bar{x}(\bar{t_\Sigma})\right) = 0$. Thus:

$$h_A\left(x(t_\Sigma) + \delta x_- + f_-(\bar{x}(t_\Sigma), t_\Sigma)\delta t\right) = 0$$

Expanding according to the Taylor Series:

$$h_A(x(t_\Sigma)) + n^T(\delta x_- + f_-(\bar{x}(t_\Sigma), t_\Sigma)\delta t) = 0 \tag{2.22}$$

where $n = \nabla h_A(x_\Sigma, t_\Sigma)$. However, $h_A(x(t_\Sigma)) = 0$. Hence, (2.22) can be written as follows:

$$n^T\delta x_- + n^T f_-(\bar{x}(t_\Sigma), t_\Sigma)\delta t = 0$$

$$\delta t = \frac{-n^T\delta x_-}{n^T f_-(\bar{x}(t_\Sigma), t_\Sigma)} \tag{2.23}$$

Recall (2.21):

$$\begin{aligned}
\delta x_+ &= \delta x_- + (f_-(\bar{x}(t_\Sigma), t_\Sigma) - f_+(x(t_\Sigma), t_\Sigma))\delta t \\
\delta x_+ &= \delta x_- + (f_-(\bar{x}(t_\Sigma), t_\Sigma) - f_+(x(t_\Sigma), t_\Sigma))\frac{-n^T\delta x_-}{n^T f_-(\bar{x}(t_\Sigma), t_\Sigma)} \\
\delta x_+ &= \left(I + \frac{(f_+(x(t_\Sigma), t_\Sigma) - f_-(\bar{x}(t_\Sigma), t_\Sigma))\, n^T}{n^T f_-(\bar{x}(t_\Sigma), t_\Sigma)}\right)\delta x_- \\
S &= I + \frac{(f_+(x(t_\Sigma), t_\Sigma) - f_-(\bar{x}(t_\Sigma), t_\Sigma))\, n^T}{n^T f_-(\bar{x}(t_\Sigma), t_\Sigma)}
\end{aligned}$$

In the case where the switching manifold also depends on time, the previous expression can be modified to as follows

$$S = I + \left.\frac{(f_+(x(t), t) - f_-(\bar{x}(t), t))\, n^T}{n^T f_-(\bar{x}(t), t) + \frac{\partial h_A}{\partial t}}\right| \begin{array}{l} t = t_\Sigma \\ x(t) = x(t_\Sigma) \end{array} \tag{2.24}$$

This is termed the Saltation matrix and links the events just before and after switching occurs [8]. For notation purposes, (2.24) is rewritten as:

$$S = I + \left.\frac{(f_+ - f_-)\, n^T}{n^T f_- + \frac{\partial h}{\partial t}}\right| \begin{array}{l} t = t_\Sigma \\ x(t) = x(t_\Sigma) \end{array} \tag{2.25}$$

Thus, the perturbation at time t_1 related to that at time t_0 is given as

$$\Delta x(t_1) = \Phi_M \Delta \boldsymbol{x}(t_0) \tag{2.26}$$

where

$$\Phi_M = \Phi_+(t_1, t_{\Sigma+}) S \Phi_-(t_{\Sigma-}, t_0) \tag{2.27}$$

which is termed the Monodromy matrix, Φ_- and Φ_+ are the state transition matrices outlined in (2.16) before and after switching. This method can be extended to any number of switching events. The state transition matrices are used for each topology and the saltation matrix (2.25) is calculated for each switching event. The stability of the system is then determined by assessing the eigenvalues of the Monodromy matrix. If the eigenvalues lie inside the unit circle, the system is asymptotically stable. Thus, the Monodromy matrix is similar to the Jacobian matrix presented in Section 2.3 but takes into account the switching between topologies. The Monodromy matrix is sometimes referred to as the Jacobian of the Poincaré map.

2.7 Conclusions

In this chapter, the basic concepts of linear system theory were introduced as well as the types of steady state behaviours found in systems and the types of instabilities that can occur. How these instabilities can lead to a chaotic output was discussed. Finally, a detailed derivation of the Filippov method was presented. This method is used in chapter 4 and chapter 5 to predict bifurcations and to design adaptive control schemes.

3 Power Electronics

3.1 Introduction

Power electronics is concerned with the processing and control of electrical power using electronic devices. These convert voltage and current from one form to another. They find applications in consumer electronics, the automobile industry and many devices that require such power electronics so as to operate efficiently. The efficiency of the power conversion is of paramount importance with commercial reasons being the main driving force behind high efficiency [9]. Thus, for most practical applications, switch-mode power supplies or "switching converters" are used as opposed to linear regulators. In switching converters, the input power is processed as specified by a control law to give the conditioned output power. A key feature of these converters is that they can achieve high efficiency in the range of 80-90% or even higher [10]. One particular branch of these converters are dc-dc converters in which a dc supply voltage is converted and conditioned to a higher or lower dc voltage. This chapter provides the background theory for dc-dc converters as well as the mathematical tools to model these systems and the analytical methods to study their dynamics.

3.2 DC-DC converters

DC-DC converters convert voltage at one level to voltage at another level. They employ both switching components such as transistors and diodes, to shape the input signal, and reactive components such as inductors and capacitors, to filter the output signal so that it is close to being a dc signal. When a converter is required to produce a constant output, irrespective of load variations, it is termed a regulator.

The buck converter is an example of a step-down dc-dc converter whose circuit diagram is illustrated in Figure 3.1 (a). The purpose of the buck converter is to step down an input voltage, V_{in}, to an output voltage, v_o^*, where $v_o^* = dV_{in}$ and d is the duty cycle of SW_1. The output voltage should be close to the reference voltage, V_{ref}. This is achieved by opening and closing switches SW_1 and SW_2 in a complementary manner i.e. when SW_1 is open, SW_2 is closed. The equivalent circuits for when SW_1 is closed and when SW_1 is open are shown in Figure 3.1 (b) and (c), respectively.

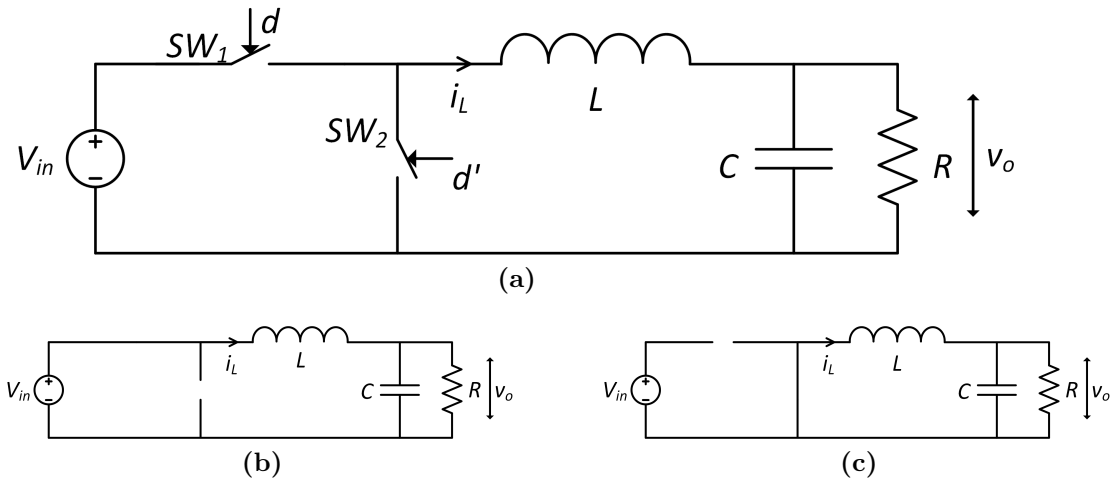

Figure 3.1: (a) Buck converter circuit. Topologies of the buck converter with SW_1 closed (b) and SW_1 open (c).

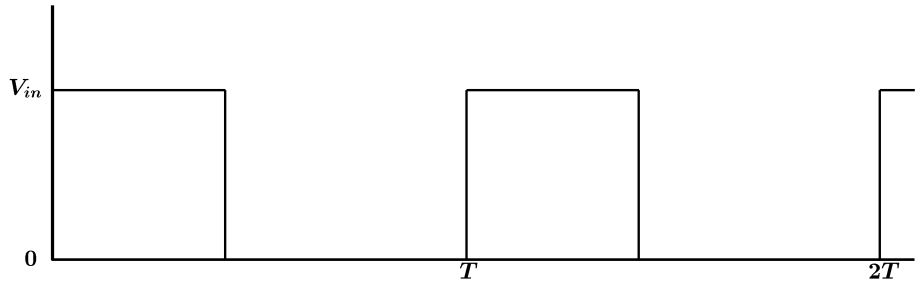

Figure 3.2: Voltage across SW_2 which corresponds to the output of the PWM.

The switches are controlled using PWM. With this form of control, the switches turn on and off periodically and the state of the switches is modulated by some control signal. If the switches are reset every T, where T is the switching period, and SW_1 starts closed, SW_1 will remain closed for dT, where d exists between 0 and 1. SW_1 will remain open for the remainder of the switching period i.e. $(1-d)T$. Figure 3.2 shows the voltage across SW_2, which is given by:

$$v_{avg} = \frac{V_{in}dT + 0(1-d)T}{T}$$
$$v_{avg} = dV_{in} \tag{3.1}$$

Thus, the average value across switch 2 is the desired dc output value. The inductor and capacitor act as a low-pass filter which smooth the voltage and current so that it approximates that of a dc voltage and current. However, owing to the periodic nature of the PWM and since it is impossible to build a perfect low-pass filter (one that only allows the dc component to pass and completely removes the components at the switching frequency and its harmonics) the output voltage and current will

have some ripple as shown in Figure 3.3 (a) and (b). This type of operation is the desired output voltage for practical applications and is termed v_o. Thus, the output voltage v_o consists of the desired dc component v_o^* plus a small undesired ac component, at the switching frequency, due to the incomplete attenuation of the switching harmonics by the low-pass filter. The magnitude of this ripple is much smaller than that of the dc component in a well-designed converter [9]. Throughout this research, ideal components are assumed unless specifically stated.

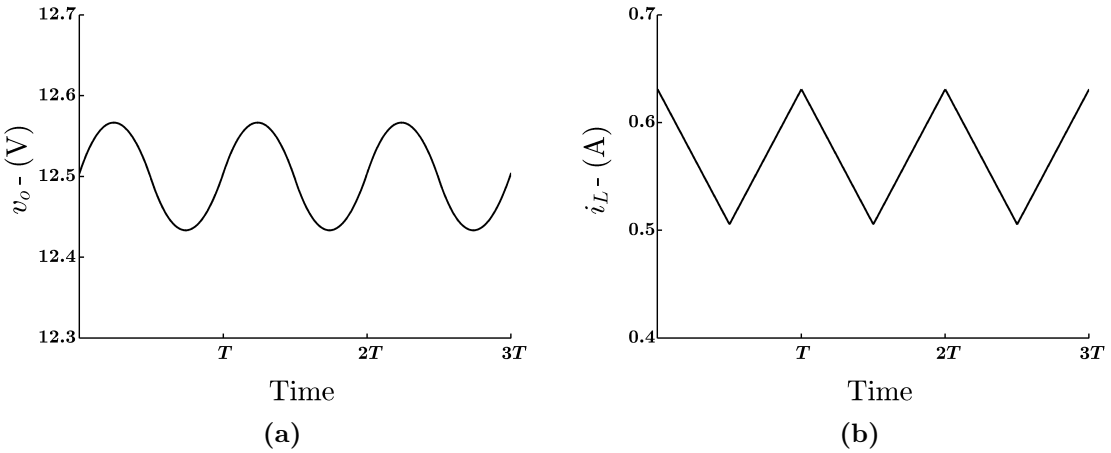

Figure 3.3: Waveforms of (a) the output voltage and (b) the inductor current for a buck converter with the following parameters: $R = 22\,\Omega$, $C = 47\,\mu F$, $L = 20\,mH$, $V_{in} = 25\,V$, $T = 400\,\mu s$ and $d = 0.5$.

In ideal circumstances, the output voltage is a function of the input voltage and the duty cycle. However, in real circuits, due to the nonideal properties of components, the output is also a function of the load current. The output of a dc-dc converter is controlled by modulating the duty cycle ratio to compensate for circuit changes or changes in the load conditions. These changes may be due to circuit parameters varying, supply voltage changes and/or external disturbances. A feedback control system for dc-dc converters compares the output voltage to a reference voltage and converts the error to a duty cycle ratio. This method is termed Voltage-Mode Control (VMC) as the output voltage is the input to the control scheme. Another form of control is Current-Mode Control (CMC). It consists of a current loop where the inductor current is compared to a reference current. Traditionally, analog controllers are employed to regulate these circuits [9]. However, in recent years, the use of digital control has been proposed and researched [11]. Digital control has many potential advantages which include their low power, immunity to analog component variations, compatibility with digital systems and a faster design process [1].

Figure 3.4 (a) outlines the control loop typically used for a VMC buck converter. The output voltage is measured against a reference voltage, V_{ref}, which is at the desired steady-state output. This gives the error voltage, v_e. The error voltage is then compared against a ramp signal which has a period of T and varies from a lower

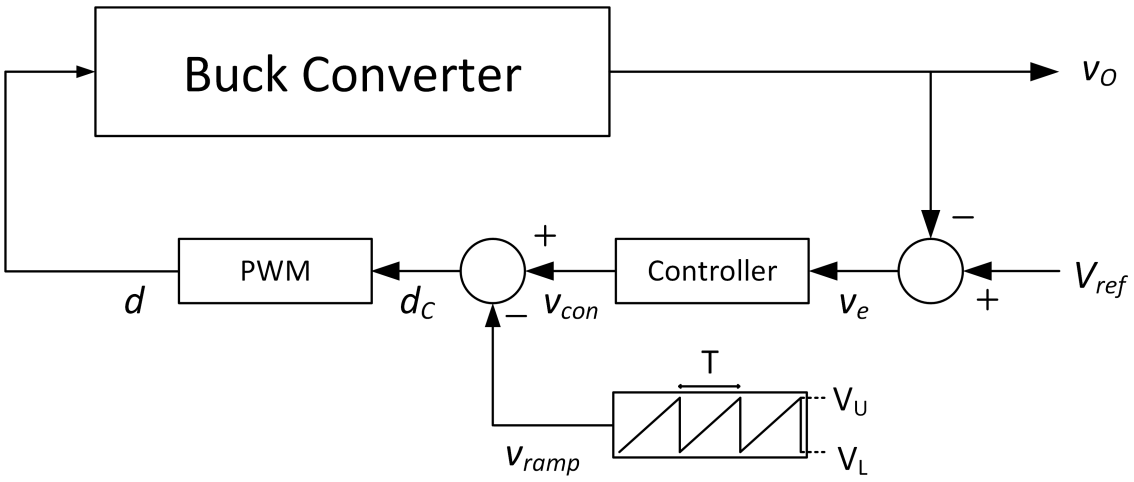

(a)

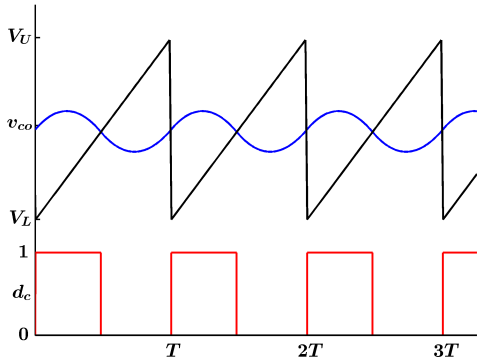

(b)

Figure 3.4: (a) Analog control loop for a VMC buck converter (b) Plot of the ramp signal (black), control voltage (blue) and PWM (red).

value, V_L, to an upper value, V_U. When the control signal is greater than the ramp signal, the output voltage is below the desired value. Thus, the PWM is high and SW_1 is closed. When the polarity of the error signal changes, i.e. when the control signal is less than the ramp signal, the output voltage is above the desired value and the PWM is low causing SW_1 to open. SW_1 remains open for the remainder of the switching period. Figure 3.4 (b) illustrates how the control voltage, ramp voltage and PWM interact.

3.3 Modeling of converters

The operation of dc-dc converters can be described as an orderly repetition of a fixed sequence of circuit topologies [12]. Such toggling between topologies is achieved by placing switches at suitable positions and turning them off and on in such a manner that the desired sequence of topologies is achieved. Thus, the overall result is time-varying and nonlinear. Recall the generalised state-space for dc-dc converters:

$$\dot{x} = A_j x + B_j x_{in} \tag{3.2}$$

where x contains the state variables that fully describe the system at any point in time and (3.2) describes how these variables change over time. The circuit topology determines the matrices A_j and B_j, where the subscript j denotes which topology the circuit is operating with. The modeling of (3.2) has evolved around two basic approaches, namely; the *averaging approach* and the *discrete-time approach*.

3.3.1 Averaging approach

The averaging approach was developed by Middlebrook and Ćuk [13]. The main objective of the averaging approach is to remove time-varying parameters from the system equations. The averaged model ignores dynamics between switching events and focuses on the envelope of dynamical motion. Thus, this method characterises converters in the low-frequency domain.

Consider a dc-dc converter that switches between K topologies. In one switching cycle, it spends a proportion of time on each topology. The proportion of time it spends on the j^{th} topology is d_j, where $d_1 + d_2 + ... + d_K = 1$. The state equations for the system are:

$$\dot{x} = \begin{cases} A_1 x + B_1 u & \text{if } t_k < t < t_k + d_1 T \\ A_2 x + B_2 u & \text{if } t_k + d_1 T < t < t_k + (d_1 + d_2) T \\ ... & \\ A_K x + B_K u & \text{if } t_k + (1 - d_K) T < t < t_{k+1} \end{cases} \tag{3.3}$$

where A_j and B_j are the system matrices for the j^{th} topology. Averaging out the system matrices yields the following continuous-time averaged model [13]:

$$\dot{x} = A_m x + B_m u \tag{3.4}$$

where

$$A_m = \sum_{j=1}^{K} d_j A_j \text{ and } B_m = \sum_{j=1}^{K} d_j B_j \tag{3.5}$$

The averaged model retains the low-frequency components while ignoring the dynamics within a switching cycle. The validity of the averaged model is restricted to the low-frequency range up to an order of magnitude below the switching frequency [12]. This is due to the Nyquist-Shannon sampling theorem. Thus, the averaged

model is suited to studying slow-scale instabilites but not suited to fast-scale instabilities; dynamics occuring at frequencies higher than the switching frequency. For this reason, the averaged model is not used in this thesis. Instead, the discrete-time approach is used.

3.3.2 Discrete-time approach

A switching converter is modelled using a series of topologies that repeat themselves periodically. One way to model such a kind of operation is to split a system into a series of sub-systems. Each sub-system is responsible for describing the system in one sub-interval of time. If the solution to the state equations at time t is required, starting at time t_0, each sub-system is solved iteratively until time t is reached. Sub-system k is linked to sub-system $k+1$ by a stitching process; the final values of k are used as the input values for $k+1$. Consider equation (3.2). Given $\boldsymbol{x}(t_0)$ as the initial condition for the state vector $\boldsymbol{x}$ at time t_0, the solution to the equation is given by [12]:

$$x(t) = e^{A_j t}x(t_0) + \int_{t_0}^{t} e^{(t-\tau)A_j}B_j u d\tau \tag{3.6}$$

This solution is valid as long as the system stays within the j^{th} topology. In continuous-conduction mode (CCM), when theq inductor current is always greater than 0, the buck converter switches between two topologies; $j = 1$ for dT and $j = 2$ for $(1-d)T$. The discrete-time mapping is found by stitching the solutions together at the time instant that switching occurs. If t_0 marks the start of a switching period, then at the point of switching between topologies the state is given by:

$$x(t_0 + dT) = e^{dTA_1}x(t_0) + \int_{t_0}^{t_0+dT} e^{(t-\tau)A_1}B_1 u d\tau \tag{3.7}$$

and the state at the next switching instant is given by:

$$x(t_0 + T) = e^{(1-d)TA_2}x(t_0 + dT) + \int_{t_0+dT}^{t_0+T} e^{(t-\tau)A_2}B_2 u d\tau \tag{3.8}$$

Using (3.7) and (3.8), values of the state vector at the end of one switching period can be obtained as well as capturing the high-frequency dynamics. Since the discrete-time model samples the system at time instants, the information contained in the model is limited by the sampling rate. If the system is sampled at the switching frequency, the model is capable of capturing all dynamics up to half of the switching frequency. For higher frequencies, the sampling rate must be increased.

The discrete-time approach is capable of analysing both slow-scale and fast-scale instabilities but the averaged model enjoys mathematical simplicity.

3.4 Nonlinear effects of analog-controlled power electronic converters

In 1927, Van der Pol was studying the Van der Pol oscillator [14]; a relaxation oscillator comprising of a battery, a bulb, a capacitor and a resistor. The circuit was driven by a 1 kHz sinusoidal signal and tuned to obtain subharmonics. However, at certain drive frequencies, an irregular noise was heard. This is one of the first examples of deterministic chaos in electronic circuits. However, there was little interest in explaining the spurious oscillations for the next 50 years. In 1980, Baillieul, Brockett and Washburn [15] suggested that chaos may occur in dc-dc converters and other systems that are driven by a PWM. In 1981, Linsay published the first modern day experimental report of chaos in an electronic system [16].

In 1984, Brockett and Wood presented a paper showing that a controlled buck converter can exhibit bifurcations and chaos. A letter by Hamill and Jefferies in 1988 [17] was one of the first detailed analyses of chaos in a CMC buck converter. The use of difference equations and zigzag return maps were used to qualitatively study the system. Wood further described chaotic behaviour in 1989 [18] using an experimental setup for a VMC controlled buck converter, termed a ripple regulator. Setting the input voltage as the bifurcation parameter and plotting the bifurcation diagram and associated phase portraits, the work demonstrates that the system underwent the period-doubling route to chaos. In a 1990 paper [19], Deane and Hamill identify several other possible routes to chaos exhibited by different power electronic circuits. This work is then extended in [20, 21, 22] for a VMC buck converter, a CMC buck converter and a CMC boost converter, respectively. Using a combination of iterated maps and experimental results, these works mainly focus on the prediction and experimental confirmation of chaos in dc-dc converters under various control schemes.

The early work in the analysis of chaos in dc-dc converters typically used exact differential equations which were integrated to find the trajectories [23]. This allows qualitative analysis to be performed but it is difficult to perform any quantitative analysis due to the complex mathematics involved. Other methods included devising linear system models using methods like state-space averaging which, while theoretically sound, are approximate and fail to predict fast-scale instabilities [24]. Hamill and Deane proposed nonlinear map-based modelling [25]. In this method, one of the state variables is sampled at specific time-instants. The three possible time-instants are:

1. Stroboscopic sampling: Sample at the beginning of each switching period. This method is used in this thesis.
2. S-switching or synchronous switching: Sampling at the clock instants when switching occurs thus, multiple pulsings and skipped cycles are possible.
3. A-switching or asynchronous switching: Sampling at each switching event i.e. when $v_{con} = v_{ramp}$.

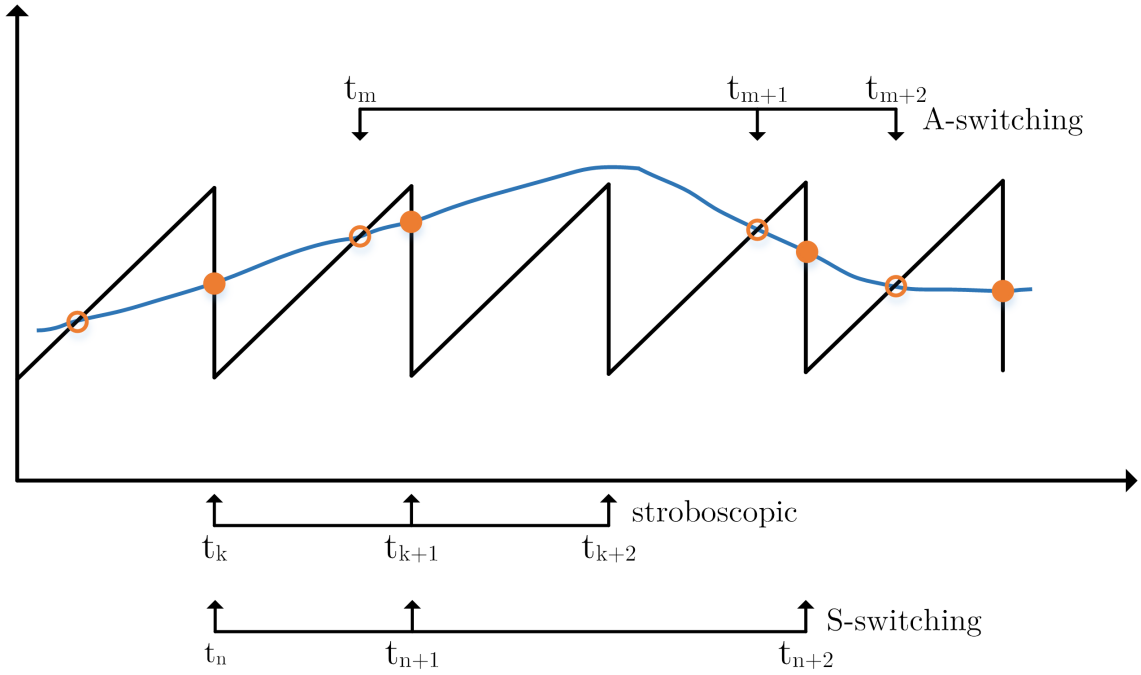

Figure 3.5: Three possible time instants for discrete-time sampling. Ramp signal (black) and control signal (blue).

This sparked research to move in two directions. Firstly, Banerjee and Chakrabarty [26] added non-idealities to the system and demonstrated that a closed-form model could still be obtained. It was shown by Deane and Hamill and Banerjee et al. that the discrete-time model could be reduced to a one-dimensional piecewise-linear map using switch-on sampling and stroboscopic sampling which can be used for quantitative analysis of chaotic behaviour as the discrete-modeling procedure reduces the problem of the stability of the trajectory in the state-space to that of a fixed point of the sampled data model [21, 27].

An important study into the bifurcation behaviour in buck converters was published by Chakrabarty and Banerjee [28]. Varying the input voltage, load capacitance, inductance and load resistance, it was found that the system does not always go through the usual period-doubling route to chaos. There are regions between period-doubling zones where period-halving occurs and there are abrupt changes in behaviour as parameters vary from one value to the next.

[29, 30] Fossas and Olivar presented further studies into the nonlinear dynamics of the buck converter showing the topology of its chaotic attractor. The authors study

the eigenvalues of the system by deriving the stroboscopic map and linearising about a fixed point. This enables the analysis of period-1 and period-2 orbits.

Border-collision bifurcations were first explained by Banerjee et al. [27, 31] and have been analysed by Banerjee [32, 33]. This is a common feature in dc-dc converters and has been studied by many researchers [34, 35, 36]. Quasi-periodic routes to chaos, where two system frequencies interact with one another, have also been observed and studied [36, 37, 38, 39, 40].

The intermittency route to chaos was discovered by Manneville and Pomeau and reported in [41]. Intermittent operation, heard as sizzle with a rather long period, occurs in periodically driven nonlinear systems, where the frequency of the interference signal is not consistent with the system's driving frequency. It was first reported in [42]. Such intermittency has been observed in power supplies which are not protected against the intrusion of spurious signals. [43] studies a CMC boost converter with a sinusoidal signal injected directly into the compensation ramp. Intermittent operation has been studied in a VMC buck converter which superimposes the spurious perturbation directly onto the control voltage by [44]. However, in all of these works, only sinusoidal interference signals were considered. [45] considers perturbing the input voltage and control voltage with a noise signal that has a sinusoidal, saw-tooth and triangular waveform. In [42] and [45], discrete maps are derived which enable the derivation of the Jacobian matrix, whose eigenvalues indicate the stability of the system. However, the application of this method requires that the frequency ratio and the type of bifurcation that occurs be taken into account. Thus, the discrete map method cannot be generalised for all frequency ratios or noise shapes in order to derive conditions to avoid instability. The mapping function changes depending on the frequency ratio and type of bifurcation. Hence, this method is algebraically complex and not suited to controller design.

At present, fast-scale instabilities are mostly checked through experimentation or simulation over large parameter ranges. This leads to over designed components that eliminate subharmonics. However, with a push towards miniaturization, the size of the regulator is constrained. Thus, a design method for predicting fast-scale instabilities is required. Previous work [12, 23] have suggested that the Jacobian of the Poincaré map or the Monodromy matrix can be used to predict fast-scale instabilities. Other methods such as trajectory sensitivity analysis, linearising the system around the nominal periodic orbit rather than the equilibrium points, and auxiliary vector methods, determining the Jacobian matrix using small differences of the state vectors compared to their steady-state values at the beginning and end of sub-intervals, have been proposed [46, 47] but can be mathematically complicated when used in controller design. Furthermore, apart from determining the stability of the limit cycle, they offer little insight into why these instabilities occur.

The Filippov method achieves the same objective as the sampled-data model and it

is preferred when more complicated converter topologies are employed. In [48], the author applies Filippov's Method to analyse the stability of a VMC buck converter. The main benefit of the Filippov method is that it can consider each switching event separately. This enables designers to consider the transition matrix with the corresponding Saltation matrix at each switching event and compose the Monodromy matrix whose eigenvalues indicate the stability of the system. This work was then extended in [49] by Bradley, where a buck converter under proportional control is considered. The system undergoes the period-doubling route to chaos as the proportional control term, K_P, is varied. The value of K_P at which the first period-doubling bifurcation is derived using the Filippov method.

3.4.1 Previous work on controlling nonlinear phenomena

In real-world applications, it is desirable to have mechanisms that allow nonlinear phenomena that occur in nonlinear systems to be controlled. Since 1980, when the paper first suggesting the possibility of chaotic behaviour in dc-dc converters was published [15], many control methods have been proposed for controlling bifurcations and chaos. These can typically be split into two general groups; feedback control and non-feedback control.

Feedback control methods involve measuring the system variables, applying a control law and varying some control parameter to achieve the desired control output. One example of feedback control is variable ramp compensation. In this method, the ramp characteristics are varied in order to avoid chaotic behaviour. In [50], the authors use a feed-forward controller. The ramp is proportional to the input voltage and is used to eliminate subharmonic oscillations when the duty cycle exceeds 50%. In [51], analysis of a CMC buck converter without slope compensation is considered. The time-delayed feedback controller is another method that has been proposed [52, 53] to work in tandem with a P controller to increase the stability margin of dc-dc converters. This method constructs a control signal based on the difference between the present state of the system and its delayed value. However, this is more suited to digital control.

Non-feedback control methods do not measure the system variables and no specific periodic output is identified. Resonant parametric perturbation involves perturbing some parameters at appropriate frequencies and amplitudes thereby, converting a chaotic output into the desired output. [54] applies dynamic resonant perturbation for the elimination of fast-scale instabilities. In contrast to traditional resonant perturbation, the sinusoidal signal is derived from the output voltage. However, extensive simulations are still required as rigorous bounds for the elimination of period-doubling are not presented. [55] proposes exact and approximate sampled-data models for power electronic converters under current-mode control. Boundary

conditions for the occurrence of subharmonic instability are given which enable dynamic behaviour prediction. However, the results of the models presented here are strongly dependent on the initial switching instant chosen [56].

3.5 Conclusions

This chapter laid out the basic topology of dc-dc converters. The buck converter configuration was discussed and mathematical models presented. Conventional methods of modeling switching converters were studied. It was seen that while continuous time-averaging techniques are easier to understand compared to the discrete-time approach, the former method is only suitable for low-frequency analysis and discards details between switching events. Thus, the later method is required to study the system's behaviour in its entirety.

An overview of literature on nonlinear effects in analog-controlled dc-dc converters was discussed as well as previous work in controlling the nonlinear phenomena that may occur.

4 Analog PID Controller

4.1 Introduction

DC-DC converters are widely used in numerous applications because of their high efficiency, small size, low cost and weight [57]. Most power electronic systems are not equipped with redundancy. Any faults that occur to the components or subsystem can damange the interconnecting devices or lead to a shutdown of the system. For this reason, designing power electronic converters with a view to long term reliability is a concern for industrial applications [58]. Therefore, a thorough investigation into the nonlinear dynamics of dc-dc converters is required as well as a method to predict and avoid the undesireable operation.

For the satisfactory operation of the converter and the systems that it interconnects, it is imperative that the controller is suitably designed. The basic requirement is a fast and stable response over a wide operating region. In order to achieve this, the employed P or PI controller must be properly tuned [9]. From a stability point of view, two types of instabilities can occur; slow-scale instabilities and fast-scale instabilities. The use of traditional methods for the selection of the P and I terms are based on standard control theory techniques, like Bode plots. These methods use the linearised averaged model which acts like a low-pass filter and hence, cannot describe fast-scale instabilities [12]. Therefore, frequency response methods used in the tuning of PI controllers leave the controller vulnerable to various spurious behaviours. Previous works [12, 23] have suggested that the Jacobian of the Poincaré map or the Monodromy matrix can be used to predict these fast-scale instabilities. Hence, it is possible to be used in the design of a controller.

It is well known that the usage of the D-term in a dc-dc converter can cause the amplification of noise or inject significant noise into the closed-loop system. The injection of noise is mainly due to the equivalent series resistance (ESR) and the equivalent series inductance (ESL) of the capacitor. During large signal transients, the parasitic elements drive an impulse response in the derivative term with large overshoots and undershoots. During small signal transients, the ESR leads to discrete jumps at switching points that alternate in polarity. This interaction can lead to a reduction in the phase margin [59]. Traditionally, the D-term has been avoided. On the other hand, due to the requirement for fast transient responses, the D term

is required. However, little or no work exists on design procedures for PID controllers that take into consideration fast-scale instabilities. An extra difficulty can arise, the Saltation matrix required in [60] assumes a smooth scalar function for the manifold that describes the switching action. A smooth function is one that has a first derivative everywhere in its domain. The smoothness of the switching manifold is required as the Filippov method uses its derivative to the state vector. When a PID controller is employed, the resulting functions may be non-smooth. Therefore, it is not straightforward to apply the method presented in [60] for such converters.

In this chapter, the research aims to address this issue, that is, to analyse fast-scale instabilities of a PID controlled dc-dc converter and prove that the D-term, apart from providing faster dynamics, also improves the stability of the nominal operation. Initially, the main framework of how a PID controlled buck converter can be designed to include the consideration of fast-scale instabilities is introduced. Specifically, the theoretical framework for stable period-1 operation is presented and enables designers to select control parameters that will ensure stable behaviour without using high gains that can cause noise problems. An adaptive PID controller is proposed, whereby the D-term is updated at the end of every switching cycle as the load and other characteristics vary. Once this methodology has been clearly and concisely presented, the main issue of the non-smoothness of the switching manifold will be addressed by considering a VMC boost converter.

4.2 Buck Converter

4.2.1 Mathematical Model

A PID controlled synchronous buck converter is considered in Figure 4.1. It is important to note that the parameters used throughout this work do not reflect values currently employed in industry. However, there exists a large body of research which are based on these parameter values. Thus, they have been chosen to enable the comparison of the results of the current work to previous approaches. Furthermore, some of these studies have performed experimental setups of the systems described throughout this dissertation. These works validate the accuracy of the theoretical models and simulations [19, 60, 61, 42].

The buck converter is described by the equations:

$$\dot{x} = \begin{cases} f_{on}(x,t) = & A_{on}x + B_{on}x_{in} & SW_1 \text{ is on} \\ f_{off}(x,t) = & A_{off}x + B_{off}x_{in} & SW_1 \text{ is off} \end{cases} \tag{4.1}$$

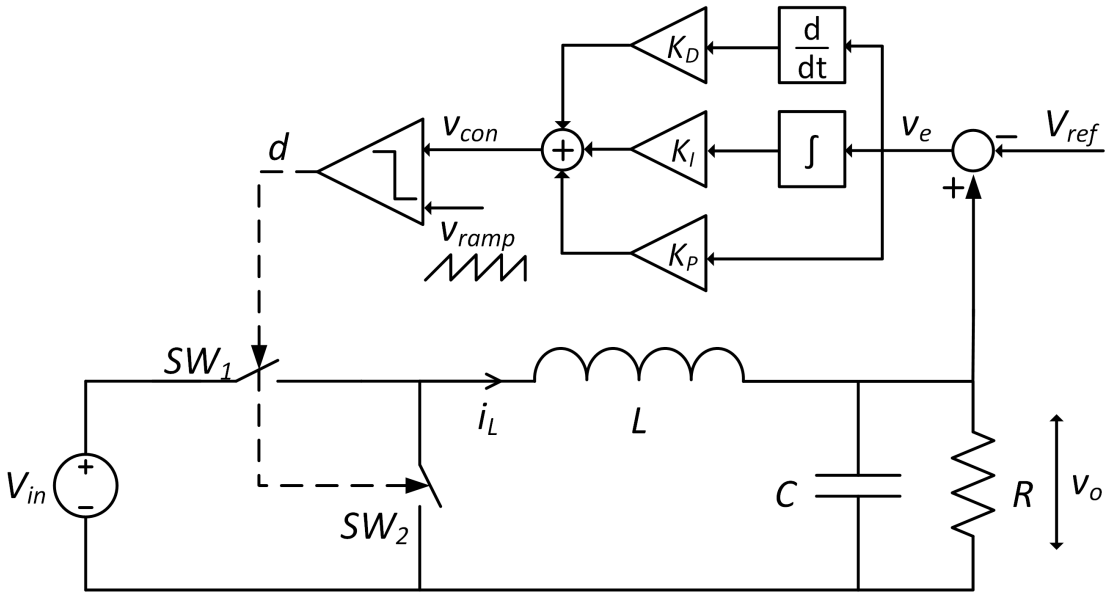

Figure 4.1: Buck converter with analog PID controller. The parameters used in this work, unless otherwise stated, are $T = 400\,\mu s$, $L = 20\,mH$, $C = 47\,\mu F$, $R = 22\,\Omega$, $V_{ref} = 11.3\,V$, $V_L = 3.8\,V$, $V_U = 8.2\,V$, $K_D = 0.0001$, $K_I = 10$, $K_P = 8.4$ and $V_{in} = 25\,V$.

where:

$$A = A_{on} = A_{off} = \begin{bmatrix} -\frac{1}{RC} & \frac{1}{C} \\ -\frac{1}{L} & 0 \end{bmatrix},\ x(t) = \begin{bmatrix} v_o \\ i_L \end{bmatrix}$$

$$B_{on} = \begin{bmatrix} 0 \\ \frac{1}{L} \end{bmatrix},\ B_{off} = \begin{bmatrix} 0 \\ 0 \end{bmatrix},\ x_{in} = V_{in}$$

To form a symmetrical system and to simplify the equations, a transformation to the (v_o, u) plane is applied. Let $i_L = \alpha v_o + \beta u$ where $u = \frac{i_L - \alpha v_o}{\beta}$. The state variables can be rewritten as:

$$\frac{dv_o}{dt} = (A_{11} + A_{12}\alpha)\, v_o + A_{12}\beta u + B_{11} V_{in} \tag{4.2}$$

$$\frac{di_L}{dt} = \alpha \frac{dv_o}{dt} + \beta \frac{du}{dt} \tag{4.3}$$

Thus:

$$\begin{aligned} \frac{du}{dt} &= \frac{1}{\beta}\left(\frac{di_L}{dt} - \alpha \frac{dv_o}{dt}\right) \\ &= \frac{1}{\beta}\left(A_{21} v_o + A_{22}\alpha v_o + A_{22}\beta u + B_{21} V_{in}\right) - \frac{\alpha}{\beta}\left(A_{11} v_o + A_{12}\alpha v_o + A_{12}\beta u + B_{11} V_{in}\right) \\ &= \frac{1}{\beta}\left(A_{21} + \alpha A_{22} - \alpha A_{11} - \alpha^2 A_{12}\right) v_o + \left(A_{22} - \alpha A_{12}\right) u + \frac{1}{\beta}\left(B_{21} - \alpha B_{11}\right) V_{in} \end{aligned}$$

The output must be in the form:

$$\frac{d}{dt}\begin{bmatrix} v_o \\ u \end{bmatrix} = \begin{bmatrix} -\sigma & \omega \\ -\omega & -\sigma \end{bmatrix}\begin{bmatrix} v_o \\ u \end{bmatrix} + \bar{B}V_{in}$$

where:

$$\bar{B} = \begin{bmatrix} B_{11} \\ \frac{B_{21}-\alpha B_{11}}{\beta} \end{bmatrix} = \begin{bmatrix} a\sigma + b\omega \\ a\sigma - b\omega \end{bmatrix}$$

Thus:

$$a = \frac{\bar{B}_{11} + \bar{B}_{21}}{2\sigma} \text{ and } b = \frac{\bar{B}_{11} - \bar{B}_{21}}{2\omega}$$

Therefore:

$$A_{11} + \alpha A_{12} = -\sigma$$
$$\alpha = \frac{-\sigma - A_{11}}{A_{12}}$$

and:

$$\beta = \frac{\omega}{A_{12}}$$

The transfer function for the system presented in (4.2) and (4.3) is:

$$\frac{R}{LCRs^2 + Ls + R}$$

with roots at $\sigma \pm j\omega$, thus $\sigma = \frac{1}{2RC}$ and $\omega = \sqrt{\frac{1}{LC} - \sigma^2}$. Because a PID controller is used in this work, the dimensions of the state space increase by 1 due to the integral action. A new state variable v_i is introduced and the buck converter circuit illustrated in Figure 4.1 is modelled with:

$$A = A_{on} = A_{off} = \begin{bmatrix} -\sigma & \omega & 0 \\ -\omega & -\sigma & 0 \\ K_I & 0 & 0 \end{bmatrix}$$

$$B_{on} = \begin{bmatrix} 0 \\ \delta_{in} \\ -K_I \end{bmatrix}, B_{off} = \begin{bmatrix} 0 \\ 0 \\ -K_I \end{bmatrix}$$

$$x(t) = \begin{bmatrix} v_o \\ u \\ v_i \end{bmatrix}, x_{in} = \begin{bmatrix} 0 \\ V_{in} \\ V_{ref} \end{bmatrix}, \delta_{in} = \frac{\omega^2 + \sigma^2}{\omega}$$

A PID controller has 3 control variables; K_P, K_I and K_D. The proportional component depends only on the error signal. The proportional gain, K_P, determines the ratio of the output response to the error signal. The integral component sums the

error term over time. The result is that even a small error will cause the integral component to slowly increase. The integral component will continue to increase until the steady-state error is zero. The derivative component causes the output to decrease if the process variable is increasing rapidly. The derivative response is proportional to the rate of change of the process variable. Increasing the derivative component will increase the speed of the overall system. As discussed in Section 3.2, the control signal is compared to a ramp signal to generate the duty cycle. The switching manifold $h(x,t)$ is given by:

$$\begin{aligned} h(x,t) &= v_{con} - v_{ramp} \\ h(x,t) &= K_P v_e + K_I \int_0^t v_e d\tau + K_D \frac{d}{dt}(v_e) - (V_L + (V_U - V_L)\, t \bmod T) \\ h(x,t) &= K_P (v_o - V_{ref}) + v_i + K_D (-\sigma v_o + \omega u) - V_L - (V_U - V_L)\, t \bmod T \end{aligned} \tag{4.4}$$

4.2.2 Transient response and stability issues

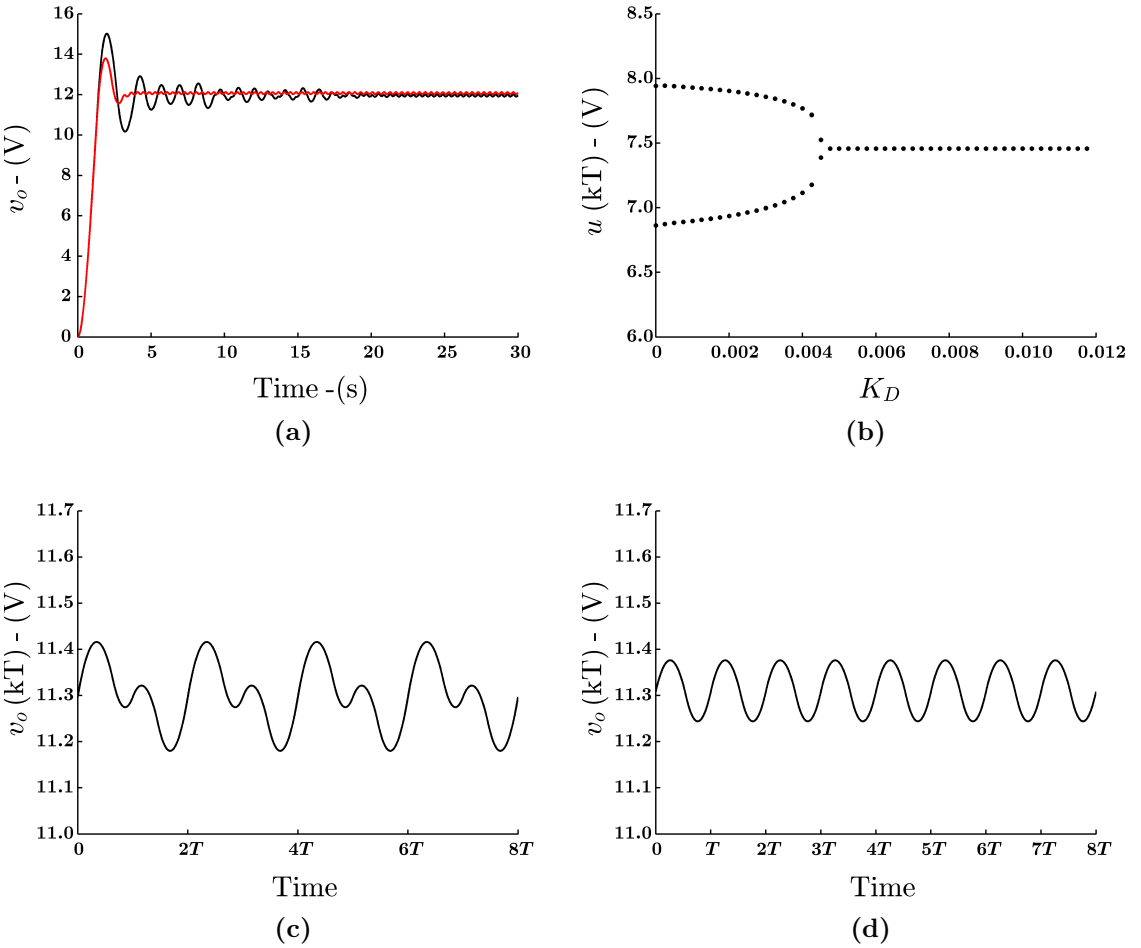

Figure 4.2: (a) Transient response comparisons $K_D = 0$ (black) and $K_D = 0.001$ (red). (b) Bifurcation diagram - K_D (c) Period-2 orbit with $K_D = 0$ (d) Period-1 orbit with $K_D = 0.01$.

As has been mentioned, the usage of the D-term is usually avoided when a fast response is not a major requirement as the D-term is sensitive to noise. On the other hand, when it is employed it can greatly improve the transient behaviour and stability margin of a system. In order to demonstrate its effects on the transient behavior of a system, it is shown that a buck converter with the parameters given in Figure 4.1, has a superior performance when the D-term is included. Figure 4.2 (a) shows the transient performance of the buck converter when the D-term is included (red) and when it is not included (black). It is clear that when the D-term is included, the settling time and overshoot are greatly reduced. However, because of the aforementioned problems, the inclusion of the D-term must be done with great caution.

A common type of instability in power electronic converters is the period-doubling bifurcation. This can greatly downgrade the efficiency and performance of the converter as it almost doubles the current ripple. This instability cannot be detected by conventional methodologies, like Bode plots, and therefore, another approach needs to be taken. In order to fully understand the effect the D-term has on the stability of the converter, all of the components of the control strategy that is employed must carefully be examined. The main components of the PID controller are the gains K_P, K_I and K_D as well as the values from the ramp comparator V_L and V_U. Figure 4.2 (b) shows the bifurcation diagram with the state variable u sampled once per switching cycle as the K_D term is varied. For low values of K_D, the system operates with a period-2 orbit. This is clear from Figure 4.2 (c), where the steady-state response of the system with $K_D = 0$ is shown. The output voltage repeats every $2T$. However, at $K_D = 0.005$ a bifurcation takes place. For values of $K_D > 0.005$, the system operates with a period-1 orbit as illustrated in Figure 4.2 (d), which shows that the output voltage has the same period as the ramp signal with $K_D = 0.01$. Thus, it is clear that the inclusion of the D-term is beneficial as it increases the stability margin of the system.

To further investigate the effect that the D-term has on the stability of the system, Figure 4.3 shows the bifurcation diagrams with K_P, V_U and V_L as the bifurcation variables for both $K_D = 0$ and $K_D \neq 0$. For the K_P bifurcation diagram, the ramp characteristics are fixed at $V_L = 3.8\,V$ and $V_U = 8.2\,V$ and (a) $K_D = 0$ and (b) $K_D = 0.004$. As expected in both cases, as the K_P term is increased, the system moves from a period-1 orbit to a period-2 orbit through a smooth period-doubling bifurcation. It is clear from these figures that the system is more stable with $K_D > 0$. A similar picture is revealed when V_U and V_L are altered, the bifurcation diagrams with $K_D = 0$ (c) and (e) and $K_D = 0.006$ (d) and (f) are shown, with V_U and V_L as the parameters of interest, respectively. By increasing the difference $V_U - V_L$, a similar behaviour as decreasing the value of K_P is observed i.e. a high $V_U - V_L$ difference is similar to a small K_P value. Figure 4.3 (c) shows the bifurcation diagram

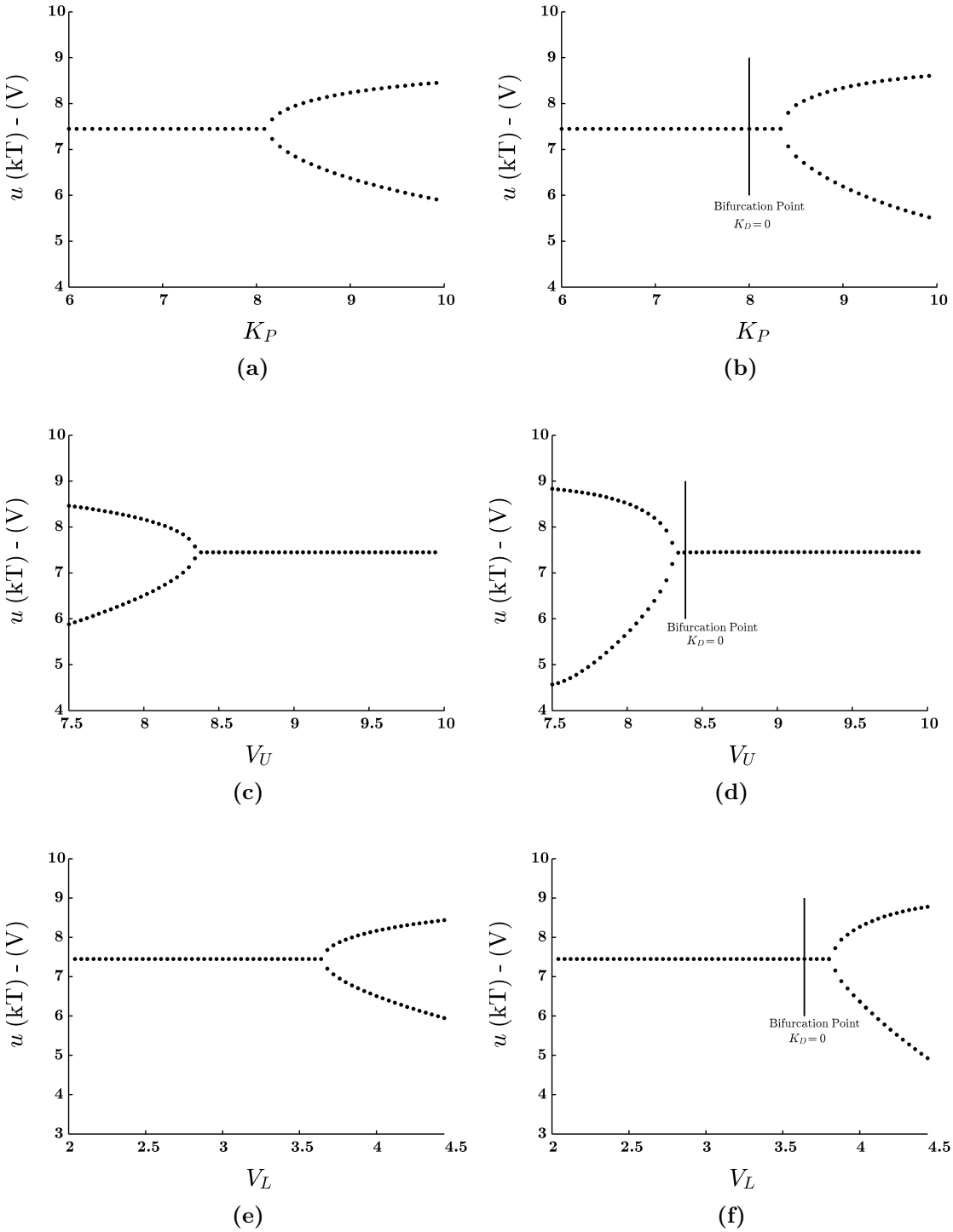

Figure 4.3: Bifurcation diagrams for (a) K_P with $K_D = 0$ (b) K_P with $K_D = 0.004$ (c) V_U with $K_D = 0$ (d) V_U with $K_D = 0.006$ (e) V_L with $K_D = 0$ (f) V_L with $K_D = 0.006$

with V_U as the bifurcation parameter. For low values of V_U, the system operates with a period-2 orbit. The $V_U - V_L$ difference is small and similar dynamics are seen for high K_P values. As V_U increases, the $V_U - V_L$ difference also increases and the system moves through a smooth period-doubling bifurcation. Similar dynamics are seen as the K_P value decreases. Figure 4.3 (e) and (f) shows the bifurcation diagrams of V_L when K_D is and is not included, respectively. Comparable results are seen but for V_L decreasing. In all three cases, the stability margin increases when K_D is included.

The aim when tuning a PID controller used in dc-dc converters is typically to achieve:

1. Zero steady-state error
2. Fast-transient behaviour
3. Low overshoot
4. Low current ripple
5. Keep the D-term as low as possible

The converter has 0 poles at the origin and is termed a type-0 system. Thus, the zero steady-state error is achieved with any value of the integral term K_I. The K_P and K_D term can be set using frequency-response methods, but it is important to ensure that the current ripple is as low as possible. To achieve this, either the K_P is decreased and the settling time is increased or K_D is increased which amplifies any noise problems. Therefore, K_D must be set to the minimum value that will not cause any serious noise problems while at the same time will force the system to operate in a stable region away from period-doubling bifurcations. This is the focus of this section of the thesis; to perform stability analysis that is required to capture the onset of a period-doubling bifurcation and through that analysis to identify the most suitable K_D value.

4.3 Stability analysis and controller tuning

In order to select the D-term to avoid period-doubling bifurcations, the value of K_D at which they occur must be predicted. This value is termed the critical K_D value or $K_{D_{CRIT}}$. It must be noted that PID controllers in power electronics are digitally implemented in order to use specifically designed filters. Therefore, the effect of the analog to digital conversion (A/D) conversion must be taken into account. Having said that, when a suitably chosen high clock frequency is employed, when compared with the system's bandwidth, the influence of the digital implementation is negligible. The analogue model can be used instead, for example [62].

4.3.1 Application of Filippov's method

The Filippov method relates events before and after switching thus, enabling dynamical analysis of systems with a set of discontinuous state space equations. The Saltation matrix, S, is given by [60]:

$$S = I + \left. \frac{(f_+ - f_-)\, n^T}{n^T f_- + \frac{\partial h}{\partial t}} \right| \begin{array}{l} t = t_\Sigma \\ \boldsymbol{x}(t) = \boldsymbol{x}(t_\Sigma) \end{array} \tag{4.5}$$

with f_- and f_+ being the right hand side of (4.1) before and after switching, $h(x,t)$ is the switching surface defined in (4.4) and n is the normal to the switching surface h. The vector fields that govern the buck converter are:

$$f_+ = \begin{bmatrix} -\sigma v_\Sigma + \omega u_\Sigma \\ -\omega v_\Sigma - \sigma u_\Sigma + \delta_{in} V_{in} \\ K_I\,(v_\Sigma - V_{ref}) \end{bmatrix} \;,\; f_- = \begin{bmatrix} -\sigma v_\Sigma + \omega u_\Sigma \\ -\omega v_\Sigma - \sigma u_\Sigma \\ K_I\,(v_\Sigma - V_{ref}) \end{bmatrix}$$

Using (4.4), the expression of the function h, it is possible to determine the normal vector to the manifold as well as its partial derivative with respect to time at $t = \bar{d}T$, where $\bar{d} = (1-d)$:

$$n = \begin{bmatrix} \frac{\partial h}{\partial v_o} \\ \frac{\partial h}{\partial u} \\ \frac{\partial h}{\partial v_i} \end{bmatrix} = \begin{bmatrix} K_P - \sigma K_D \\ \omega K_D \\ 1 \end{bmatrix} \;,\; \frac{\partial h}{\partial t} = -\frac{1}{T}\,(V_U - V_L)$$

This gives the following:

$$\begin{aligned}
(f_+ - f_-)n^T &= \begin{bmatrix} 0 \\ \delta_{in} V_{in} \\ 0 \end{bmatrix} \begin{bmatrix} K_P - \sigma K_D & \omega K_D & 1 \end{bmatrix} \\
&= \begin{bmatrix} 0 & 0 & 0 \\ \delta_{in} V_{in}\,(K_P - \sigma K_D) & \delta_{in} V_{in} \omega K_D & \delta_{in} V_{in} \\ 0 & 0 & 0 \end{bmatrix} \\
n^T f_- + \frac{\partial h}{\partial t} &= \begin{bmatrix} K_P - \sigma K_D & \omega K_D & 1 \end{bmatrix} \begin{bmatrix} -\sigma v_\Sigma + \omega u_\Sigma \\ -\omega v_\Sigma - \sigma u_\Sigma \\ K_I\,(v_\Sigma - V_{ref}) \end{bmatrix} - \frac{1}{T}\,(V_U - V_L) \\
&= K_P\,(-\sigma v_\Sigma + \omega u_\Sigma) + K_I\,(v_\Sigma - V_{ref}) \\
&\quad + K_D\left[\left(\sigma^2 - \omega^2\right) v_\Sigma - 2\sigma\omega u_\Sigma\right] - \frac{1}{T}\,(V_U - V_L)
\end{aligned}$$

For brevity, let $x_C = K_P\left(-\sigma v_\Sigma + \omega u_\Sigma\right) + K_I\left(v_\Sigma - V_{ref}\right) + K_D\left[\left(\sigma^2 - \omega^2\right)v_\Sigma - 2\sigma\omega u_\Sigma\right] - \frac{1}{T}\left(V_U - V_L\right)$. Thus, the Saltation matrix at $\bar{dT}$, is:

$$S_1 = \begin{bmatrix} 1 & 0 & 0 \\ S_{21} & 1 + S_{22} & S_{23} \\ 0 & 0 & 1 \end{bmatrix} \tag{4.6}$$

where

$$S_{21} = \frac{\delta_{in} V_{in}\left(K_P - \sigma K_D\right)}{x_C}\ ,\ S_{22} = \frac{\delta_{in} V_{in}\omega K_D}{x_C}\ ,\ S_{23} = \frac{\delta_{in} V_{in}}{x_C} \tag{4.7}$$

The second switching point occurs at the falling edge of the ramp signal, thus $\partial h/\partial t$ approaches ∞. Hence, S_2 is the identity matrix with the same dimension as S_1. The overall Monodromy matrix is:

$$\Phi_M(T, 0) = e^{A(1-\bar{d})T} S_1 e^{A\bar{d}T} \tag{4.8}$$

where the exponential matrix is given by:

$$e^{AT} = e^{-\sigma T}\begin{bmatrix} \cos\left(\omega T\right) & \sin\left(\omega T\right) & 0 \\ -\sin\left(\omega T\right) & \cos\left(\omega T\right) & 0 \\ K_I Y_I & K_I Y_2 & e^{\sigma T} \end{bmatrix}$$

with

$$Y_1 = \frac{\sigma e^{\sigma T} - \sigma\cos\left(\omega T\right) + \omega\sin\left(\omega T\right)}{\sigma^2 + \omega^2}\ ,\ Y_2 = \frac{\omega e^{\sigma T} - \sigma\sin\left(\omega T\right) - \omega\cos\left(\omega T\right)}{\sigma^2 + \omega^2}$$

Obviously, for the calculation of the Monodromy matrix, the duty cycle and the value of the state vector at $t = \bar{dT}$ are required. The analytical expression of the solution of a linear ODE $\dot{x}(t) = Ax(t) + Bu$ is as follows:

$$x(t) = e^{A(t-t_0)}x(t_0) + \int_{t_0}^{t} e^{A(t-\tau)}Bud\tau \tag{4.9}$$

Using (4.9), the state vector at time $t = \bar{dT}$ and $t = T$ can be found:

$$x\left(\bar{dT}\right) = \Phi_{off}\left(\bar{dT}, 0\right)x\left(0\right) + I_{off}\left(\bar{dT}\right) \tag{4.10}$$

$$x(T) = \Phi_{on}\left(T, \bar{dT}\right)x\left(\bar{dT}\right) + I_{on}\left(T\right) \tag{4.11}$$

where:

$$I_{off}\left(\bar{dT}\right) = \int_{0}^{\bar{dT}} e^{A(\bar{dT}-\tau)}B_{off}x_{in}d\tau$$

$$I_{on}\left(T\right) = \int_{\bar{d}T}^{T} e^{A(T-\tau)} B_{on} x_{in} d\tau$$

$$\Phi_{off}\left(\bar{d}T, 0\right) = e^{A\bar{d}T} \text{ and } \Phi_{on}\left(T, \bar{d}T\right) = e^{A(1-\bar{d})T}$$

Using the Newton-Raphson method, the duty cycle and switching points can be found [63].

4.3.2 Proposed design strategy

The characteristic equation of the Monodromy matrix (denoted by Φ_M instead of $\Phi_M\left(T, 0\right)$ for brevity) is given by [64]:

$$-\lambda^3 + \mathrm{tr}\left(\Phi_M\right)\lambda^2 - 0.5\left(\mathrm{tr}\left(\Phi_M\right)^2 - \mathrm{tr}\left({\Phi_M}^2\right)\right)\lambda + \det\left(\Phi_M\right) \tag{4.12}$$

where tr and det are the trace and determinant of the matrix, respectively, which are:

$$\det\left(\Phi_M\right) = e^{-2\sigma T} + e^{-2\sigma T} S_{22} \tag{4.13}$$

$$\mathrm{tr}\left(\Phi_M\right) = e^{-\sigma T}\left(2\cos\left(\omega T\right) + S_{21}\sin\left(\omega T\right) + S_{22}\cos\left(\omega T\right) + S_{23} K_I Y_2\right) + 1 \tag{4.14}$$

Thus, the coefficient of the λ term in (4.12) is:

$$e^{-\sigma T}\Bigg(2\cos\left(\omega T\right) + e^{-\sigma T} + S_{21}\sin\left(\omega T\right) + S_{22}\left(e^{-\sigma T} + \cos\left(\omega T\right)\right) + S_{23}\left(e^{-\sigma T} K_I Y_2 \cos\left(\omega T\right) - e^{-\sigma T} K_I Y_1 \sin\left(\omega T\right)\right)\Bigg)$$

4.3.2.1 Saddle-node bifurcation

Even though the main focus of this work is to tune a PID controller to avoid fast-scale instabilities, it is important to ensure that other types of instabilities do not occur. Saddle-node bifurcations effectively change the operating point of the converter. This can be catastrophic in many applications and therefore, must be avoided at all costs. The system undergoes a saddle-node bifurcation when one of the eigenvalues is equal to +1. Setting $\lambda = +1$, (4.12) becomes:

$$-1 + \mathrm{tr}\left(\Phi_M\right) - 0.5\left(\mathrm{tr}\left(\Phi_M\right)^2 - \mathrm{tr}\left({\Phi_M}^2\right)\right) + \det\left(\Phi_M\right) = 0 \tag{4.15}$$

Evaluating(4.15), yields:

$$\begin{aligned} e^{-\sigma T} K_I S_{23} \left(e^{-\sigma T} Y_1 \sin(\omega T) + Y_2 \left(1 - e^{-\sigma T} \cos(\omega T) \right) \right) = 0 \\ e^{-\sigma T} Y_1 \sin(\omega T) + Y_2 \left(1 - e^{-\sigma T} \cos(\omega T) \right) = 0 \end{aligned} \tag{4.16}$$

Since (4.16) contains no terms that depend on the controller parameters, i.e. K_P,K_I and K_D, the controller has no effect on the occurrence of saddle-node bifurcations.

4.3.2.2 Period-doubling bifurcation

The system undergoes a period-doubling bifurcation when one of the eigenvalues is equal to -1. Setting $\lambda = -1$ in (4.12) yields:

$$1 + \operatorname{tr}(\Phi_M) + 0.5 \left(\operatorname{tr}(\Phi_M)^2 - \operatorname{tr}\left({\Phi_M}^2 \right) \right) + \det(\Phi_M) = 0 \tag{4.17}$$

Evaluating (4.17):

$$\begin{aligned} c_1 + e^{-\sigma T} \Big[& 2 \sin(\omega T) S_{21} + \\ & \left(2e^{-\sigma T} + 2 \cos(\omega T) \right) S_{22} + \\ & \left(\left(1 + e^{-\sigma T} \right) K_I Y_2 \cos(\omega T) - e^{-\sigma T} K_I Y_1 \sin(\omega T) \right) S_{23} \Big] = 0 \end{aligned}$$

where $c_1 = 2 + e^{-\sigma T} \left(4 \cos(\omega T) + 2e^{-\sigma T} \right)$. Using (4.7):

$$\begin{aligned} x_C c_1 + e^{-\sigma T} \Big[& 2 \sin(\omega T) \delta_{in} V_{in} (K_P - \sigma K_D) + \\ & \left(2e^{-\sigma T} + 2 \cos(\omega T) \right) \delta_{in} V_{in} \omega K_D + \\ & \left(\left(1 + e^{-\sigma T} \right) K_I Y_2 \cos(\omega T) - e^{-\sigma T} K_I Y_1 \sin(\omega T) \right) \delta_{in} V_{in} \Big] = 0 \end{aligned}$$

Grouping the terms dependent on K_P, K_I, K_D, V_U and V_L:

$$P K_P + D K_D + I K_I + C(V_U - V_L) = 0 \tag{4.18}$$

where

$$\begin{aligned} P &= 2\delta_{in} V_{in} e^{-\sigma T} \sin(\omega T) + (-\sigma v_\Sigma + \omega u_\Sigma) c_1 \\ D &= \delta_{in} V_{in} e^{-\sigma T} \left(2\omega e^{-\sigma T} + 2\omega \cos(\omega T) - 2\sigma \sin(\omega T) \right) + \left(\left(\sigma^2 - \omega^2 \right) v_\Sigma - 2\sigma\omega u_\Sigma \right) c_1 \\ I &= \delta_{in} V_{in} e^{-\sigma T} \left(Y_2 + e^{-\sigma T} Y_2 \cos(\omega T) - e^{-\sigma T} Y_1 \sin(\omega T) \right) + (v_\Sigma - V_{ref}) c_1 \\ C &= -\frac{1}{T} c_1 \end{aligned}$$

Using (4.18), the specific closed form analytical expressions that describe the stability boundaries (assuming all other parameters are kept constant) are as follows:

$$V_{U_{CRIT}} = \frac{-K_P P - K_I I - K_D D + C V_L}{C} \tag{4.19}$$

$$V_{L_{CRIT}} = \frac{K_P P + K_I I + K_D D + C V_U}{C} \tag{4.20}$$

$$K_{D_{CRIT}} = \frac{-K_P P - K_I I - C\left(V_U - V_L\right)}{D} \tag{4.21}$$

From Figure 4.2 (b), a period-doubling bifurcation is seen at $K_D \backsimeq 0.0050$ and, from (4.21), the predicted bifurcation point is at $K_D = 0.0053$. Thus, the simulated and predicted results are in very good agreement. Similar results can be shown for other controller parameters.

4.3.2.3 Numerical example

Using the circuit parameters outlined in Figure 4.1, consider the case when $K_D = 0.000235$. From Figure 4.2 (b), it is clear that the system is unstable and is operating with a period-2 orbit. The switching points are given by:

$$\begin{bmatrix} v_\Sigma \\ u_\Sigma \\ v_{i_\Sigma} \end{bmatrix} = \begin{bmatrix} 11.2389 \\ 4.4793 \\ 6.6455 \end{bmatrix}$$

and $\bar{d} = 0.4577$. Thus, the Saltation matrix is found using (4.6) and gives:

$$S_1 = \begin{bmatrix} 1 & 0 & 0 \\ -9.7246 & 0.7487 & -1.1736 \\ 0 & 0 & 1 \end{bmatrix}$$

The Monodromy matrix is found using (4.8):

$$\Phi_M = \begin{bmatrix} -0.7754 & -0.0076 & -0.2075 \\ -8.0112 & -0.7349 & -1.0361 \\ 0.0018 & 0.0003 & 0.9998 \end{bmatrix}$$

and gives eigenvalues at:

$$\lambda = \begin{bmatrix} -1.0027 \\ -0.5074 \\ 0.9995 \end{bmatrix}$$

Since one of the eigenvalues is outside the unit circle, $\lambda_1 = -1.0027$, the system is unstable. Hence, the output is period-2. It is important to note that while $\lambda_3 = 0.995$, this is very close to $+1$ and is the contributed by the integrator in

the controller. This term is dominated by the integral term and it should not be considered when estimating the stability margin [60].

Now consider the case where $K_D = 0.01$. From Figure 4.2 (b), the system operates with a period-1 orbit and is stable. Following the same procedure as above, the switching points are:

$$\begin{bmatrix} v_\Sigma \\ u_\Sigma \\ v_{i_\Sigma} \end{bmatrix} = \begin{bmatrix} 11.2874 \\ 4.5533 \\ 19.4161 \end{bmatrix}$$

and $\bar{d} = 0.4577$. Thus, the Saltation matrix is found using (4.6) and gives:

$$S_1 = \begin{bmatrix} 1 & 0 & 0 \\ -0.8040 & -1.0551 & -0.2256 \\ 0 & 0 & 1 \end{bmatrix}$$

The Monodromy matrix is found using (4.8):

$$\Phi_M = \begin{bmatrix} 0.7185 & 0 & -0.0339 \\ -0.6034 & -0.9972 & -0.2039 \\ 0.0035 & 0.0004 & 1 \end{bmatrix}$$

and gives eigenvalues at:

$$\lambda = \begin{bmatrix} -0.9972 \\ -0.7190 \\ 0.9995 \end{bmatrix}$$

Since all of the eigenvalues lie inside the unit circle, the system is stable.

The duty cycle and state vector were calculated using the Newton-Raphson method with the tolerance set to 13 decimal places. The critical K_D term was calculated to 6 decimal places. Using Matlab® R2013a [65] with a 1.5 (GHz) Intel® i3 processor, the script took 16 (s) to determine the critical K_D value and the eigenvalues when $K_D = 0.000235$ and $K_D = 0.01$. At present fast-scale instabilities are checked by extensive simulations or experimentation over a large parameter range [60]. The proposed method allows for an accurate prediction of when fast-scale instabilities will occur in a more efficient manner. Similar methods are used in the proceeding work.

4.3.2.4 Controller design

(4.21) can be used in controller design to avoid fast-scale instabilities. The steps to tune the controller are as follows:

1. Tune the value of K_P and K_I using standard linear control theory e.g. Bode plots.

2. Check if the converter requires a better transient performance or if the current/voltage ripple is higher than expected.

   a) If the answer is no, the D-term is not required.

   b) If the answer is yes, the D-term is required and the designer should proceed to step 3.

3. A faster transient response or a less oscillatory response is required. Thus, the D-term should now be included and be tuned using (4.21) or using a figure similar to Figure 4.4. Selecting a value higher than that given by (4.21) will lead to a stable system with the desired response.

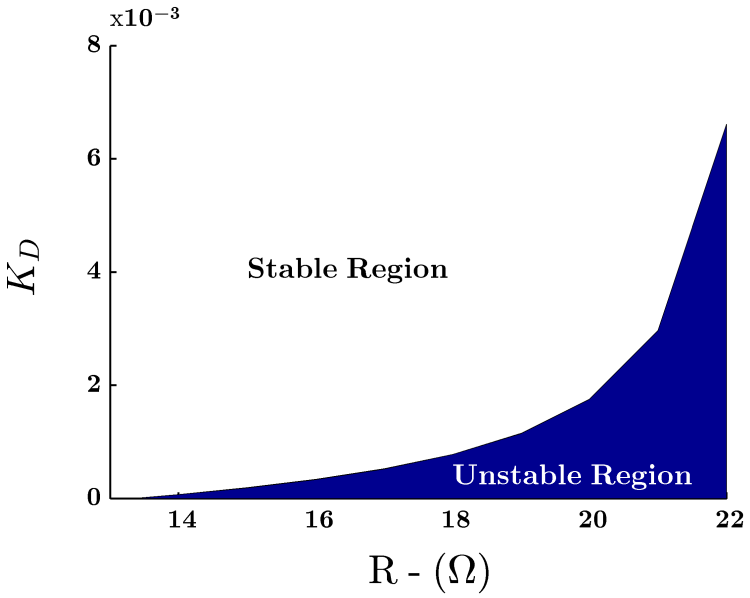

Figure 4.4: Values of K_D at which period-doubling bifurcations occur as R varies.

Figure 4.4 shows the critical K_D value as the load resistance varies. When K_D is in the shaded region, the system is unstable. This can be used by a designer in order to properly tune the PID controller. For example, using the parameters given in Figure 4.1, the nominal output load is 22 Ω. Thus, in order to guarantee stability, the D-term must be set so $K_D > 0.0053$. On the other hand, if the load resistance is varying between 16 Ω to 22 Ω, then in order to ensure stability, $K_D > 0.0053$ even if the system only spends a fraction of time at 22 Ω and the majority of its time at 16 Ω. In this scenario, the K_D value is unnecessarily high for large portions of time and puts the system at risk to amplification of noise. Ideally, a method of changing the D-term as the load varies in such a way as to retain the benefits of PID control and at the same time guaranteeing a stable response is required. In the next section an adaptive PID controller that constantly monitors the changes in the supply voltage and output load and updates the K_D term appropriately is proposed.

4.4 Adaptive PID controller

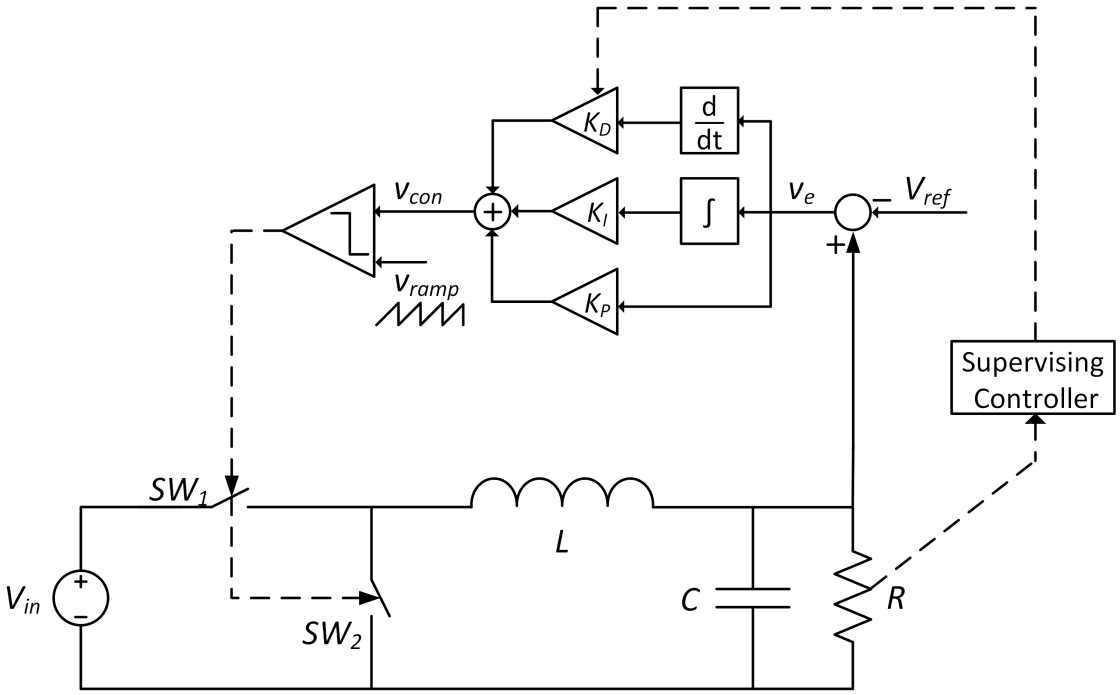

Figure 4.5: Adaptive PID control scheme

In the previous section, the Monodromy matrix was calculated and Floquet multipliers were derived as a function of the controller parameters (4.19)-(4.21). These results allow the proper tuning of the PID controller to avoid fast-scale instabilities. In cases where the parameters are fixed, (4.21) or Figure 4.4 can be used to tune the controller in order to have satisfactory operation. In cases where the parameters are not fixed, e.g. varying load resistance, supply voltage, one option is to tune for the worst-case scenario. For example, if the output load varies between $14 - 22\,\Omega$, a K_D term can be selected that will give a stable period-1 response for all resistance values. In this case, $22\,\Omega$ has the highest $K_{D_{CRIT}}$ value at 0.0053 (as explained in the previous section). This will ensure stability across the entire operating range. However, if the system only spends a fraction of time at $22\,\Omega$, it is a lot better if the D-term can be varied according to the value of the load resistance as this retains the benefits of using the K_D term while minimizing the amplification of noise. Thus, using (4.21) the adaptive PID controller can be tuned.

Figure 4.5 illustrates the proposed control scheme where the input voltage and load resistance are monitored using estimators [66, 67, 68] and then the K_D term is adjusted accordingly. The function of the supervising controller is to update the K_D term and ensures reliable period-1 orbits while maintaining the advantages of the D-term. For practical applications, it may be desirable to perform off-board calculations using (4.21) to develop a look-up table for the supervising controller. Table 4.1[1] shows a sample look-up table for a buck converter, with parameters out-

[1] In order to guarantee robustness, (4.21) was multiplied by 1.25.

lined in Figure 4.1, where R and V_{in} may vary. The values of R and V_{in} were selected to demonstrate that as R and V_{in} increase, the critical K_D value also increases. Since a $1\,(\Omega)$ range for R is given in the table, the D-term is tuned for the worst-case scenario e.g. in the $13-14\,(\Omega)$ range, the D-term is tuned to ensure stability when $R = 14\,(\Omega)$.

$V_{in}\,(V)/R\,(\Omega)$	$13-14$	$15-16$	$17-18$	$19-20$	$21-22$
24.6	0	0	0.00010	0.00036	0.00077
24.7	0	0.00002	0.00020	0.00005	0.00108
24.8	0	0.00013	0.00045	0.00097	0.00217
24.9	0	0.00027	0.00068	0.00147	0.00383
25.0	0.00009	0.00042	0.00097	0.00220	0.00830

Table 4.1: Sample look-up table for the supervising controller

Consider a buck converter system where the output load varies with time causing the system to slip in and out of stability. Figure 4.6 (b) shows a stable period-1 orbit for $R = 16\,\Omega$ with K_D set to 0.00042 and $V_{in} = 25$ (V). The system is operating as desired. However, R increases to $17\,\Omega$. If the D-term is not updated, this causes the system to lose stability through a period-doubling bifurcation as shown in Figure 4.6 (c) where the output is a period-2 orbit. However, if a supervising controller which updates the D-term to take this change into account is present, the period-1 orbit can be re-established. Figure 4.6 (d) shows the output when the supervising controller is active and updates K_D to 0.00097. It is clear that the inclusion of the supervising controller using (4.21) can be used to ensure stability over a wide operating region.

Figure 4.6 (a) shows the transient response as R and K_D vary. Notice that even for small variations of the load resistance, $1\,\Omega$, the voltage ripple of the system increases when K_D is not updated. It then returns to its previous value when K_D is updated. A similar response is seen when the supply voltage is varied thus demonstrating the effectiveness of the controller.

4.5 Application to discontinuous switching manifold

In the previous sections, the proper tuning of a PID controller for a VMC buck converter was thoroughly presented. This was achieved by considering the Saltation matrix. The switching condition was described by the smooth function $h(x,t)$. The smoothness of h is required as the Filippov method (4.5) uses its derivative with respect to the state vector, $\partial h/\partial x$. However, the smoothness of h cannot be guaranteed when other converter topologies are used. For example, when a PID controller is applied to a CMC buck converter, the inclusion of the $\partial i/\partial t$ term

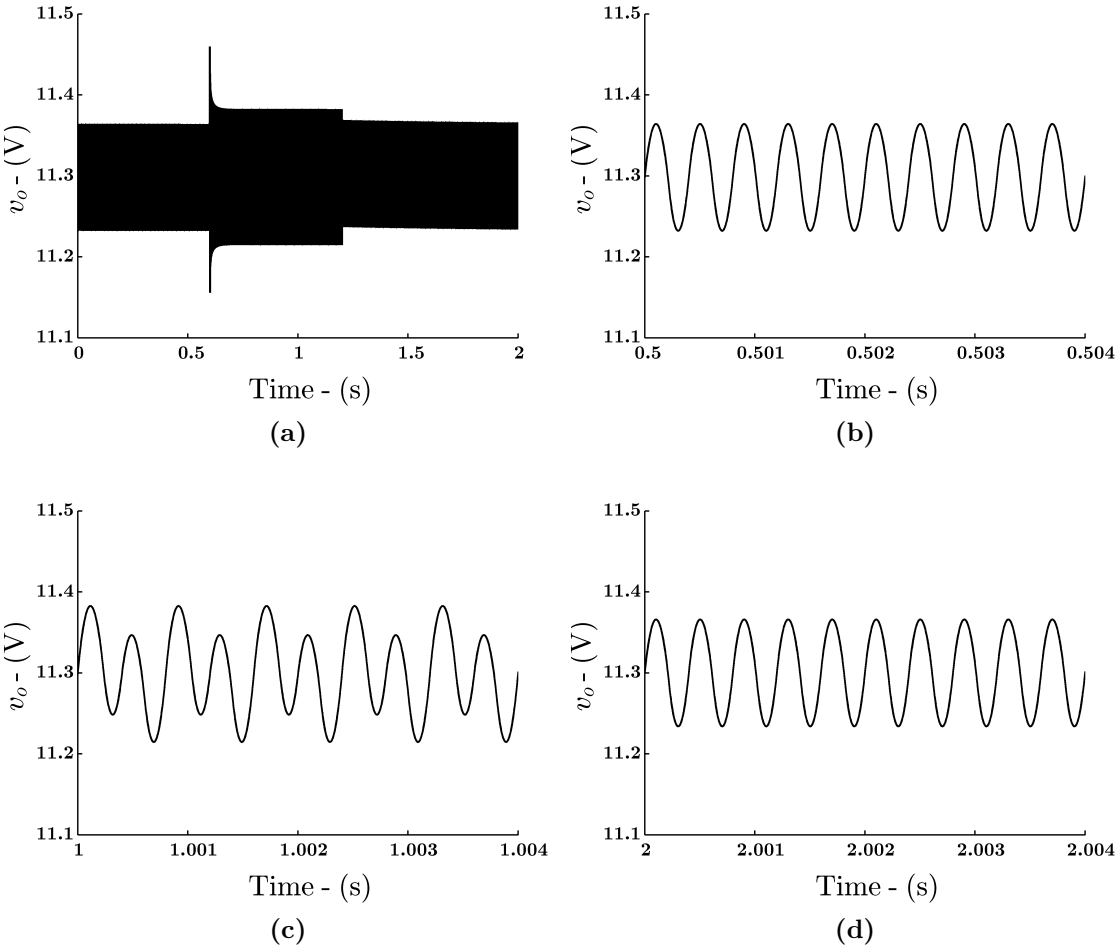

Figure 4.6: Application of adaptive PID control with step change in the load resistance (a) Transient response (b) Period-1 orbit with $R = 16\,\Omega$, $K_D = 0.00042$ (c) Period-2 orbit with $R = 17\,\Omega$, $K_D = 0.00042$ (d) Period-1 orbit with $R = 17\,\Omega$, $K_D = 0.00097$.

creates a discontinuous function. Another case where this can be observed is the VMC boost converter when a PID controller is used. This causes an added difficulty for the method proposed for the proper tuning of a PID controller. Thus, the issue of non-smoothness and the application of the proposed control strategy are investigated in this section.

4.5.1 Boost converter model

The circuit diagram for the boost converter is shown in Figure 4.7 (a). The boost converter is a step-up dc-dc converter used to convert an input voltage, V_{in}, to a higher output voltage, v_o. The switch, SW, is closed at the start of the switching period for a time dT and then opens and remains open for the remainder of the switching period $(1 - d)T$. The boost converter with a PID controller is described by the equations:

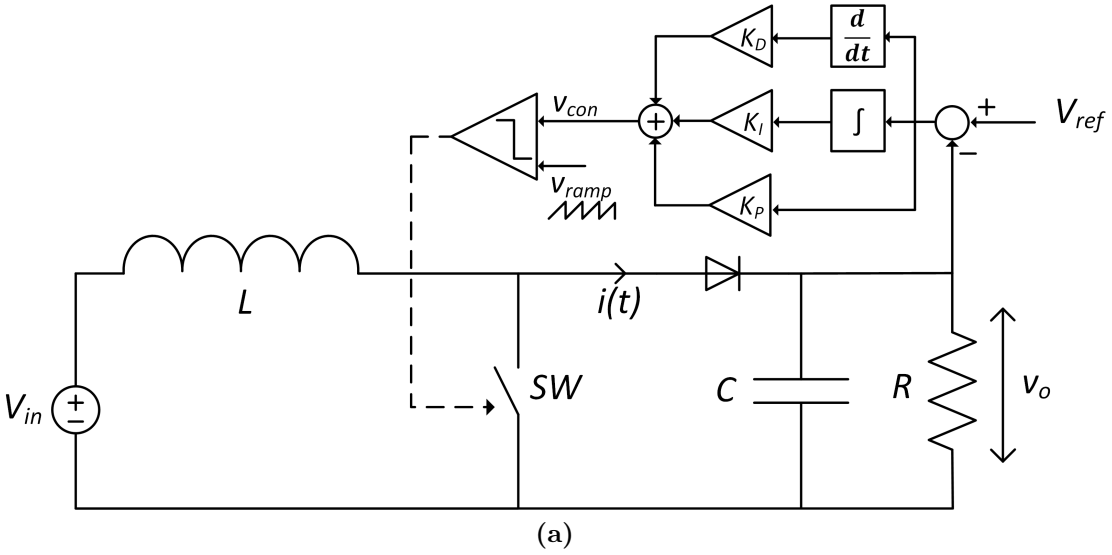

(a)

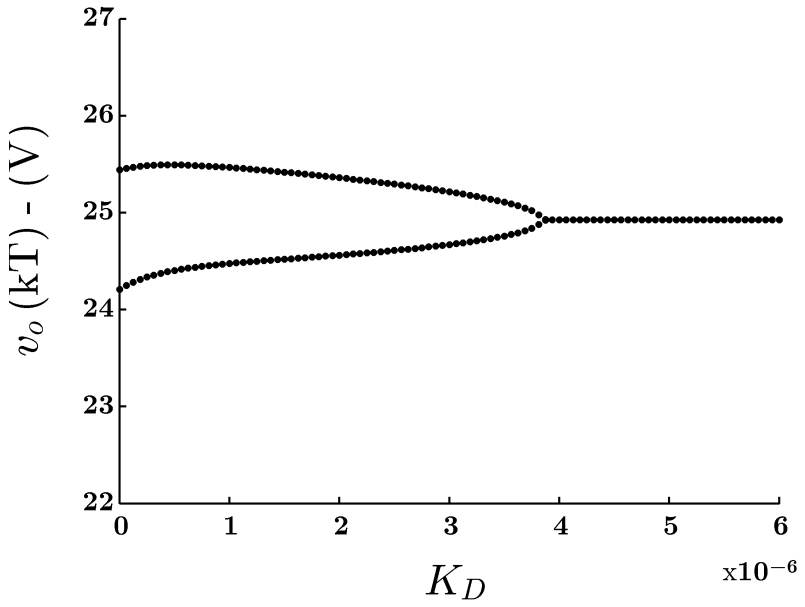

(b)

Figure 4.7: (a) VMC boost converter with a PID controller circuit diagram (b) Bifurcation diagram with K_D as the bifurcation variable with circuit parameters $V_{in} = 16\,V$, $L = 208\,\mu H$, $C = 222\,\mu F$, $R = 12.5\,\Omega$, $V_{ref} = 25\,V$, $V_L = 0$, $V_U = 1$, $K_P = 0.075$, $K_I = 0.01$ and $T = 333\,\mu s$.

$$\dot{x} = \begin{cases} f_{on}(x,t) = & A_{on}x + B_{on}x_{in} & SW_1 \text{ is on and } i > 0 \\ f_{off}(x,t) = & A_{off}\boldsymbol{x} + B_{off}x_{in} & SW_1 \text{ is off and } i > 0 \\ f_{dcm}(x,t) = & A_{dcm}x + B_{dcm}x_{in} & SW_1 \text{ is off and } i = 0 \end{cases} \tag{4.22}$$

where

$$A_{on} \begin{bmatrix} -\frac{1}{RC} & 0 & 0 \\ 0 & 0 & 0 \\ -K_I & 0 & 0 \end{bmatrix}, \; A_{off} = \begin{bmatrix} -\frac{1}{RC} & \frac{1}{C} & 0 \\ -\frac{1}{L} & 0 & 0 \\ -K_I & 0 & 0 \end{bmatrix}, \; A_{dcm} = \begin{bmatrix} -\frac{1}{RC} & 0 & 0 \\ 0 & 0 & 0 \\ -K_I & 0 & 0 \end{bmatrix}$$

$$B_{on} = B_{off} = \begin{bmatrix} 0 \\ \frac{1}{L} \\ K_I \end{bmatrix}, \; B_{dcm} = \begin{bmatrix} 0 \\ 0 \\ K_I \end{bmatrix}$$

$$x(t) = \begin{bmatrix} v_o & i & v_i \end{bmatrix}^T, \; x_{in} = \begin{bmatrix} 0 & V_{in} & V_{ref} \end{bmatrix}^T.$$

The circuit spends $d_{on}T$ operating in the ON-topology, $d_{off}T$ operating in the OFF-topology and $d_{dcm}T$ operating in the DCM-topology, where $d_{on} + d_{off} + d_{dcm} = 1$. The opening and closing of SW is determined by comparing the control signal to the ramp signal. When the control signal is greater than the ramp signal, SW is closed and the circuit is modelled with the ON-topology. When the control signal is less than the ramp signal, SW is open and the circuit is modelled with either the OFF-topology or the Discontinuous Conduction Mode (DCM) topology depending on whether $i > 0$. The control signal is given as

$$\begin{aligned} v_{co} =& K_P v_e + K_I \int_0^t v_e d\tau + K_D \frac{d}{dt}(v_e) \\ v_{co\_on} = v_{co\_dcm} =& K_P (V_{ref} - v_o) + v_i + K_D \left(\frac{1}{RC} v_o \right) \\ v_{co\_off} =& K_P (V_{ref} - v_o) + v_i + K_D \left(\frac{1}{RC} v_o - \frac{1}{C} i \right) \end{aligned}$$

The control signal is non-smooth as the derivative at the switching instant is undefined.

4.5.2 Application of the Filippov method

In order to investigate the effect of the non-smoothness of h, a boost converter with a PID controller is considered. Unlike the VMC buck converter, the switching manifold is given by a piece-wise function:

$$h(x,t) = \begin{cases} h_A(x,t), & x \, \epsilon \, G_A \\ h_B(x,t), & x \, \epsilon \, G_B \end{cases}$$

where $h(x,t)$ is smooth in the G_A and G_B region but is discontinuous when switching between the two regions at the border. As before, switching from $A \rightarrow B$ occurs when $h_A(x,t) = 0$ where t_Σ is the time instant when switching takes place. However, in this case $h_A(x,t) \neq h_B(x,t)$. Thus, when switching occurs $h_B(x,t_\Sigma) \neq 0$. Recall that in the derivation of the Filippov method in Section 2.6 and in (2.22), the Taylor series is used and the function $h_A(x,t)$ is expanded with respect to both time and state vectors at $t = t_\Sigma$ and $x = x(t_\Sigma)$. This is equated to zero because as the trajectory approaches the switching manifold in the state space $h(x,t_\Sigma) = h_A(x,t_\Sigma) = 0$. The Saltation matrix has the form:

$$S = I + \left. \frac{(f_+(\boldsymbol{x}(t),t) - f_-(\bar{\boldsymbol{x}}(t),t))\, n^T}{n^T f_-(\bar{\boldsymbol{x}}(t),t) + \frac{\partial h_A}{\partial t}} \right| \begin{array}{l} t = t_\Sigma \\ \boldsymbol{x}(t) = \boldsymbol{x}(t_\Sigma) \end{array} \tag{4.23}$$

$$n = \left. \frac{\partial h_A(x,t)}{\partial x} \right| \begin{array}{l} t = t_\Sigma \\ \boldsymbol{x}(t) = \boldsymbol{x}(t_\Sigma) \end{array}$$

For the boost converter with circuit parameters as in Figure 4.7, the topology order is as follows: ON $\rightarrow$OFF$\rightarrow$DCM. Thus, there are two switching conditions to consider occurring at $t_{\Sigma 1}$, $x_{\Sigma 1}$ and $t_{\Sigma 2}$, $x_{\Sigma 2}$. The switching condition from ON$\rightarrow$OFF is given as

$$h_1(x,t) = K_P\left(V_{ref} - v_o\right) + v_i + K_D\left(\frac{1}{RC} v_o\right) - v_{ramp}$$

In order the have DCM operation $i = 0$ and the switching manifold is given by:

$$h_2(x,t) = x_2 = i$$

The derivation of S_1 is:

$$f_+ = \begin{bmatrix} \frac{Ri_{\Sigma 1} - v_{\Sigma 1}}{RC} \\ \frac{V_{in} - v_{\Sigma 1}}{L} \\ K_I\left(V_{ref} - v_{\Sigma 1}\right) \end{bmatrix} \quad , \quad f_- = \begin{bmatrix} -\frac{v_{\Sigma 1}}{RC} \\ \frac{V_{in}}{L} \\ K_I\left(V_{ref} - v_{\Sigma 1}\right) \end{bmatrix}$$

$$n_1 = \begin{bmatrix} -K_P + K_D\left(\frac{1}{RC}\right) & 0 & 1 \end{bmatrix} \quad , \quad \frac{\partial h_1}{\partial t} = -\frac{1}{T}\left(V_U - V_L\right)$$

Using (4.6), S_1 is:

$$S_1 = \begin{bmatrix} 1 + \frac{i_{\Sigma 1}\left(-K_P + K_D\left(\frac{1}{RC}\right)\right)}{Cx_{B1}} & 0 & \frac{i_{\Sigma 1}}{Cx_{B1}} \\ -\frac{v_{\Sigma 1}}{Lx_{B1}}\left(-K_P + K_D\left(\frac{1}{RC}\right)\right) & 1 & -\frac{v_{\Sigma 1}}{Lx_{B1}} \\ 0 & 0 & 1 \end{bmatrix} \tag{4.24}$$

where $x_{B1} = K_I\left(V_{ref} - v_{\Sigma 1}\right) - \frac{v_{\Sigma 1}}{RC}\left(-K_P + K_D\left(\frac{1}{RC}\right)\right) - \frac{V_U - V_L}{T}$. At the second switching instant, i.e. OFF→DCM:

$$f_+ = \begin{bmatrix} -\frac{v_{\Sigma 2}}{RC} \\ 0 \\ K_I\left(V_{ref} - v_{\Sigma 2}\right) \end{bmatrix} \quad , \quad f_- = \begin{bmatrix} \frac{Ri_{\Sigma 2} - v_{\Sigma 2}}{RC} \\ \frac{V_{in} - v_{\Sigma 2}}{L} \\ K_I\left(V_{ref} - v_{\Sigma 2}\right) \end{bmatrix}$$

$$n_2 = \begin{bmatrix} 0 & 1 & 0 \end{bmatrix} \quad , \quad \frac{\partial h_2}{\partial t} = 0$$

The second Saltation matrix is:

$$S_2 = \begin{bmatrix} 1 & \frac{L}{C}\frac{i_\Sigma}{V_{in} - v_{\Sigma 2}} & 0 \\ 0 & 0 & 0 \\ 0 & 0 & 1 \end{bmatrix}$$

However, switching occurs when $i = 0$ thus, $i_\Sigma = 0$ and S_2 is

$$\begin{bmatrix} 1 & 0 & 0 \\ 0 & 0 & 0 \\ 0 & 0 & 1 \end{bmatrix} \tag{4.25}$$

The third switching point occurs at the falling edge of the ramp signal, thus $\partial h_3/\partial t = \infty$. Hence, S_3 is the identity matrix with the same dimension as S_1 and S_2. The overall Monodromy matrix is:

$$\Phi_M = S_3 \Phi_{dcm} S_2 \Phi_{off} S_1 \Phi_{on} \tag{4.26}$$

where

$$\Phi_{dcm} = e^{A_{dcm} d_{dcm} T} \quad , \quad \Phi_{off} = e^{A_{off} d_{off} T} \quad , \quad \Phi^{A_{on} d_{on} T}$$

The bifurcation diagram of the PID controlled boost converter is illustrated in Figure 4.7 (b). It is clear from this, that a period doubling bifurcation takes place at $K_D = 0.000003938$. In Table 4.2, the fixed point $x(0)$ and the corresponding Floquet multipliers which were calculated using (4.26) are shown. It is clear that as the value of K_D decreases, one of the Floquet multipliers moves closer to -1. Between $K_D = 0.0000039375$ and 0.0000038750, the eigenvalue crosses the unit circle at -1 and a period-doubling bifurcation takes place. Therefore, (4.23) is the correct expression for calculating the Saltation matrix when the switching manifold is given by a discontinuous function.

It is important to note, that the eigenvalue in Table 4.2 that is closest to $+1$ is as a result of the integrator in the controller and does not contribute to the system's stability [60]. Furthermore, the eigenvalue at 0 is owing to the fact that the system

K_Dx10^{-6}	$x(0)$	Eigenvalues
4.0625	$[24.9264 - 0.00000.1910]^T$	$[\ -0.9979 \quad 0 \quad 0.9999\ ]$
4.0000	$[24.9266 - 0.00000.1916]^T$	$[\ -0.9985 \quad 0 \quad 0.9999\ ]$
3.9375	$[24.9269 - 0.00000.1921]^T$	$[\ -0.9991 \quad 0 \quad 0.9999\ ]$
3.8750	$[24.9224 - 0.00000.1927]^T$	$[\ -1.0026 \quad 0 \quad 0.9999\ ]$
3.8125	$[24.8779 - 0.00000.1933]^T$	$[\ -1.0300 \quad 0 \quad 0.9999\ ]$
3.7500	$[24.8379 - 0.00000.1938]^T$	$[\ -1.0545 \quad 0 \quad 0.9999\ ]$

Table 4.2: Floquet multipliers of fixed point

is operating in DCM. Having established a method for the formation of the Saltation matrix, equation (4.26) can be used to find the eigenvalues of the system and thus, tune the K_D term of the controller. This can be used off-line when the parameters are fixed or in an adaptive controller, similar to Section 4.4, in the case when the parameters are not fixed.

4.6 Conclusions

This chapter examined the tuning of a PID controller used in dc-dc converters in order to guarantee a fast and stable response. The advantage and drawbacks of including the derivative term were clearly and thoroughly highlighted and studied. It was shown that the inclusion of the D-term not only improves the transient response but also increases the stability margin of the system. However, its inclusion increases the noise levels in systems and must be used with caution. Thus, design guidelines were developed to find its minimum value to retain the benefits of the D-term while minimising the amplification of noise. An adaptive controller was presented, which is used when the parameters of the converter are not fixed, that guarantees a fast and stable response.

The inclusion of the D-term in the mathematical analysis of converters where the function that describes the switching conditions is non-smooth required a modification of the formation of the Saltation matrix. This chapter presented a technique for this modification and verified is validity. This work detailed how the Filippov method can be used to derive the Saltation matrix with a non-smooth switching manifold.

5 Intermittent instability in power electronic converters

5.1 Introduction

Traditionally, analog controllers are employed to regulate circuits [9]. However, with advances in technology, digital control has become a viable alternative with many potential advantages which include their low power, immunity to analog component variations, compatibility with digital systems, faster design process and the possibility for more advanced control schemes [1]. Advanced control schemes enable converters to operate with higher efficiencies. Hence, digital state-feedback controllers are frequently used in dc-dc converters when high/optimal performance is required [69]. However, little work exists on the nonlinear dynamics of such converters. [69] and [70] both detail some of the possible nonlinear dynamics exhibited by such systems. However, this research assumes ideal operating conditions, which cannot be guaranteed in practical applications.

Intermittent operation can qualitatively be described as distributed periods of irregular motion such as bursts of unstable or chaotic operation separated by long periods of stable operation. It can arise in periodically driven nonlinear systems, where the frequency of the coupled signal is not consistent with the system's driving frequency. It occurs when a crucial parameter is being modulated by the coupling signal. Such intermittency has been observed in switch-mode power supplies which are not protected against spurious signals or where parasitic capacitances or inductances are present causing unwanted oscillations of the control signals [45]. The noise can also take the form of coupling along radiated paths on the same circuit board. These unwanted oscillations affect the efficiency of the system and thus, a better analysis of the nonlinear dynamics is required to provide design guidelines in order to eliminate this type of operation. Previous works have developed discrete maps to derive the Jacobian matrix for noise perturbed dc-dc converters [42, 45], these methods are algebraically complex and not suitable for tuning controller parameters in order to eliminate intermittency.

The aim of this research is to study the effect of noise on a buck converter with a digital state-feedback controller. Once the nonlinear behaviour exhibited by the

circuit has been characterised, the theoretical framework for stable period-1 operation is presented which enables designers to select control parameters in order to eliminate such unstable behaviour.

5.2 Survey of previous works

The intermittency route to chaos was first discovered by Manneville and Pomeau [41]. By considering the Lorenz model, presented in [2], the authors observed the system lose stability and give birth to a limit cycle for a short period of time. As one of the variables of the system was varied, the duration the limit cycle existed varied. Intermittent operation was first observed in dc-dc converters in [44] by considering a VMC buck converter with the ramp signal being perturbed by a disturbance signal. By considering a disturbance signal of both sinusoidal and rectangular waveforms, the output voltage was seen to go through distributed periods of irregular motion. As the strength of the interference signal increased, the duration of the unstable operation also increased. If the strength of the interference signal was sufficiently high, the output was chaotic. While no quantitative analysis of this work was performed, the author details at what signal strength intermittent operation is first observed and when the output is chaotic. From this, the author concludes that for high feedback gains or large input voltage, the system is more likely to exhibit intermittent operation.

Similar work was carried out in [43] for a CMC boost converter. Through the use of time-bifurcation diagrams, period-doubling bifurcations are observed as time varies. For sufficiently high intruding signal strengths, the system exhibits subharmonic and chaotic operation. Using discrete-maps, the author derives the eigenvalues of the system and the critical spurious signal strength at which period-doubling bifurcations first occur.

In [42], the author considers perturbing the control signal of a VMC buck converter with a sinusoidal disturbance signal. Three cases are considered that relates the frequency of the disturbance signal to the frequency of the external clock; rational ratios, irrational ratios and rational ratios close to the rational multiples. Quasi-periodic orbits are observed for irrational ratios. When the interference signal is a rational multiple of the external clock frequency, the system operates with an orbit equal to the denominator of the rational multiple. Intermittent operation is observed for the third case. In order to apply conventional bifurcation analysis techniques, the authors apply a transformation that relates changes in time to changes in another variable. This enables the derivation of an iterative discrete-time map and allows the examination of the movement of the eigenvalues of the system as the variable changes. Similar works are carried out in [45] where sinusoidal, triangu-

lar and sawtooth disturbance signals perturbing the input voltage, control voltage and reference voltage are considered. The authors also investigate the effect of two interference signals perturbing input voltage and reference voltage simultaneously.

Little work has been carried out in the way of control of intermittent operation. [71] applies resonant parametric perturbation, where a control parameter is perturbed in order to ensure stability, to a parallel-buck converter with the input voltage being perturbed by a noise signal as a method for the avoidance of intermittent operation. However, little or no work exists on design procedures for controllers in order to avoid intermittent operation.

5.3 System model

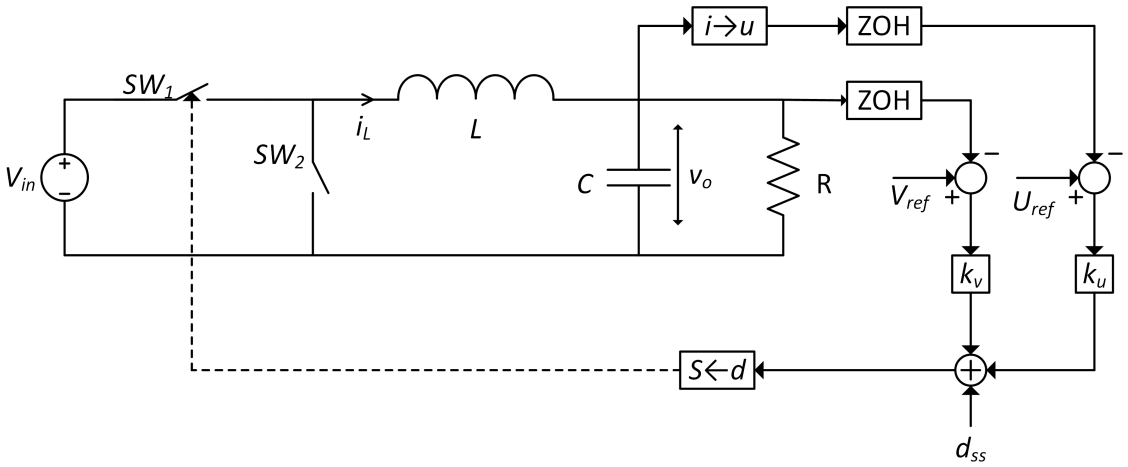

Figure 5.1: Buck converter with digital state-feedback controller.

Recall the equations used to model the buck converter in Section 4.2

$$\dot{x} = \begin{cases} f_{on}(x,t) = & A_{on}x + B_{on}x_{in} & SW_1 \text{ is on} \\ f_{off}(x,t) = & A_{off}x + B_{off}x_{in} & SW_1 \text{ is off} \end{cases} \tag{5.1}$$

where

$$A = A_{on} = A_{off} = \begin{bmatrix} -\sigma & \omega \\ -\omega & -\sigma \end{bmatrix}$$

$$B_{on} = \begin{bmatrix} 0 \\ \delta_{in} \end{bmatrix}, \; B_{off} = \begin{bmatrix} 0 \\ 0 \end{bmatrix}$$

$$x(t) = \begin{bmatrix} v_o \\ u \end{bmatrix}, \; x_{in} = V_{in}, \; \delta_{in} = \frac{\omega^2 + \sigma^2}{\omega}$$

Note: no integrator is present in the controller and the state-space is given by a 2x2 matrix. A buck converter with a digital state-feedback controller is considered in

Figure 5.1. As a digital controller is employed, the state vector is sampled at the switching frequency, using a zero-order hold (ZOH), and compared to the demanded value $x_{ref} = \begin{bmatrix} V_{ref} & U_{ref} \end{bmatrix}^T + \begin{bmatrix} \frac{\Delta v_o}{2} & \frac{1}{2\omega C}\Delta i_L - \frac{\sigma}{2\omega}\Delta v_o \end{bmatrix}^T$, where Δv_o and Δi_L are the estimated voltage and current ripple given by [72]:

$$\Delta i_L = \frac{V_{in} - v_{ref}}{L} dT$$
$$\Delta v_o = \frac{\Delta i_L T}{8C}$$

By knowing the circuit parameters and estimating the current and voltage ripples, the proper selection of the x_{ref} terms means the control scheme has an indirect integral action. The state-feedback control law is formed by adding the two state error terms together and multiplying by the gain $\begin{bmatrix} k_v & k_u \end{bmatrix}$, as well as adding a constant affine term equal to the desired steady-state value of the system $d_{ss} = V_{ref}/V_{in}$. The control signal is given by:

$$d\,(kT) = \begin{bmatrix} k_v & k_u \end{bmatrix} (x(kT) - x_{ref}) + d_{ss} \tag{5.2}$$

At this point, it is important to note that digital implementation requires A/D and digital to analog (D/A) conversion. This means that the sampled values must be quantized; quantization is the mapping of values in a continuous set to a discrete set. However, quantization can cause limit cycling to occur [1]. The aim of this work is to study the effect of noise on the occurrence of intermittent operation. In order to distinguish between the effects of noise and the effects of quantization, the resolution of the quantizers is assumed to be infinitely small. The effect of quantization on the nonlinear dynamics of the converter is investigated in chapter 6.

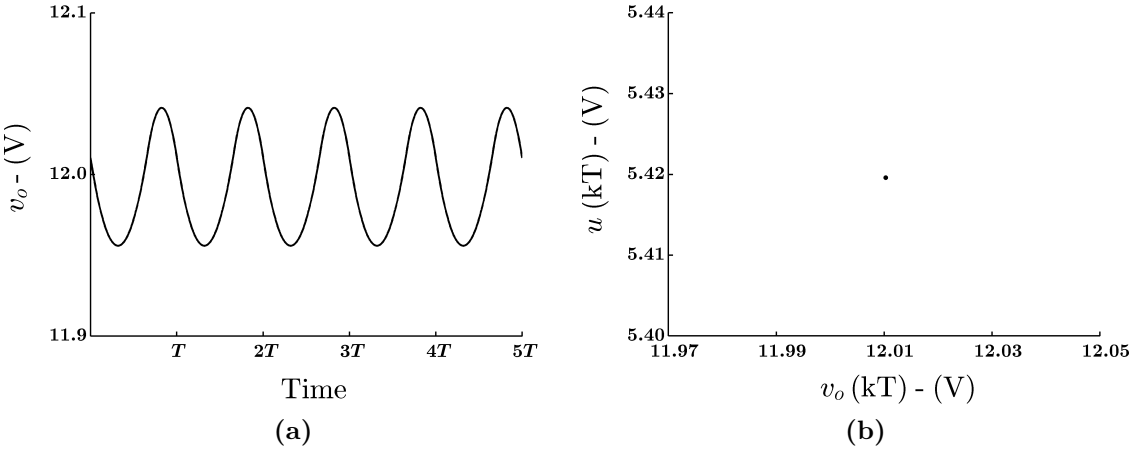

Figure 5.2: (a) Steady-state output voltage and (b) Poincaré section with the following circuit parameters $L = 20\,(mH)$, $C = 47\,(\mu F)$, $R = 22\,(\Omega)$, $T = 400\,(\mu s)$, $V_{ref} = 12.4381\,(V)$, $U_{ref} = 11.677\,(V)$, $k_v = -0.1334$ and $k_u = 0.0092$.

Figure 5.2 shows (a) the steady-state output voltage and (b) the Poincaré section of

the buck converter operating under ideal conditions. The Poincaré section samples both of the state variables once per switching cycle and plots them against each other. If the systems trajectory intersects the Poincaré plane n times, then n points are seen on the section. In this case, a single point is shown illustrating that the system is operating with the desired period-1 orbit. The effect of perturbing the input voltage with an undesirable noise signal is now considered.

5.4 Influence of sinusoidal interference signal at the input voltage

The unperturbed buck converter operates with a stable period-1 orbit. This assumes ideal operating conditions and ideal sources. In practical applications, noise sources can affect the input voltage of a buck converter. Noise signals may arise because of finite input capacitances, ESR of the input capacitor or stray inductance and stray capacitance in the circuit [73]. Consider an interference signal, v_s, which is injected directly into the input voltage. This coupling can be modelled as an additive process which superposes the disturbance directly on the input voltage. The perturbed input voltage V_{in}^* is now given by:

$$V_{in}^* = V_{in} + v_s \tag{5.3}$$

If the interference signal is periodic, the simplest case to consider is a sinusoidal disturbance signal with an amplitude $\hat{v}_s$. Then the perturbed signal is:

$$V_{in}^* = V_{in} + \hat{v}_s \sin(2\pi f_n t) = V_{in}(1 + \alpha_v \sin(2\pi f_n t)) \tag{5.4}$$

where α_v is the strength of the interference which is defined as the ratio of $\hat{v}_s$ to V_{in} i.e. $\alpha_v = \hat{v}_s/V_{in}$ and f_n is the frequency of the noise where $f_n = \alpha_f f$ and $\alpha_f \epsilon \mathbb{R}$ which is the ratio of the noise frequency to the switching frequency. Since α_f can be any value, there are three cases to consider:

1. α_f is an irrational number.
2. α_f is a rational number.
3. α_f is a rational number and the noise frequency is close to the switching frequency or one of its integer multiples.

5.4.1 Multiples of the switching frequency

For rational frequency ratios, $\alpha_f \epsilon \mathbb{Q}$ and can be expressed in the form N_{num}/N_{den}, where N_{num} and N_{den} are positive integers. In this case, the buck converter operates with a periodicity equal to the denominator of α_f i.e. a period-N_{den} orbit.

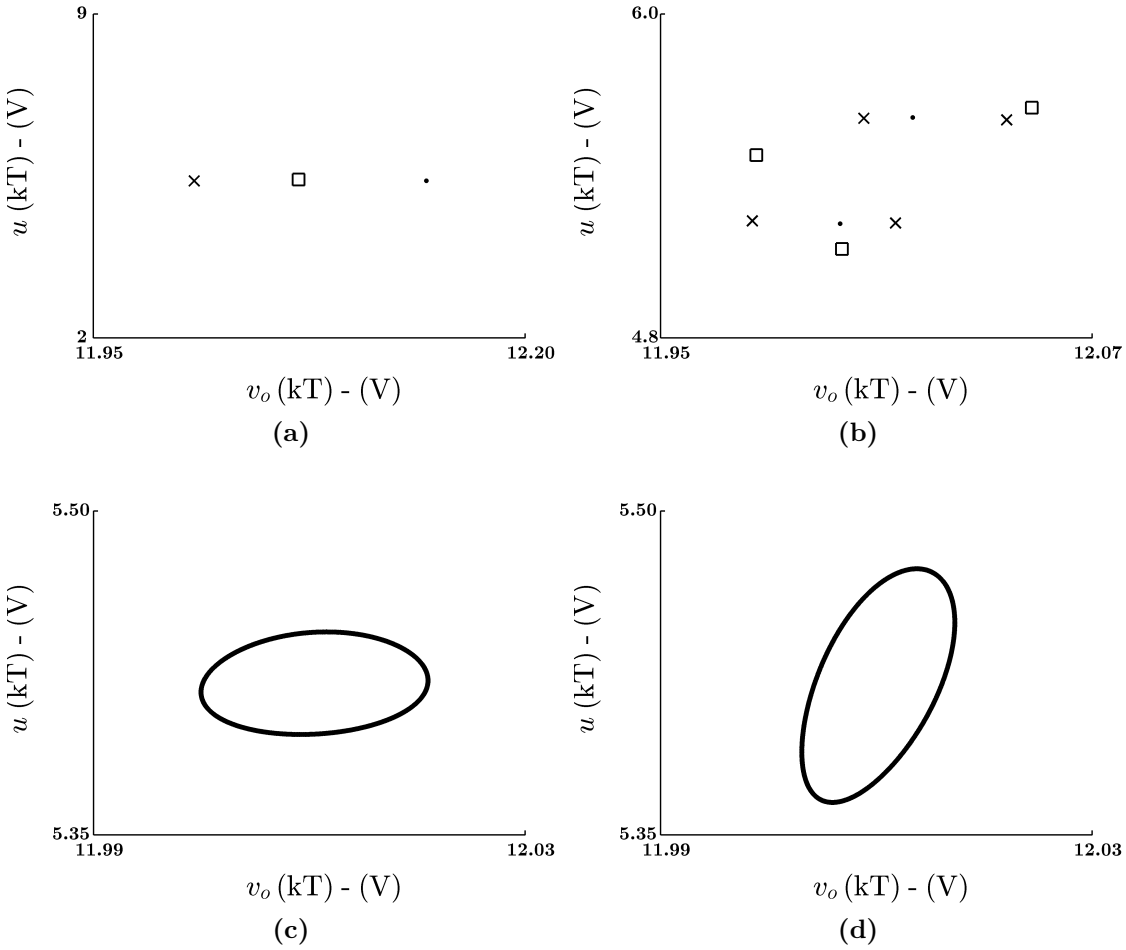

Figure 5.3: Poincaré section with sinusoidal disturbance signal and $\alpha_v = 0.5$ for different frequency ratios (a) $\alpha_f = 1$, 2 and 3 (dot, square and x, respectively) (b) $\alpha_f = 1/2$, 1/3 and 3/4 (dots, squares and xs, respectively) (c) $\alpha_f =$ Golden ratio and (d) $\alpha_f =$ Silver ratio.

For example, Figure 5.3 (a) shows the Poincaré section for integer multiples of α_f. Specifically, $\alpha_f = 1$, 2 and 3. In this case, $N_{den} = 1$ and the system operates with a period-1 orbit which is characterised by a single point on the Poincaré section. In contrast to this, (b) shows the Poincaré section for fractional multiples of α_f i.e. when $N_{den} \neq 1$. Specifically, $\alpha_f = 1/2$, 1/3 and 3/4 which corresponds to period-2, period-3 and period-4 operation, respectively. This is characterised by 2,3 and 4 intersections on the Poincaré section. It is clear that the buck converter operates with a period-N_{den} orbit.

In Figure 5.3 (c) and (d), irrational values of α_f are considered. Specifically, the effect of the Golden ratio $\alpha_f = \left(1 + \sqrt{5}\right)/2$ and the Silver ratio $\alpha_f = 1 + \sqrt{2}$. Since f_n and f are not commensurate, a low oscillating frequency modulating the other frequency is expected and the steady state is quasi-periodic. This is confirmed on the Poincaré section which shows the trajectory intersecting the Poincaré plane an infinite number of times. This type of behaviour is termed a torus (as explained in chapter 2).

In the next section, the case where the frequency of the noise signal is close to the switching frequency or its integer multiples is considered.

5.4.2 Interference frequency approaching the switching frequency or its integer multiples

Since the interference signal is coupled unintentionally, it is possible that the frequency of the noise will be close to the switching frequency or its integer multiples. In this instance, $f_n = pf + \hat{f}$ where p is an integer and $\hat{f}$ is a number which is less than half the switching frequency. This kind of interference signal leads to intermittent operation. The perturbed input voltage can be rewritten as

$$V_{in}^* = V_{in}\left(1 + \alpha_v \sin\left(2\pi\left(pf + \hat{f}\right)t\right)\right) \tag{5.5}$$

Taking $\hat{f} = 1$ and $p = 1$ and 2, the interference frequencies considered are 2501 (Hz) and 5001 (Hz). In order to reveal the periodicity of the output and the intermittent behaviour, the output voltage is sampled once per switching cycle and plotted against the sampling instant. From the resulting plot, it is possible to determine how the system trajectory evolves over time. In order to distinguish this from the conventional parameter-bifurcation diagram, these plots are termed *time-bifurcation* diagrams. Figure 5.4 and Figure 5.5 show the time-bifurcation diagrams for 2501 (Hz) and 5001 (Hz), respectively. From these figures, the following observations can be made:

- For low signal strengths, $\alpha_v = 0.16$, the converter maintains its expected period-1 orbit, though the operating point fluctuates due to the oscillating input voltage. The effect of the disturbance signal is not significant at this stage and the system does not exhibit intermittent operation. Figure 5.4 (a) and Figure 5.5 (a) show the corresponding time-bifurcation diagrams.
- As the strength of the interference signal increases, the system cannot maintain the expected period-1 orbit. Instead, the system operates with a period-1 orbit for the majority of the time with small bursts of unstable operation. The system loses stability for a short period of time through a Hopf bifurcation and operates with a limit-cycle present on the output. However, the system does regain stability after a short period of time. Intermittent operation is observed as α_v increases. Figure 5.4 (b) and Figure 5.5 (b) show the corresponding time-bifurcation plots.
- Further increases to the interference signal strength cause the amplitude of the limit cycle to increase and the period of instability to increase. Figure 5.4 (c) and (d) and Figure 5.5 (c) and (d) show the corresponding time-bifurcation plots.

- The intermittent period, T_{int}, is represented by

$$T_{int} = \frac{1}{N_{den}\hat{f}}$$

where $\hat{f} = pf - f_n$. Thus, if the interference frequency is close to the switching frequency, the period of intermittency is very long.

5.5 Stability analysis

As there is no steady-state fixed point in the system which can be used to perform bifurcation analysis of the time-bifurcation plots above, a transformation must take place. The transformation must convert changes in time to change in another variable. This enables parameter-bifurcation analysis to be performed. The new parameter, ϕ, is considered as a conceptual phase shift to model the equivalent drift of the system from the switching frequency, or its integer multiples, and the perturbed input voltage in (5.4) is now rewritten as:

$$V_{in}^{*} = V_{in}\left(1 + \alpha_v \sin\left(2\pi p f t + \phi\right)\right) \tag{5.6}$$

where $\phi = 2\pi\hat{f}t$. Using the above perturbed control voltage, a parameter-bifurcation diagram can be constructed by selecting ϕ as the bifurcation parameter. Figure 5.8 and Figure 5.9 show the resulting plots which are equivalent to those presented in Figure 5.4 and Figure 5.5. When the time-bifurcation and the parameter-bifurcation diagrams are compared, the results are in very close agreement. This transformation enables standard bifurcation analysis to be performed and the results can be transformed from the parameter-domain to the time-domain. Essentially, the parameter-bifurcation diagram over the interval of $0 \leq \phi \leq 2\pi$ is the same as the time-bifurcation diagram over the intermittent period, T_{int}, shown in Figure 5.4 and Figure 5.5. The Filippov method is now used to derive the Monodromy matrix for the system which enables its stability to be assessed.

As demonstrated in chapter 4, the Filippov method is a technique that is used to analyse the stability of systems with a discontinuous state-space. By relating events before and after switching, its stability can be assessed. Recall the formula for the saltation matrix:

$$S = I + \left.\frac{\left(f_+ - f_-\right) n^T}{n^T f_- + \frac{\partial h}{\partial t}}\right| \begin{array}{l} t = t_\Sigma \\ \boldsymbol{x}(t) = \boldsymbol{x}(t_\Sigma) \end{array} \tag{5.7}$$

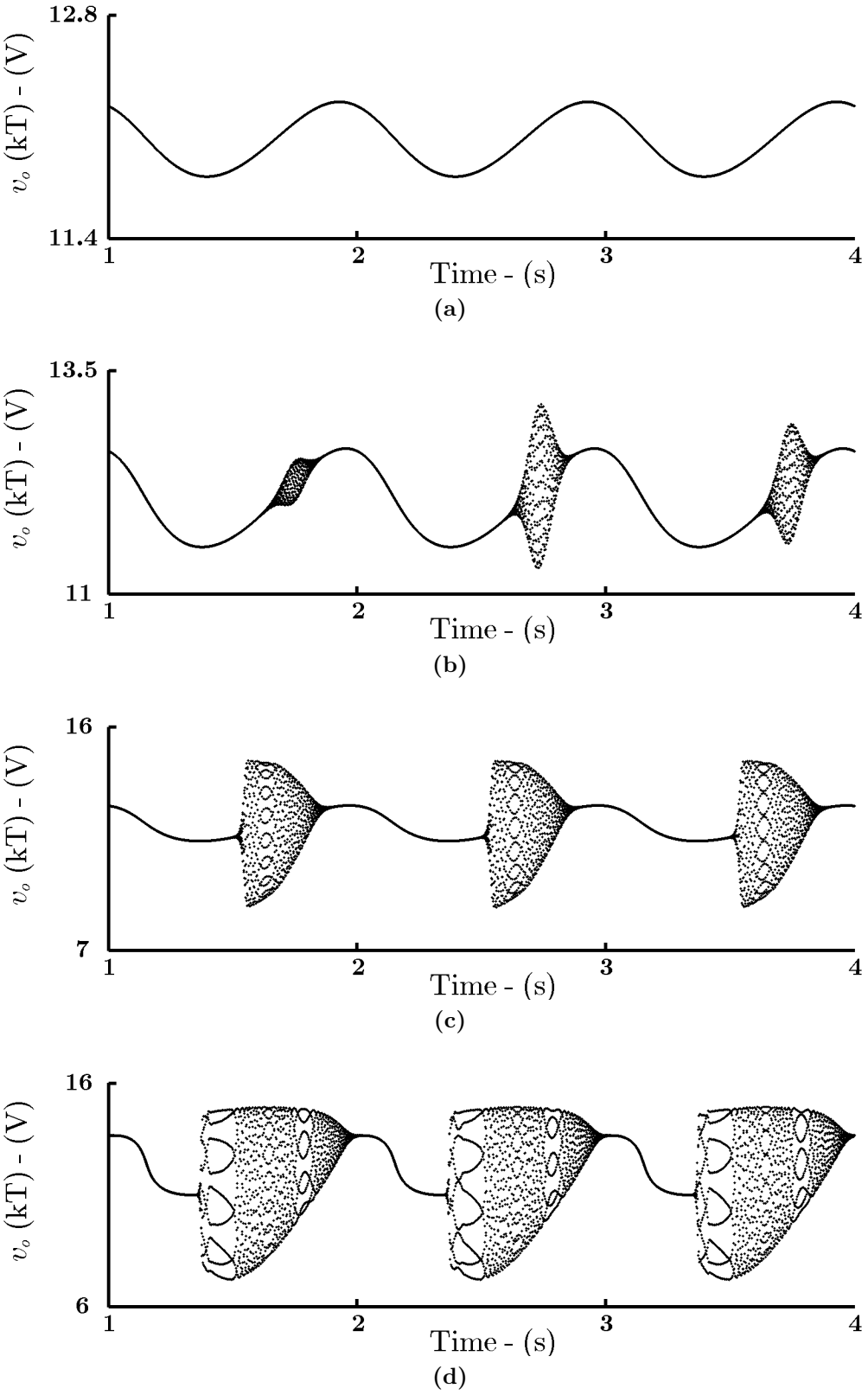

Figure 5.4: Time-bifurcation diagram with a sinusoidal interference signal with a frequency of $f_n = 2501$ for (a) $\alpha_v = 0.16$ (b) $\alpha_v = 0.38$ (c) $\alpha_v = 0.5$ and (d) $\alpha_v = 1$.

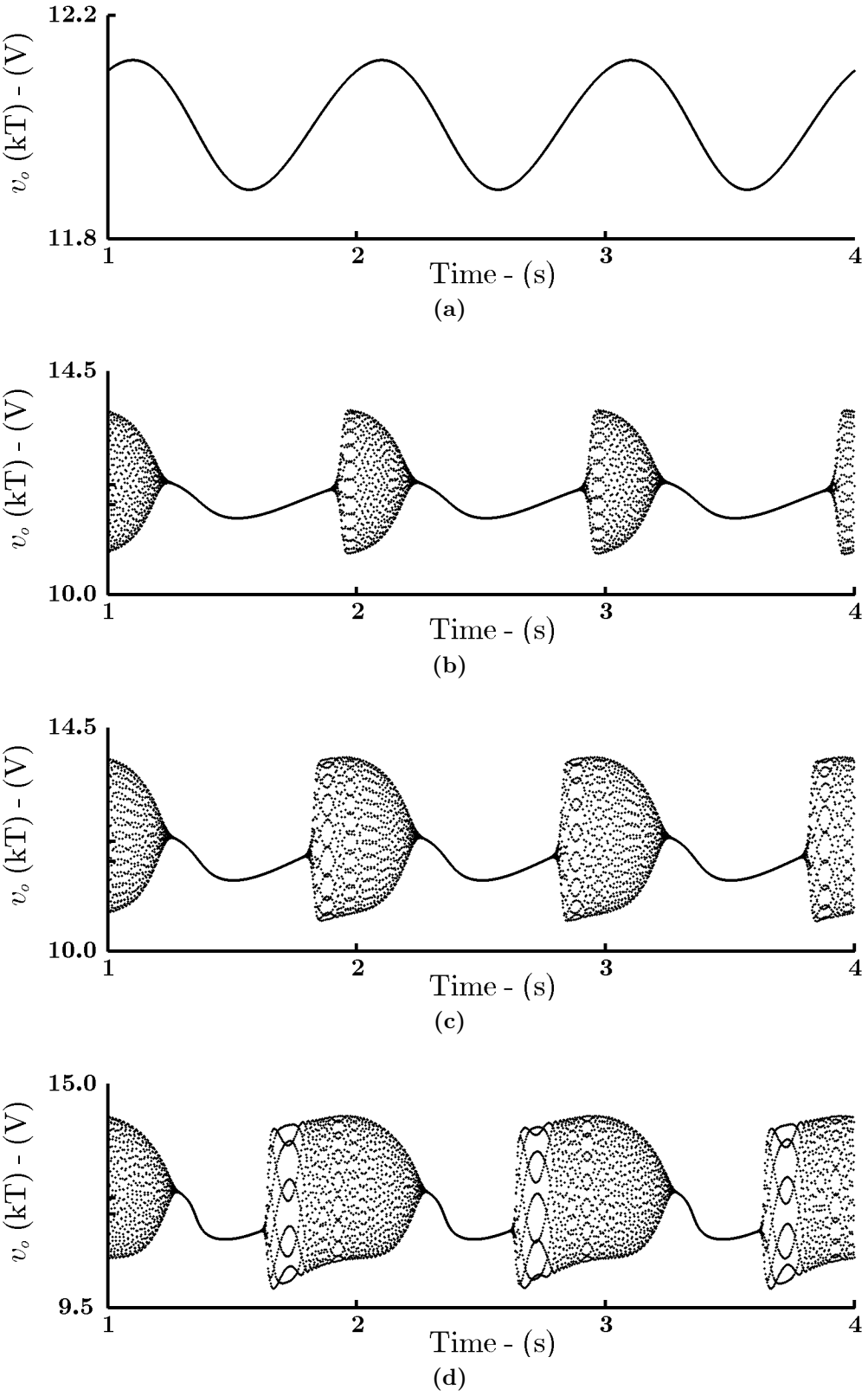

Figure 5.5: Time-bifurcation diagram with a sinusoidal interference signal with a frequency of $f_n = 5001$ for (a) $\alpha_v = 0.16$ (b) $\alpha_v = 0.57$ (c) $\alpha_v = 0.7$ and (d) $\alpha_v = 1$.

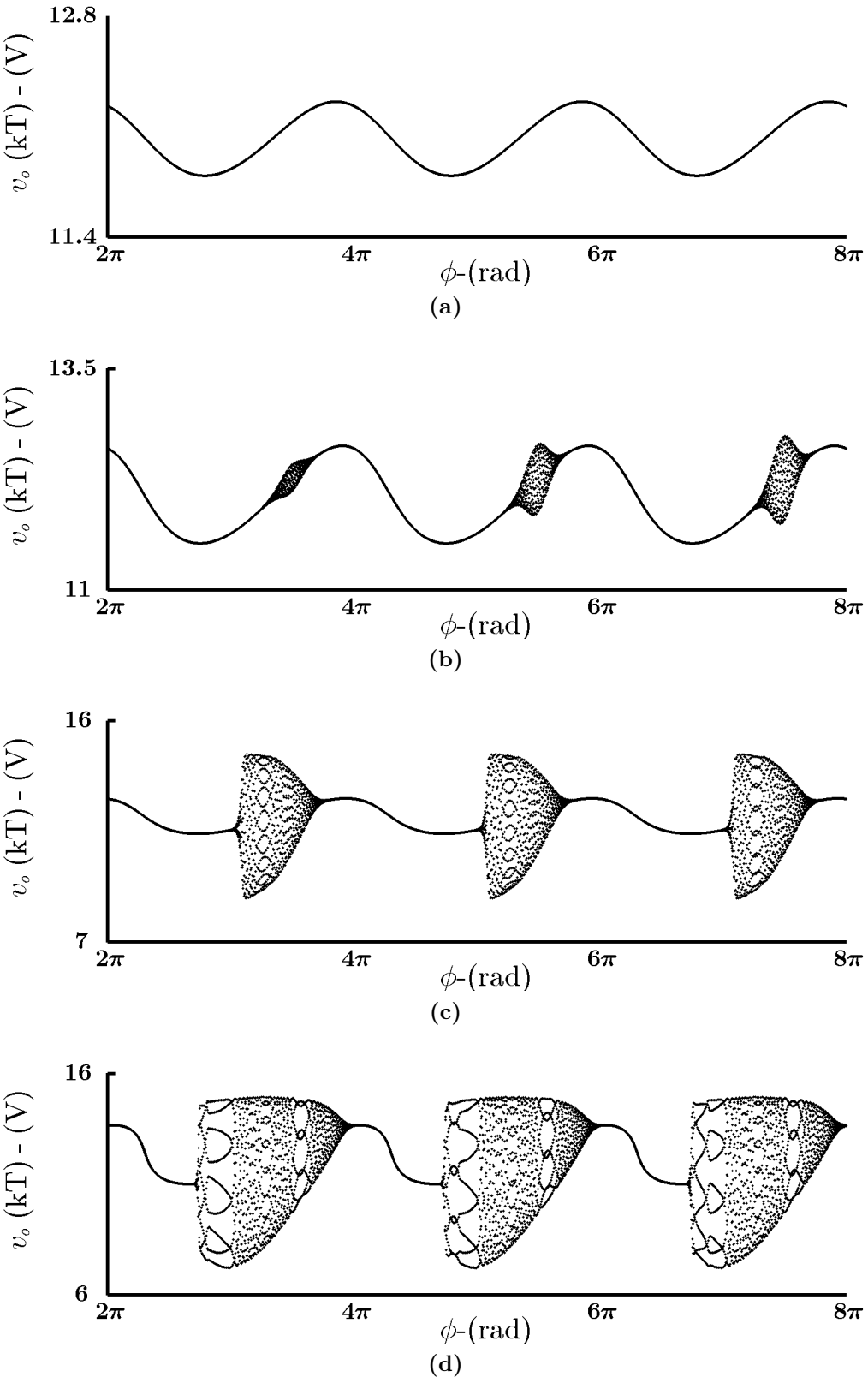

Figure 5.6: Parameter-bifurcation diagram with a sinusoidal interference signal with $p = 1$ for (a) $\alpha_v = 0.16$ (b) $\alpha_v = 0.38$ (c) $\alpha_v = 0.5$ and (d) $\alpha_v = 1$.

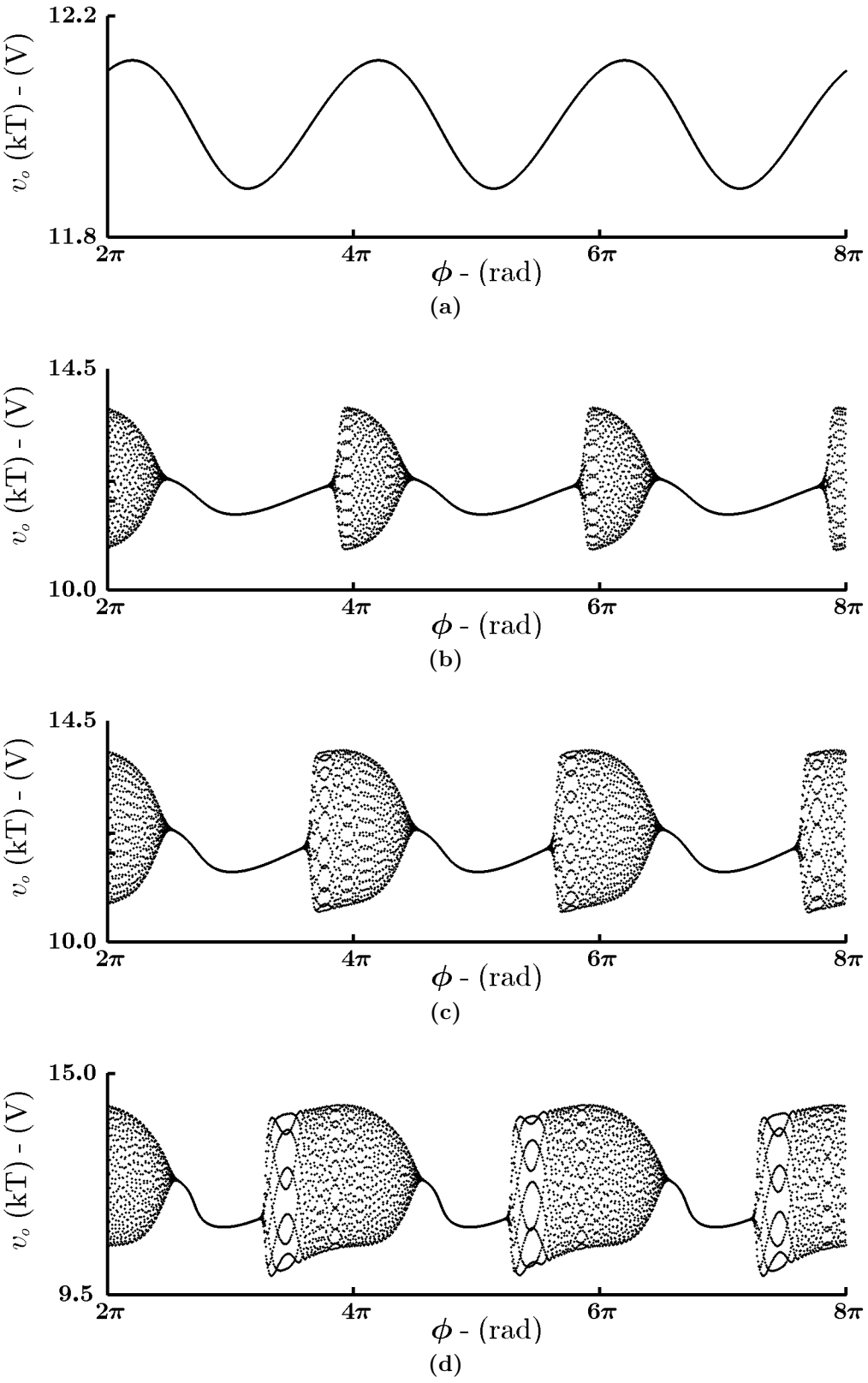

Figure 5.7: Parameter-bifurcation diagram with a sinusoidal interference signal with $p = 2$ for (a) $\alpha_v = 0.16$ (b) $\alpha_v = 0.57$ (c) $\alpha_v = 0.7$ and (d) $\alpha_v = 1$.

f_- and f_+ are the right hand side of (5.1) before and after switching, respectively.

$$f_- = \begin{bmatrix} -\sigma v_\Sigma + \omega u_\Sigma \\ -\omega v_\Sigma - \sigma u_\Sigma + \delta_{in} V_{in} \end{bmatrix} \quad , \quad f_+ = \begin{bmatrix} -\sigma v_\Sigma + \omega u_\Sigma \\ -\omega v_\Sigma - \sigma u_\Sigma \end{bmatrix}$$

The switching manifold for the system is:

$$h(x,t) = d_{ss} + \begin{bmatrix} k_v & k_u \end{bmatrix} (x(kT) - x_{ref}) - t \bmod T \tag{5.8}$$

The switching manifold in (5.8) depends on the value of the state vector at the start of the switching period. However, both n and $\partial h/\partial t$ are evaluated at the switching instant i.e. $t = (k+d)\,T$. Thus, (5.8) must be rewritten to reflect this. SW_1 is closed at the start of the switching period and remains closed for dT. Thus, the switch is closed from $kT \to (k+d)\,T$. Therefore, the solution to (5.1) is given by:

$$\int_{kT}^{(k+d)T} \frac{d}{dt}\left(e^{-At}x\right) dt = \int_{kT}^{(k+d)T} e^{-At} B V_{in}^* dt$$

However, $V_{in}^* = V_{in}\left(1 + \alpha_v \sin\left(2\pi f_n t\right)\right)$:

$$x\left((k+d)\,T\right) = e^{AdT}x(kT) - A^{-1}\left(I - e^{AdT}\right)BV_{in} + \alpha_v e^{A(k+d)T} \int_{kT}^{(k+d)T} e^{-At} \sin\left(2\pi f_n t\right) dt B V_{in} \tag{5.9}$$

Let $N_{dT} = e^{A(k+d)T} \int_{kT}^{(k+d)T} e^{-At} \sin\left(2\pi f_n t\right) dt$. Using integration by parts, N_{dT} can be derived to be:

$$N_{dT} = e^{A(k+d)T}\left(A^2 + \left(2\pi f_n\right)^2\right)^{-1} \left(-Ae^{-At}\sin\left(2\pi f_n t\right) - 2\pi f_n e^{-At}\cos\left(2\pi f_n t\right)\right)\Big|_{t=kT}^{t=(k+d)T}$$

Inserting the limits yields:

$$N_{dT} = \left(A^2 + \left(2\pi f_n\right)^2\right)^{-1} \Bigg(Ae^{AdT}\sin\left(2\pi f_n kT\right) + 2\pi f_n e^{AdT}\cos\left(2\pi f_n kT\right) - A\sin\left(2\pi f_n (k+d)T\right) - 2\pi f_n \cos\left(2\pi f_n (k+d)T\right) \Bigg)$$

Evaluating (5.9), the state variable at the start of the switching period can be related

to the state variable at the switching instant:

$$x\left(\left(k+d\right)T\right) = e^{AdT}x(kT) - A^{-1}\left(I - e^{AdT}\right)BV_{in} + \alpha_v N_{dT}BV_{in} \tag{5.10}$$

Rearranging (5.10) so that the value of the state vector at the start of the switching period is expressed in terms of its value at the switching instants gives:

$$x(kT) = e^{-AdT}x\left(\left(k+d\right)T\right) + A^{-1}\left(e^{-AdT} - I\right)BV_{in} + \alpha_v N_T BV_{in} \tag{5.11}$$

where

$$\begin{aligned} N_T = \left(A^2 + \left(2\pi f_n\right)^2\right)^{-1} \Bigg(& -AI\sin\left(2\pi f_n kT\right) \\ & -2\pi f_n I\cos\left(2\pi f_n kT\right) \\ & +Ae^{-AdT}\sin\left(2\pi f_n(k+d)T\right) \\ & +2\pi f_n e^{-AdT}\cos\left(2\pi f_n(k+d)T\right)\Bigg) \end{aligned}$$

Using (5.11), n and $\partial h/\partial t$ are:

$$n = \left.\begin{bmatrix} \frac{\partial h}{\partial v_o} \\ \frac{\partial h}{\partial u} \end{bmatrix}\right|_{t=(k+d)T} = e^{\sigma dT}\begin{bmatrix} k_v\cos\left(\omega dT\right) + k_u\sin\left(\omega dT\right) \\ -k_v\sin\left(\omega dT\right) + k_u\cos\left(\omega dT\right) \end{bmatrix} \tag{5.12}$$

$$\begin{aligned} \left.\frac{\partial h}{\partial t}\right| = -\frac{1}{T} + e^{\sigma dT}\Bigg(& \left(k_v\sin\left(\omega dT\right) - k_u\cos\left(\omega dT\right)\right)\delta_{in}V_{in}^* \\ & +\left(\left(\sigma k_v + \omega k_u\right)\cos\left(\omega dT\right) + \left(\sigma k_u - \omega k_v\right)\sin\left(\omega dT\right)\right)v_\Sigma \\ & +\left(\left(-\sigma k_v - \omega k_u\right)\sin\left(\omega dT\right) + \left(\sigma k_u - \omega k_v\right)\cos\left(\omega dT\right)\right)u_\Sigma\Bigg) \end{aligned} \tag{5.13}$$

The Saltation matrix defined in (5.7) is given by:

$$S_1 = \begin{bmatrix} 1 & 0 \\ S_{21} & 1 + S_{22} \end{bmatrix} \tag{5.14}$$

with

$$\begin{aligned} S_{21} =& Te^{\sigma dT}\delta_{in}V_{in}^*\left(k_v\cos\left(\omega dT\right) + k_u\sin\left(\omega dT\right)\right) \\ S_{22} =& Te^{\sigma dT}\delta_{in}V_{in}^*\left(-k_v\sin\left(\omega dT\right) + k_u\cos\left(\omega dT\right)\right) \end{aligned}$$

The second switching point occurs at the falling edge of the ramp signal. Hence, $\partial h/\partial t = \infty$ and S_2 is the identity matrix of the same dimension as S_1. The Mon-

odromy matrix is:

$$\Phi_M = e^{A(1-d)T} S_1 e^{AdT} \tag{5.15}$$

where the exponential matrix is given by:

$$e^{At} = e^{-\sigma t} \begin{bmatrix} \cos(\omega t) & \sin(\omega t) \\ -\sin(\omega t) & \cos(\omega t) \end{bmatrix}$$

Figure 5.8 and Figure 5.9 show the parameter-bifurcation plots with ϕ as the bifurcation parameter for varying signal strengths and for $p = 1$ and $p = 2$, respectively. Consider the case where $p = 1$ and $\alpha_v = 0.5$, the corresponding bifurcation diagram is shown in Figure 5.8 (c). This diagram can be broken into three key regions:

1. $0 \leq \phi \leq 1.885$: In this region, the system is stable and operates with a period-1 orbit.
2. $1.885 \leq \phi \leq 4.964$: The system is unstable and undergoes a bifurcation at $\phi = 1.885$. This is confirmed by assessing the eigenvalues presented in Table 5.1 which were calculated using (5.15). Since the $|\lambda| > 1$ and λ has a non-zero imaginary part, it is determined that a Hopf bifurcation takes place.
3. $4.964 \leq \phi \leq 6.28$: The system is stable and operating with a period-1 orbit.

Similar dynamics occur in Figure 5.8 (b)-(d) and Figure 5.9 (b)-(d), where the system moves from a stable orbit to an unstable orbit through a Hopf bifurcation. Table 5.1 and Table 5.2 present the eigenvalues at the bifurcation points for $p = 1$ and $p = 2$, respectively.

5.5.1 Hopf bifurcation

It was shown above that the system undergoes a Hopf bifurcation as ϕ varies. This type of operation can be catastrophic in many applications, and therefore, it must be avoided. Given that the Monodromy matrix, Φ_M, is a 2x2 matrix, the characteristic equation is given by:

$$\lambda^2 - \mathrm{tr}(\Phi_M)\lambda + \det(\Phi_M) \tag{5.16}$$

The following matrix properties are useful

$$\mathrm{tr}(XY) = \mathrm{tr}(YX) \tag{5.17}$$

$$\det(XY) = \det(X)\det(Y) \tag{5.18}$$

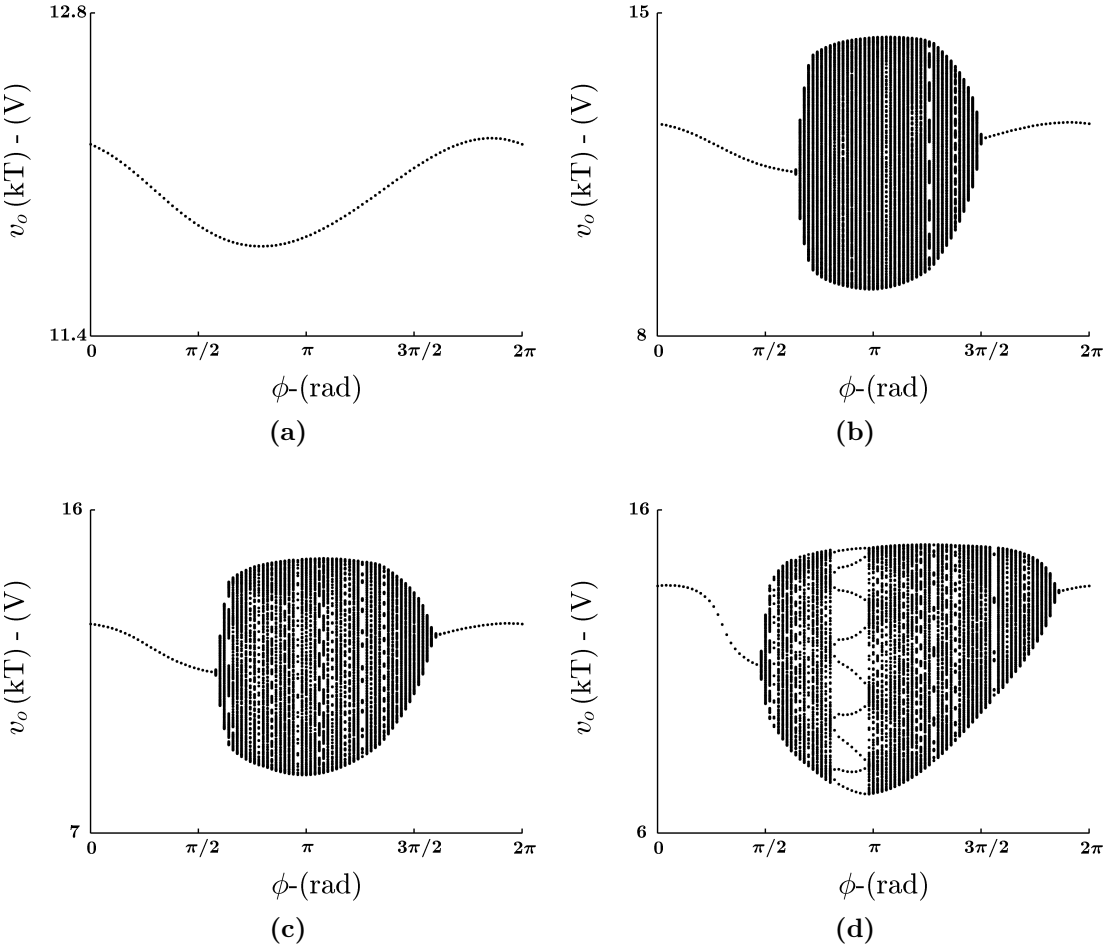

Figure 5.8: Parameter-bifurcation diagram with sinusoidal interference signal with $p = 1$ for (a) $\alpha_v = 0.16$ (b) $\alpha_v = 0.38$ (c) $\alpha_v = 0.5$ and (d) $\alpha_v = 1$.

α_v	ϕ	$\lambda_{1,2}$	$\lvert\lambda_{1,2}\rvert$
0.38	1.8221	$0.7549 \pm 0.6558i$	0.9999
	1.8850	$0.7535 \pm 0.6588i$	1.0009
	4.9637	$0.7167 \pm 0.6973i$	1.0000
	5.0265	$0.7169 \pm 0.6930i$	0.9971
0.50	1.8221	$0.7549 \pm 0.6558i$	0.9999
	1.8850	$0.7535 \pm 0.6588i$	1.0009
	4.9637	$0.7167 \pm 0.6973i$	1.0000
	5.0265	$0.7169 \pm 0.6930i$	0.9971
1.00	1.4451	$0.7611 \pm 0.6248i$	0.9847
	1.5080	$0.7613 \pm 0.6486i$	1.0001
	5.7805	$0.6725 \pm 0.7403i$	1.0002
	5.8434	$0.6716 \pm 0.7366i$	0.9967

Table 5.1: Eigenvalues of the system with $p = 1$ at the bifurcation point for varying signal strengths.

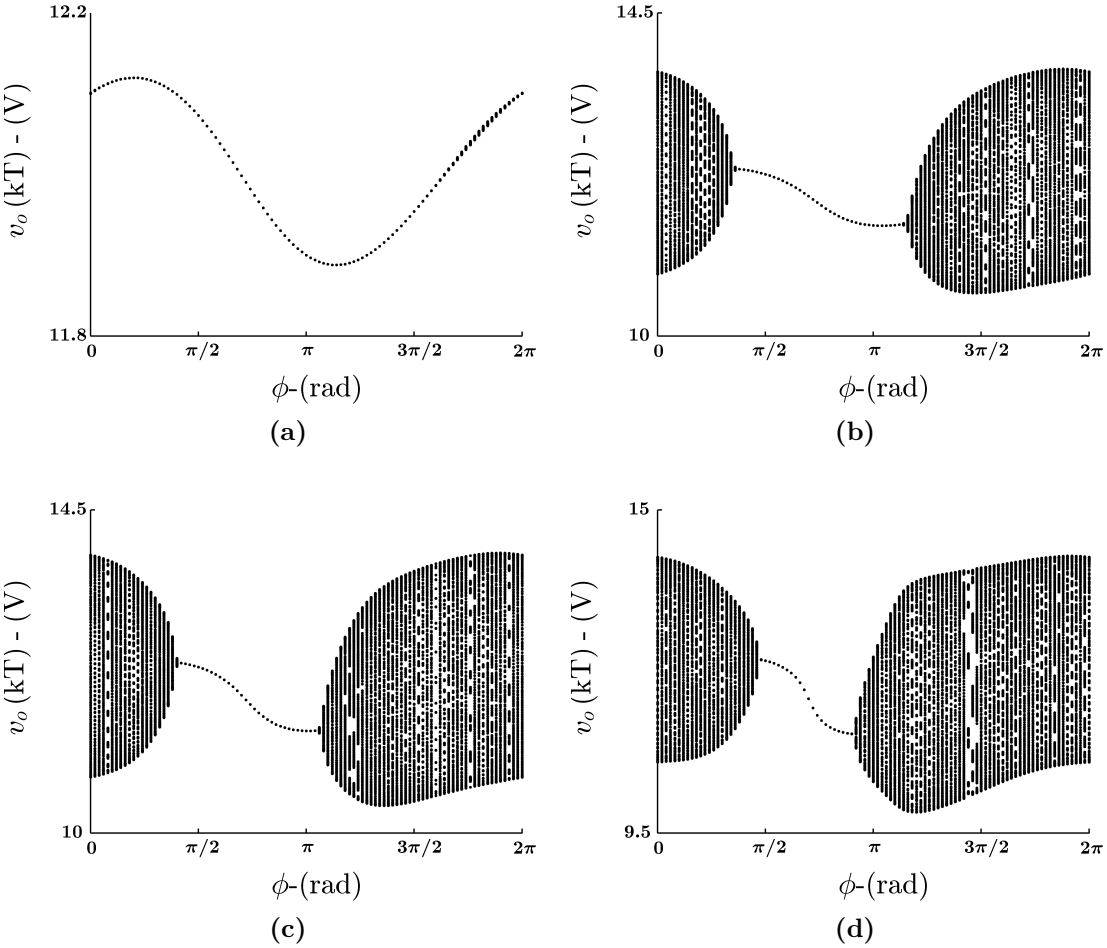

Figure 5.9: Parameter-bifurcation diagram with sinusoidal interference signal with $p = 2$ for (a) $\alpha_v = 0.16$ (b) $\alpha_v = 0.57$ (c) $\alpha_v = 0.7$ and (d) $\alpha_v = 1$.

α_v	ϕ	$\lambda_{1,2}$	$\lvert\lambda_{1,2}\rvert$
0.57	1.0681	$0.7246 \pm 0.6894i$	1.0002
	1.1310	$0.7259 \pm 0.6821i$	0.9961
	3.5814	$0.7521 \pm 0.6514i$	0.9950
	3.6642	$0.7515 \pm 0.6599i$	1.0001
0.70	1.2566	$0.7220 \pm 0.6919i$	1.0000
	1.3195	$0.7256 \pm 0.6762i$	0.9918
	3.3301	$0.7560 \pm 0.6565i$	1.0013
	3.3929	$0.7551 \pm 0.6589i$	1.0021
1.00	1.4451	$0.7201 \pm 0.6949i$	1.0007
	1.5080	$0.7216 \pm 0.6846i$	0.9947
	2.8274	$0.7628 \pm 0.6338i$	0.9918
	2.8903	$0.7624 \pm 0.6489i$	1.0012

Table 5.2: Eigenvalues of the system with $p = 2$ at the bifurcation point for varying signal strengths.

Using (5.17), the trace of the Monodromy matrix is:

$$\begin{aligned}\mathrm{tr}\left(\Phi_M\right) = &\underbrace{2e^{-\sigma T}\cos\left(\omega T\right)}_{M} + \\ &\underbrace{Te^{-\sigma(1-d)T}\delta_{in}\left(k_v\sin\left(\omega(1-d)T\right)+k_u\cos\left(\omega(1-d)T\right)\right)}_{P}V_{in}^{*}\end{aligned} \tag{5.19}$$

and using (5.18) the determinant is:

$$\det\left(\Phi_M\right) = e^{-2\sigma T} + Te^{-\sigma(2-d)T}\delta_{in}V_{in}^{*}\left(-k_v\sin\left(\omega dT\right)+k_u\cos\left(\omega dT\right)\right) \tag{5.20}$$

From (5.16), it is clear that the eigenvalues are given by

$$\lambda_{1,2} = \frac{\mathrm{tr}\left(\Phi_M\right) \pm \sqrt{\mathrm{tr}\left(\Phi_M\right)^2 - 4\det\left(\Phi_M\right)}}{2} \tag{5.21}$$

The discriminant of (5.21) is

$$\begin{aligned}\Bigg(&\underbrace{4e^{-2\sigma T}\left(\cos^2\left(\omega T\right)-1\right)}_{R} + \\ &\underbrace{\left[e^{-\sigma(1-d)T}\delta_{in}T\left(k_v\sin\left(\omega\left(1-d\right)T\right)+k_u\cos\left(\omega\left(1-d\right)T\right)\right)\right]^2}_{P^2}V_{in}^{*2} + \\ &\underbrace{4e^{-\sigma(2-d)T}\delta_{in}T\left(k_v\sin\left(\omega T\right)\cos\left(\omega\left(1-d\right)T\right)-k_u\sin\left(\omega T\right)\sin\left(\omega\left(1-d\right)T\right)\right)}_{Q}V_{in}^{*}\Bigg)\end{aligned}$$

The magnitude of(5.21) is given by:

$$\left|\lambda_{1,2}\right| = \sqrt{\left(\frac{M+PV_{in}^{*}}{2}\right)^2 + \frac{-\left(P^2V_{in}^2+QV_{in}+R\right)}{4}} \tag{5.22}$$

Setting $|\lambda_{1,2}| = 1$ yields:

$$\begin{aligned}\left(2MP-Q\right)V_{in}^{*} + \left(M^2-R-4\right) &= 0 \\ 4e^{-\sigma(2-d)T}\delta_u T\left(-k_v\sin\left(\omega dT\right)+k_u\cos\left(\omega dT\right)\right)V_{in}^{*} + 4e^{-2\sigma T} - 4 &= 0\end{aligned} \tag{5.23}$$

Rearranging (5.23), the value of k_u at which a Hopf bifurcation takes place can be determined. This value is termed k_{u_crit} or the critical k_u value and is calculated by evaluating:

$$k_{u\_crit} = \frac{1-e^{-2\sigma T}}{e^{-\sigma(2-d)T}\delta_u T V_{in}^{*}\cos(\omega dT)} + k_v\tan(\omega dT) \tag{5.24}$$

Table 5.3 shows the critical k_u value for both (a) $f_n = 2501$ and (b) $f_n = 5001$ for the α_v values the same as those in Figure 5.4 and Figure 5.5, respectively. These can be used to tune the state-feedback controller in order to avoid intermittent operation.

(a)

f_n	α_v	k_{u_crit}
2501	0.16	0.0110
	0.38	0.0010
	0.50	-0.0027
	1.00	-0.0151

(b)

f_n	α_v	k_{u_crit}
5001	0.16	0.0121
	0.57	0.0002
	0.70	-0.0045
	1.00	-0.0098

Table 5.3: Values of k_{u_crit} in order to avoid intermittent operation for varying signal strengths for (a) $f_n = 2501\,(Hz)$ and (b) $f_n = 5001\,(Hz)$.

5.6 Adaptive controller

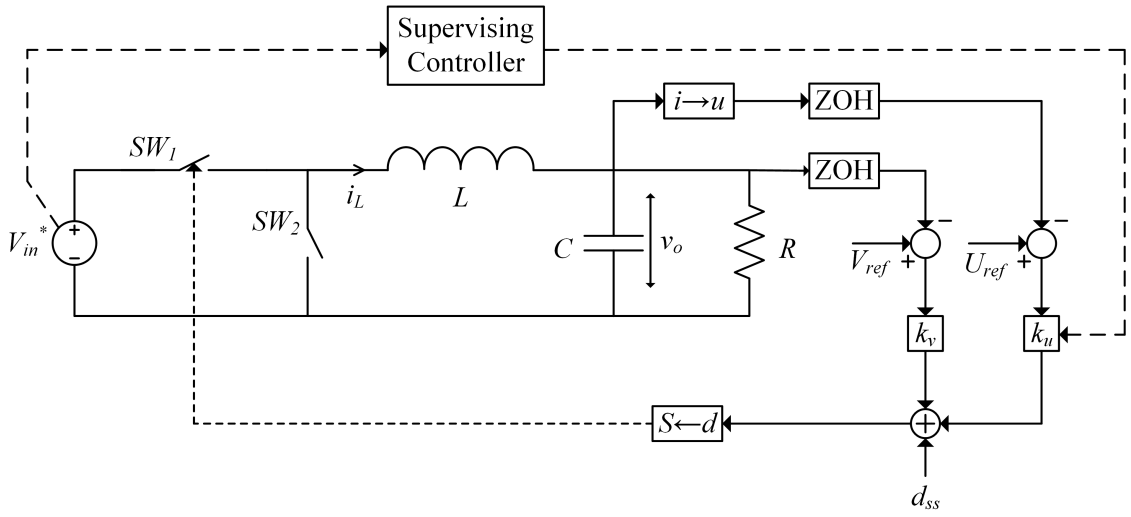

Figure 5.10: state-feedback controlled buck converter with supervising controller and perturbations at the input voltage.

In the previous section the Monodromy matrix was calculated and the Floquet Multipliers were derived as a function of the controller parameters. A formula for calculating the value of k_u which leads to a Hopf bifurcation was developed (5.24) and sample values were given in Table 5.3. This enables the development of an adaptive state-feedback controller. By modifying (5.2) and using (5.24), the proposed adaptive control scheme is illustrated in Figure 5.10. In the suggested scheme, estimators are used to monitor the input voltage [66, 67, 68] and determine the amplitude and frequency of any noise source present at the input. The function of the supervising controller is to update the k_u term in order to avoid intermittent operation. This can ensure stable period-1 orbits. The controller operates as follows:

1. The supervising controller monitors the input voltage for any input disturbances to the system. If no disturbances are present, the k_u term is not updated.

2. When a disturbance is present, the controller identifies the amplitude and frequency of the noise.

3. Using (5.15), the controller checks if the system is stable over the range $0 \leq \phi \leq 2\pi$.

   a) If the system is stable: k_u remains the same.

   b) If the system is unstable: (5.24) is evaluated and the k_u term is adjusted accordingly.

Using this method, the time-bifurcation plots are illustrated in Figure 5.11 and Figure 5.12 with $f_n = 2501$ and $f_n = 5001$, respectively. By determining k_{u_crit}, the system can avoid intermittency and operate with a stable period-1 orbit. While, in both cases, the fixed point of the system oscillates due to the periodic nature of the input, the intermittent operation seen in Figure 5.4 and Figure 5.5, when the standard control law is used, has been eliminated.

5.7 Conclusion

In this work, detailed analytical and numerical work has been carried out to investigate how the loss of stability of a digital state-feedback controlled buck converter can lead to intermittent operation due to the presence of an undesirable noise signal at the input voltage. Three cases for the ratio of the frequency of the noise to the switching frequency were considered; rational, irrational and values close to integer multiples of the switching frequency. For rational multiples, the converter was shown to operate with a period-N_{den} orbit. For irrational multiples, the system operated with a quasi-periodic orbit. Intermittent operation was observed where the frequency of the noise signal was close to the switching frequency of the system or its integer multiples. The intermittent operation was characterised by a loss in stability as time varied. However, conventional stability analysis is not applicable to time-bifurcation plots and thus, a transformation was required. The transformation converted changes in time to changes in another variable, ϕ, which was used to model the equivalent drift from the switching frequency. This enabled the application of the Filippov method to derive the eigenvalues of the system and stability criterion as a function of the controller parameters. Based on this, an adaptive digital state-feedback controller was tuned using the derived formulae which eliminated the intermittent behaviour.

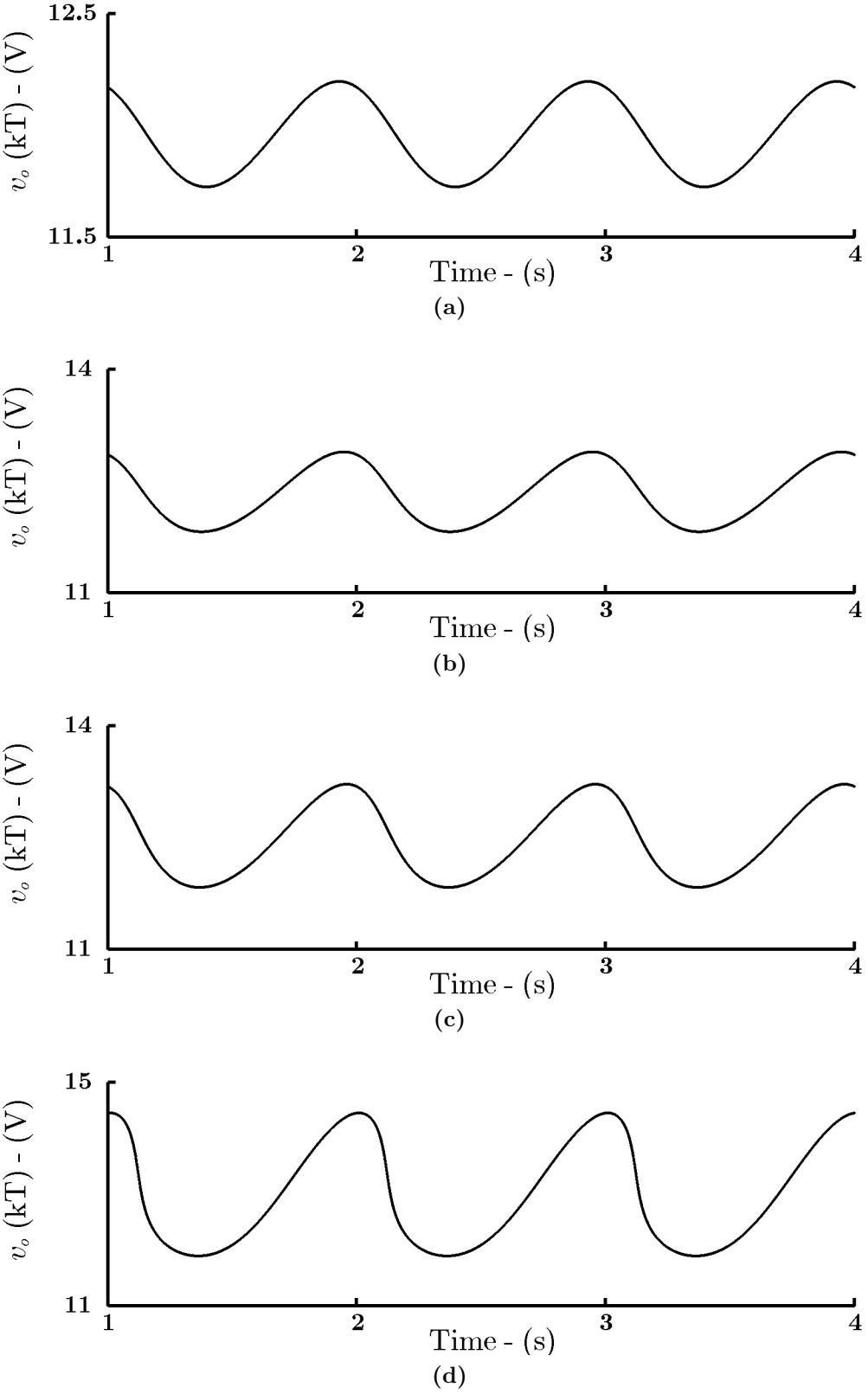

Figure 5.11: Time-bifurcation diagrams with k_u adjusted using the values from Table 5.3 (a) for (a) $\alpha_v = 0.16$ (b) $\alpha_v = 0.38$ (c) $\alpha_v = 0.5$ and (d) $\alpha_v = 1$ for $f_n = 2501$.

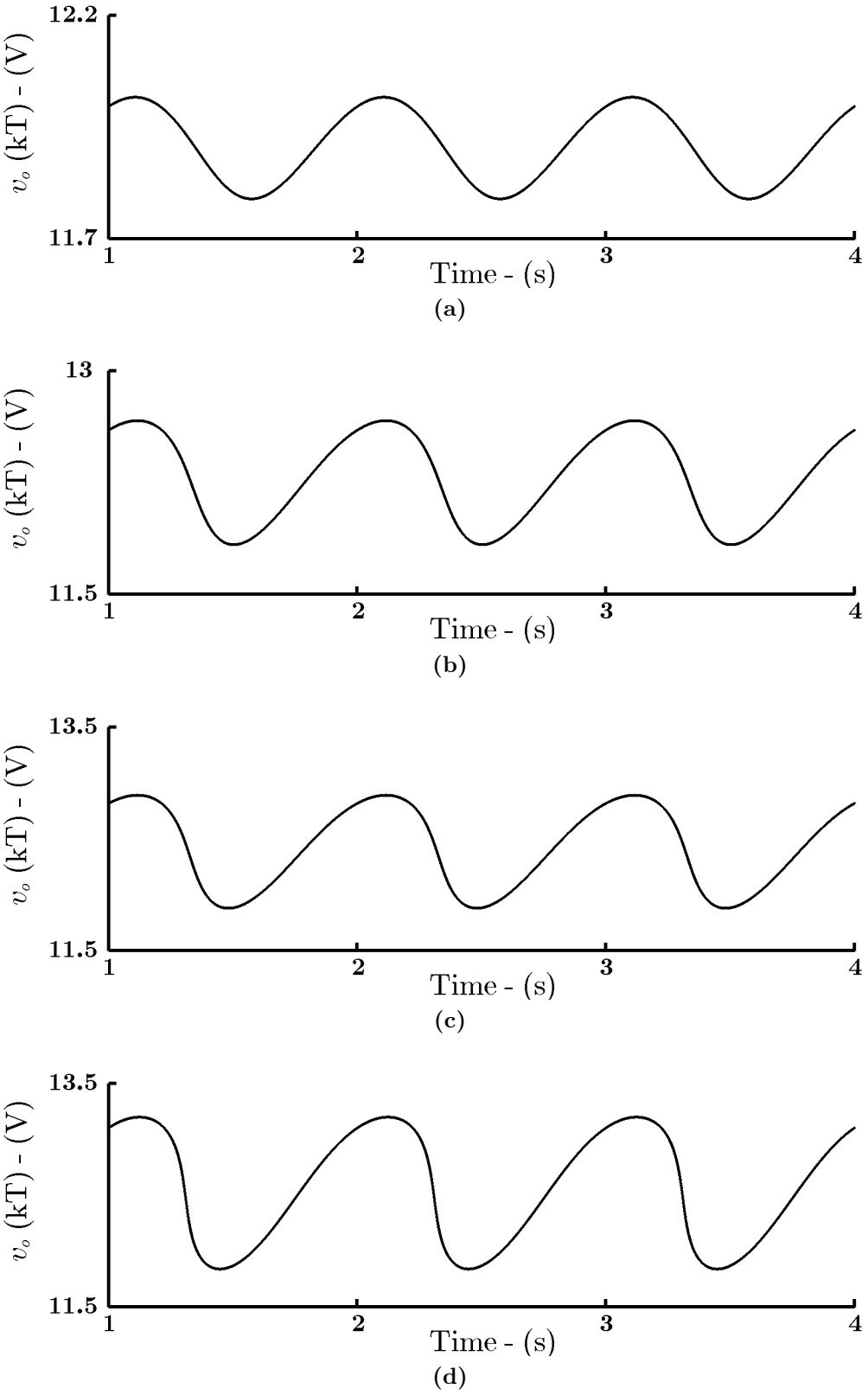

Figure 5.12: Time-bifurcation diagrams with k_u adjusted using the values from Table 5.3 (b) for (a) $\alpha_v = 0.16$ (b) $\alpha_v = 0.57$ (c) $\alpha_v = 0.7$ and (d) $\alpha_v = 1$ for $f_n = 5001$.

6 Filters in Digital Control

6.1 Introduction

In chapter 5, a buck converter operating with a digital controller was considered. However, the effects of quantization was removed in order to distinguish between the effects of noise and the digital controller. Quantization can cause limit cycling to occur [1]. A limit-cycle is a periodic orbit on the output with a frequency much smaller than that of the switching frequency. They can reduce the efficiency of the system. At present, high-resolution Digital Pulse Width Modulators (DPWMs) are used in order to reduce the effect of limit-cycle oscillations. However, the implementation of these high-resolution DPWM's is highly challenging [74]. Therefore, methods for the elimination of limit-cycles may have benefits in not only allowing for better performance but also in reducing the demand for high resolution DPWM's.

This research aims to address the issue of quantization-induced limit-cycles in a digitally controlled buck converter. Initially, how limit-cycles manifest themselves in digital systems is presented before considering filtering as a method to effect their elimination.

6.2 Previous approaches for limit-cycle control

A brief overview of previous approaches to limit-cycle control is presented.

Dithering is a method that can artificially increase the effective resolution of the DPWM . However, it can result in a decrease in the responsiveness of the system [11] and increase the output ripple [1]. Sigma-delta modulation is another method that can artificially increase the resolution of the DPWM. [75] investigates the use of a sigma-delta modulator by pre-processing the duty-cycle command and the authors state that no limit-cycles are observed. However, no rigorous analysis is done to ensure that limit-cycles do not exist. Furthermore, first-order modulators can cause unwanted tones to occur in the system. Therefore, higher-order modulators are required which are more expensive and difficult to implement. A similar approach is taken in [76].

The use of a non-uniform A/D quantizer is investigated in [77] in order to improve the dynamic response of the system and reduce the effect of limit-cycles. The describing method approach is used to analyse non-linearities and the circle criterion (a generalised approach of the Nyquist stability criterion [4]) to assess the stability of the proposed approach. However, the describing function assumes sinusoidal limit-cycles which may not always be the case. Furthermore, the author assumes that the DPWM resolution is high enough so that its influence on the non-linear dynamics can be ignored. Neither of these assumptions are always true. Another approach which considers altering the quantization process is presented in [78] by removing the zero-error bin from the system and replacing it with two error bins of finite amplitude. The author notes that this method does not remove limit-cycle oscillations but does reduce their amplitude, while not affecting the dynamic response of the system.

In [79], the authors suggest altering the reference voltage in order to minimise the amplitude of the oscillations. However, modifying the reference voltage may not be desirable or even possible in practical applications. [80] proposes applying the mean value of the duty-cycle to remove steady-state oscillations. However, the results show an increased settling time and oscillatory behaviour. A method for decreasing the effects of quantization is also presented in [81], by using geometrical considerations in order to synthesise a higher resolution A/D converter from a low resolution converter. While this method is effective at reducing the amplitude of the oscillations, it does not guarantee their complete removal.

[82] presents a mathematical model of the buck converter with digital integral control. Non-linear techniques are used to establish conditions for the existence of limit-cycles. In [83], Bradley then extends this work to a PI controller and includes the capacitor ESR. Rigorous conditions for the prediction of limit-cycles are established. In this chapter, the work of Bradley in [83] is extended from PI-control to PID-control as well as including the inductor ESR.

6.3 Behaviour of circuit

The buck converter with a digital PID controller is investigated in this chapter. Recall that the purpose of the buck converter is to step down an input voltage, V_{in}, to a lower output voltage, v_o, where $v_o = dV_{in}$ and d is the duty-cycle of switch SW_1 which is limited to the range $0 \leq d \leq 1$.

The buck converter is generally employed with a feedback mechanism. Without feedback, the system would be unable to take noise and load variations into account and consequently, the output voltage would not be guaranteed to be at the desired level. Figure 6.1 (a) shows the digital control loop used in this work. In this case,

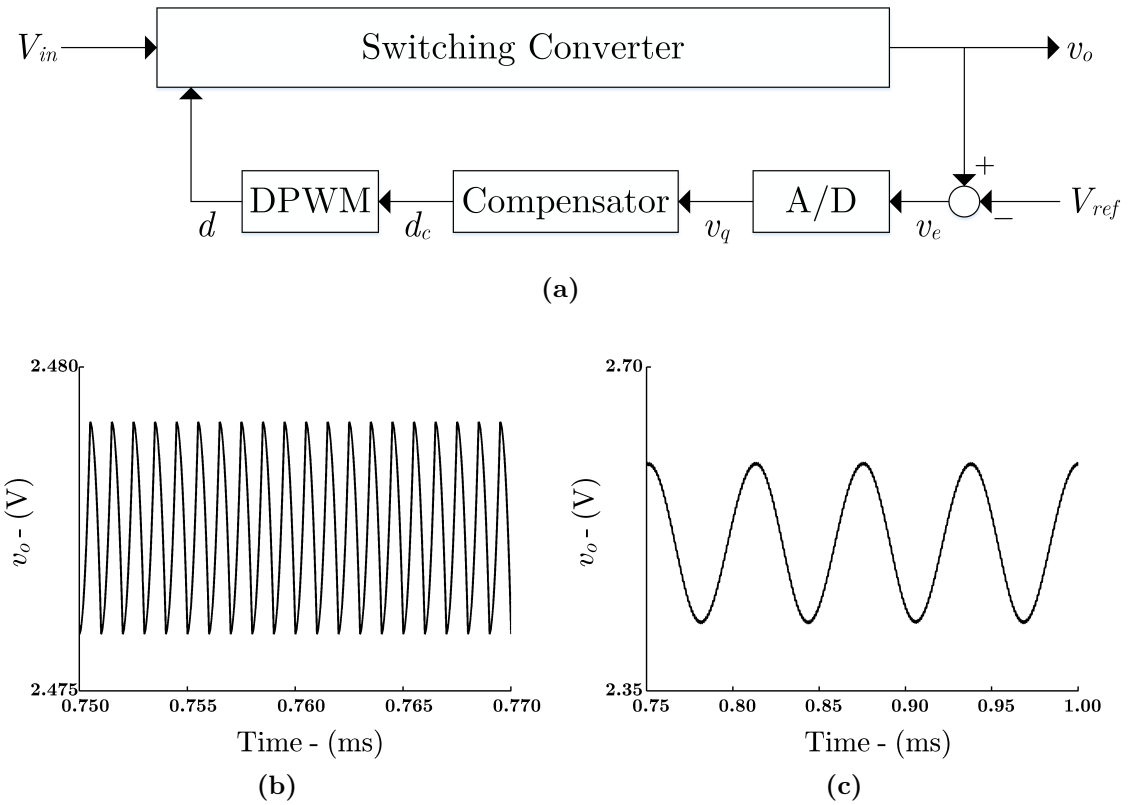

Figure 6.1: (a) Digital control loop. Steady-state response of the system with initial conditions (b) $v_o = 0\,(V)$ and $u = 0\,(V)$ and (c) $v_o = 2.47\,(V)$ and $u = 0.015\,(V)$.

the output voltage is compared to the reference voltage, V_{ref}, which is at the desired voltage. This generates the error signal, v_e. The error signal is then sampled and quantized by the A/D converter to generate the quantized error voltage, v_q. This control signal takes the form $lq_{A/D}$ where $q_{A/D}$ is the quantization step, or resolution, of the A/D converter and $l \in \mathbb{Z}$. The digital compensator then adjusts the duty-cycle command, d_c, which is sent to the DPWM. In this work, a PID control law is considered. The DPWM acts as a D/A converter taking d_c as an input and produces the duty-cycle which is used to open and close the switches. The digital to analog conversion involves some quantization. The duty-cycle command is quantized to values of the form jq_{DPWM}, where $j \in \mathbb{N}$ and q_{DPWM} is the quantization step of the DPWM.

The function of the control loop is to change the duty-cycle in order to move the output voltage closer to V_{ref}. However, owing to the effects of quantization, the duty-cycle can only take on a finite number of values and it may occur that the duty-cycle moves between two or more duty-cycle levels of the form jq_{DPWM}. This movement can cause limit-cycle oscillations on the output. In Figure 6.1 (b) and (c), some examples of the steady-state behaviour observed in the system are shown. In (b), the desired output of the system with zero initial conditions is illustrated. While there is some small ripple, which has the same frequency as the switching frequency, the output is close to the desired voltage level. However, in (c), with non-zero

initial conditions, the output voltage is seen to oscillate with a large amplitude of low frequency, compared to the ripple voltage, with the ripple voltage superimposed on this. This is a limit-cycle. It is important to note, that two different steady-state behaviours are possible with the same parameter values and thus, the steady-state behaviour is dependent on the initial conditions.

6.4 System Model

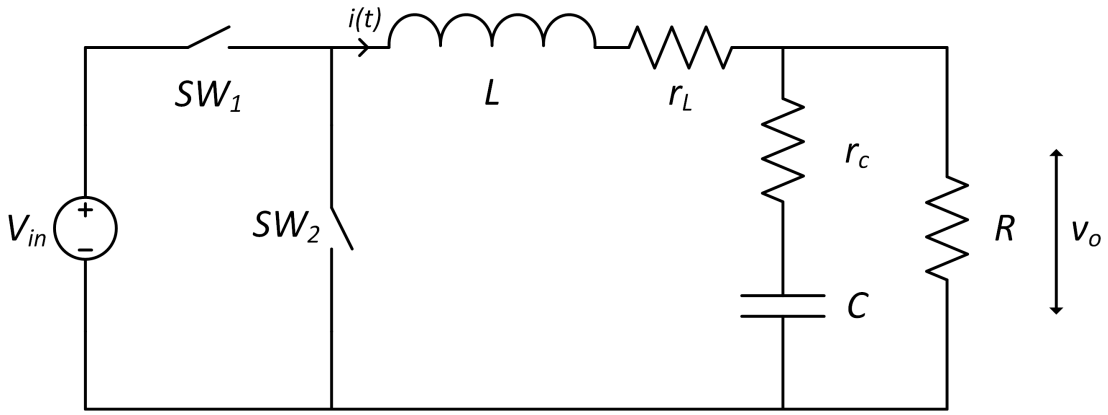

Figure 6.2: Buck converter inclusive of capacitor and inductor ESR with the following parameters: $V_{in} = 5$, $V_{ref} = 2.51\,V$, $K_I = 0.0008$, $K_P = 0.005$, $K_D = 0.00008$, $q_{A/D} = 0.101\,V$, $q_{DPWM} = 0.004\,V$, $R = 10\,\Omega$, $C = 13.52\,\mu F$, $L = 7.62\,\mu H$, $r_c = 0.02\,\Omega$ and $r_l = 0.01\,\Omega$.

The buck converter inclusive of the capacitor and inductor ESR is shown in Figure 6.2. Recall the equations describing the buck converter from chapter 4

$$\dot{x} = \begin{cases} f_{on}(x,t) = & A_{on}x + B_{on}x_{in} & SW_1 \text{ is on} \\ f_{off}(x,t) = & A_{off}x + B_{off}x_{in} & SW_1 \text{ is off} \end{cases} \tag{6.1}$$

The state variable $\boldsymbol{x}$ is the transformed state variable as in Chapter 4 which is employed to simplify the equations and form a symmetrical system. Thus, $x = \begin{bmatrix} v_o & u \end{bmatrix}$ and

$$u(t) = \left(\frac{LR - r_C r_L RC}{LCR_N\omega}\right) i(t) + \left(\frac{Rr_L - Rr_C + r_C r_L}{2LR_N\omega} - \frac{1}{2CR_N\omega}\right) v_o(t)$$

where $R_N = R + r_C$. The state matrices are given by:

$$\boldsymbol{A} = \boldsymbol{A}_{on} = \boldsymbol{A}_{off} = \begin{bmatrix} -\sigma & \omega \\ -\omega & -\sigma \end{bmatrix}$$

$$B_{on} = \begin{bmatrix} \frac{r_C R}{LR_N} \\ \frac{LR - r_C r_L RC}{L^2 CR_N\omega} + \frac{Rr_C(LCR_N\sigma - L - RCr_C)}{L^2 R_N^2 C\omega} \end{bmatrix}, \; B_{off} = \begin{bmatrix} 0 \\ 0 \end{bmatrix}$$

$$x(t) = \begin{bmatrix} v_o \\ u \end{bmatrix}, \; x_{in} = V_{in}$$

with $\sigma = \frac{Rr_L + Rr_C + r_C r_L}{2LR_N} + \frac{1}{2CR_N}$ and $\omega = \sqrt{\frac{R+r_L}{LCR_N} - \sigma^2}$. If the system operates with SW_1 closed for dT and open for $(1-d)T$, then mapping of the state variable $\boldsymbol{x}$ from the start of the switching period at t_0 to the end of the switching period at $t_0 + T$ is given by

$$x\left(t_0 + T\right) = e^{AT} x\left(t_0\right) + \left(e^{A(1-d)T} - e^{AT}\right)\left(-A^{-1} B_{on}\right) V_{in} \tag{6.2}$$

The compensator in this work is a PID controller. Its control law is

$$K_P v_e + K_I \int v_e d\tau + K_D \frac{d}{dt}\left(v_e\right)$$

Stroboscopic sampling is used thus, the start of the switching period coincides with the start of the sampling period. Assuming that any quantization in the compensator can be neglected and employing the Backward Euler method, the discrete-time control law can be written as:

$$\begin{aligned} d_c(k+1) = \; & d_c(k) - K_P\left(v_q(k+1) - v_q(k)\right) - K_I v_q(k+1) \\ & - K_D\left(v_q(k+1) - 2v_q(k) + v_q(k-1)\right) \end{aligned} \tag{6.3}$$

The A/D converter is modelled using the equation:

$$v_q(k) = Q_{A/D}\left\{v_e(k)\right\} \tag{6.4}$$

where the quantizer is modelled using:

$$Q_{A/D}\left\{v_e(k)\right\} = \left\lfloor \frac{v_e(k) + \frac{q_{A/D}}{2}}{q_{A/D}} \right\rfloor q_{A/D}$$

where the floor function, $\lfloor\rfloor$, rounds the input down to the closest integer value. This rounds the value of $v_e(k)$ to a value of the form $lq_{A/D}$. If $v_q(k) = lq_{A/D}$, the voltage is said to be in the l^{th} error bin. The duty-cycle command is also quantized to give the duty-cycle:

$$d(k) = Q_{DPWM}\left\{d_c(k)\right\} \tag{6.5}$$

where the Q_{DPWM} is defined by:

$$Q_{DPWM}\left\{d_c(k)\right\} = \left\lfloor \frac{d_c(k) + \frac{q_{DPWM}}{2}}{q_{DPWM}} \right\rfloor q_{DPWM}$$

A discrete-time map relating events at the end of the switching period to those at

the start of the switching period is given as:

$$x(k+1) = e^{AT}\boldsymbol{x}(k) + \left(e^{A(1-d)T} - e^{AT}\right)\left(-A^{-1}B_{on}\right)V_{in} \tag{6.6}$$

$$\begin{aligned} d_c(k+1) = \; & d_c(k) - K_P\left(v_q(k+1) - v_q(k)\right) - K_I v_q(k+1) \\ & -K_D\left(v_q(k+1) - 2v_q(k) + v_q(k-1)\right) \end{aligned} \tag{6.7}$$

with the quantized values $v_q(k)$ and $d(k)$ given by (6.4) and (6.5), respectively. Whenever d_c lies in the set $\left[\left(j-\frac{1}{2}\right)q_{DPWM}, \left(j+\frac{1}{2}\right)q_{DPWM}\right]$, the value of d is equal to $d_j = jq_{DPWM}$ subject to the constraint $0 \leq d \leq 1$. If $\boldsymbol{x}(k+1) = \boldsymbol{x}(k)$, then this is a fixed point in the system. (6.6) can be rewritten as $\boldsymbol{x}(k+1) - \boldsymbol{x}_j^* = e^{\boldsymbol{AT}}\left(\boldsymbol{x}(k) - \boldsymbol{x}_j^*\right)$, where:

$$x_j^* = \left(I - e^{AT}\right)^{-1}\left(e^{A(1-d_j)T} - e^{AT}\right)\left(-A^{-1}B_{on}\right)V_{in}$$

For each value of $d = d_j = jq_{DPWM}$, trajectories in $\boldsymbol{x}$ are logarithmic spirals winding towards the corresponding fixed point, x_j^*. Every trajectory consists of successive logarithmic spirals winding towards different fixed points as d_c passes from one quantization level to another. The change in d_c is determined by the quantization level occupied by v_o:

- When the output is in the l^{th} error bin, $v_q(k+1) = lq_{A/D}$. There is a step in the control law due to the integral term of $\Delta d_c(k+1) = d_c(k+1) - d_c(k) = -K_I v_q(k+1)$.
- When the output moves between two error bins, there is a step in the control law due to the proportional term of $-K_P\left(v_q(k+1) - v_q(k)\right)$ and the derivative term of $-K_D\left(v_q(k+1) - 2v_q(k) + v_q(k-1)\right)$ and the integral term of $-K_I v_q(k+1)$.
- When the output voltage stays in the same error bin for three or more iterations then $v_q(k+1) = v_q(k) = v_q(k-1)$, the proportional term and the derivative term have no effect. Any change in d_c is due to the integral component.
- When the output voltage is in the zero error bin for three or more iterations, there is no change in d_c due to $v_q(k+1) = v_q(k) = v_q(k-1) = 0$ i.e. the duty-cycle command is fixed.

6.5 Occurrence of limit-cycles

In order to establish the effect that quantization has on the nonlinear dynamics of the buck converter, the system is first modelled without quantization and compared to the case with quantization. With quantization removed, $v_e(k) = v_q(k)$ and $d(k) = d_c(k)$, subject to the constraint $0 \leq d \leq 1$.

The sampled steady-state response of the system without and with quantization is illustrated in Figure 6.3 (a) and (b). In (a), the system is seen to settle to a

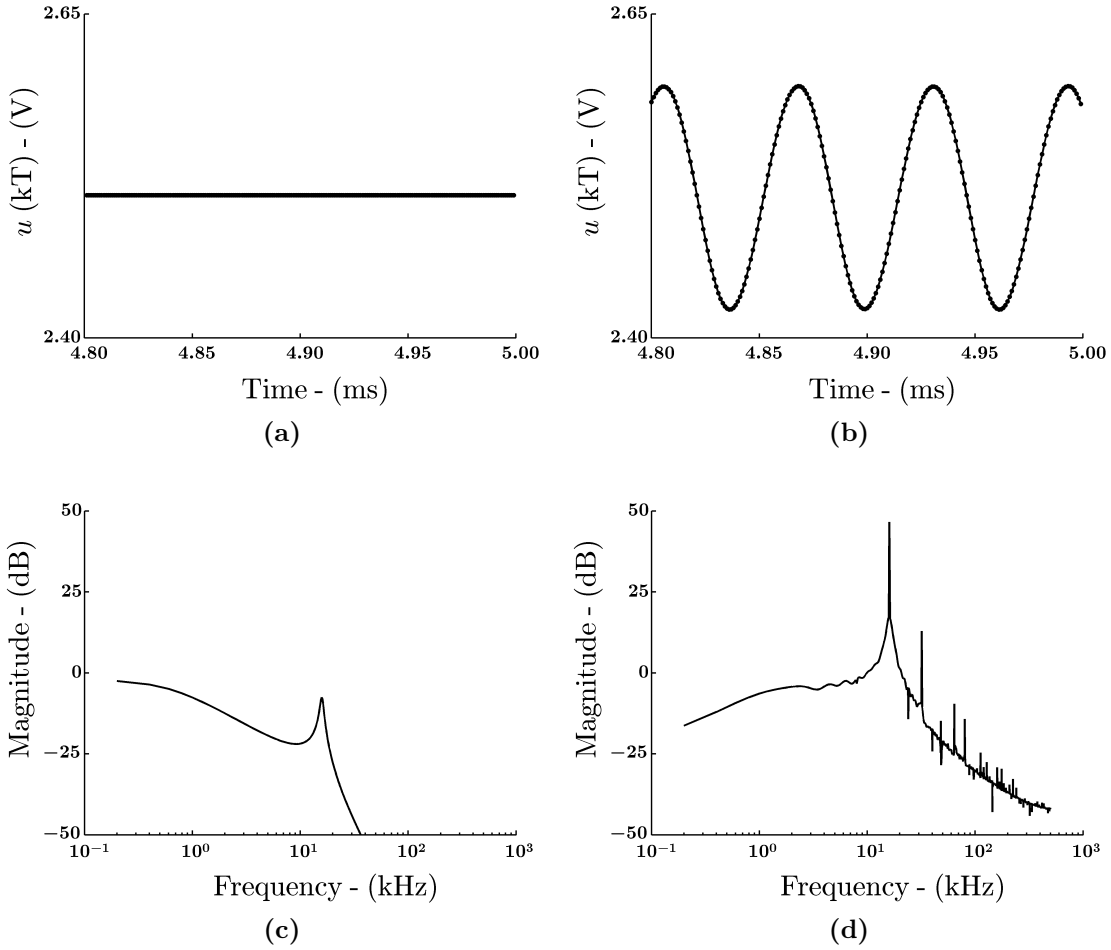

Figure 6.3: Sampled steady-state response (a) without quantization (b) with quantization. Frequency response of system (c) without quantization and (d) with quantization.

steady-state value with no oscillations on the output. It is important to note that voltage ripple is present in the system. However, since the output is sampled once per switching cycle, the ripple is excluded from the plot. In (b), when quantization is employed, the output does not settle to a steady-state value and instead oscillates between $2.4 \rightarrow 2.6\,(V)$ i.e. a limit-cycle is present.

A similar scenario can be seen in (c) and (d), where the frequency response of the system without quantization and with quantization is plotted, respectively. A large spur is present in (d) that is not present in (c) at approximately $16\,(kHz)$. This is much lower than the switching frequency of $1\,(MHz)$ and indicates the system is oscillating at this frequency. It is clear that the introduction of quantization has induced limit-cycle oscillations on the output. The frequency of the limit-cycle is $16\,(kHz)$.

An obvious question is, how do limit-cycles manifest themselves through quantization? Consider the simplest case; a limit-cycle oscillation over two duty-cycle levels. This is illustrated in Figure 6.4 (a). In this instance, the phase portrait of the sin-

gle loop limit-cycle from Figure 6.3 (b) is shown. The limit-cycle is confined to the ± 1 and 0 error bins. The duty-cycle switches between two levels at $d = 0.5$ and $d = 0.504$. Starting at $SP_{0.5}$ and moving clockwise, the output rotates about the fixed point $\boldsymbol{x}^*_{0.5}$ with $d = 0.5$. At $SP_{0.504}$, the duty-cycle changes to $d = 0.504$ and the system winds about the fixed point $\boldsymbol{x}^*_{0.504}$ until $SP_{0.5}$ is reached again. The dynamics of this motion and the interaction between the duty-cycle command, the duty-cycle and the error bins is now discussed.

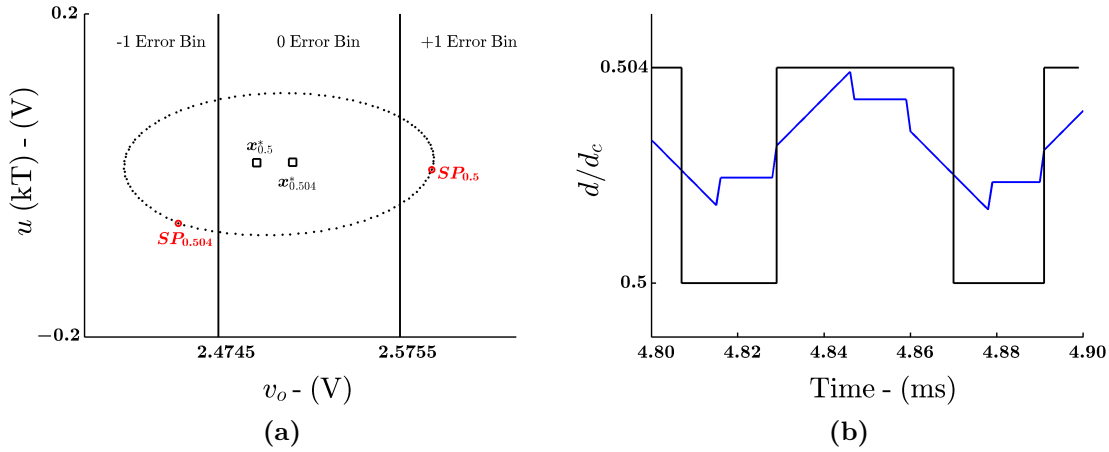

Figure 6.4: (a) Single loop limit-cycle rotating about two fixed point $x^*_{0.5}$ and $x^*_{0.504}$. The trajectory is marked with black dots, the switching points between duty levels with red circles and the fixed points with black squares. (b) How d (black) and d_c (blue) vary with time when a limit-cycle is present.

In Figure 6.4 (a), let the trajectory have P iterations. The frequency of the limit is therefore given by $\omega_{osc} = \frac{2\pi}{PT}$. Starting at $SP_{0.5}$, and moving clockwise, the trajectory winds about $\boldsymbol{x}^*_{0.5}$. Let this motion have p_1 iterations. At $SP_{0.504}$, the duty-cycle changes to 0.504 and the trajectory winds about $\boldsymbol{x}^*_{0.504}$. Let this motion have p_2 iterations. Thus, $P = p_1 + p_2$. Oscillations moving in this manner about fixed points are deemed to be limit-cycles.

Recall the control law for the PID controller given in (6.7). Figure 6.4 (b) illustrates how the duty-cycle, d, and the duty-cycle command, d_c, vary for the limit-cycle presented in (a).

Consider the evolution of the limit-cycles trajectory from $SP_{0.5}$ to $SP_{0.504}$. Let there be N_b iterations in the +1 error bin, N_0 iterations in the 0 error bin and N_c iterations in the -1 error bin. In the +1 error bin $v_q = q_{A/D}$, in the 0 error bin $v_q = 0$ and in the -1 error bin $v_q = -q_{A/D}$. The trajectory starts in the +1 error bin, assuming it has occupied this bin for three or more switching cycles, $v_q(k+1) - v_q(k) = 0$ meaning that the proportional term has no effect. Also, $v_q(k+1) - 2v_q(k) + v_q(k-1) = 0$, meaning that the derivative term has no effect. However, since $v_q(k+1) = q_{A/D}$, the integral term causes d_c to decrease by $-K_I q_{A/D}$ for each iteration in the +1 error bin. The total change in d_c for this section is $\Delta d_{cb} = N_b \left(-K_I q_{A/D}\right)$.

The trajectory then enters the 0 error bin.

- The first iteration in the bin. In this case, $v_q(k+1) = 0$ and $v_q(k) = v_q(k-1) = q_{A/D}$. The proportional term causes the duty-cycle command to jump by a distance $K_P q_{A/D}$ and the derivative term causes a jump of $-K_D(-2q_{A/D} + q_{A/D}) = K_D q_{A/D}$. The integral term has no effect. Thus, the net change in d_c is $(K_P + K_D)q_{A/D}$.
- The second iteration in the bin. In this case, $v_q(k+1) = v_q(k) = 0$ and $v_q(k-1) = q_{A/D}$. The integral and proportional term have no effect. However, the derivative term causes a jump of $-K_D q_{A/D}$.
- The remaining $N_0 - 2$ iterations. Since $v_q(k+1) = v_q(k) = v_q(k-1) = 0$, none of the control terms will alter d_c. Thus, the duty-cycle command remains constant during this period.
- The net change in d_c in the zero error bin is $\Delta d_{c0} = K_P q_{A/D}$.

Upon leaving the 0 error bin, the trajectory enters the -1 error bin.

- The first iteration in the bin. In this case $v_q(k+1) = -q_{A/D}$ and $v_q(k) = v_q(k-1) = 0$. All three control terms have an effect on d_c. The proportional term causes a jump of $K_P q_{A/D}$, the derivative term causes a jump of $K_D q_{A/D}$ and the integral term a jump of $K_I q_{A/D}$. The combined effect of the three terms is $(K_P + K_I + K_D)\, q_{A/D}$.
- The second iteration in the bin. In this case $v_q(k+1) = v_q(k) = -q_{A/D}$ and $v_q(k-1) = 0$. Since $v_q(k+1) - v_q(k) = 0$, the proportional term has no effect. The change due to the integral term is $K_I q_{A/D}$ and the change due to the derivative term is $-K_D\,(v_q(k+1) - 2v_q(k)) = -K_D q_{A/D}$. The combined change is therefore the net change is $(K_I - K_D)q_{A/D}$.
- The output stays in this bin for $N_c - 2$ iterations before reaching $SP_{0.504}$. For the remaining $N_c - 2$ iterations, since $v_q(k+1) = v_q(k) = v_q(k-1) = -q_{A/D}$, the integral term causes the duty-cycle command to jump by $K_I q_{A/D}$ on each iteration within the bin and the proportional term and the derivative term have no effect.
- The net change in d_c in the -1 error bin is $\Delta d_{cc} = K_P q_{A/D} + N_c K_I q_{A/D}$.

Similar dynamics move the trajectory from $SP_{0.504}$ back to $SP_{0.5}$.

6.6 Filtering limit-cycle oscillations

The previous section explained in detail how quantization-induced limit-cycles can manifest themselves in a digitally controlled buck converter. Now, a method to effect their elimination is considered. The frequency of the limit-cycle is dependent

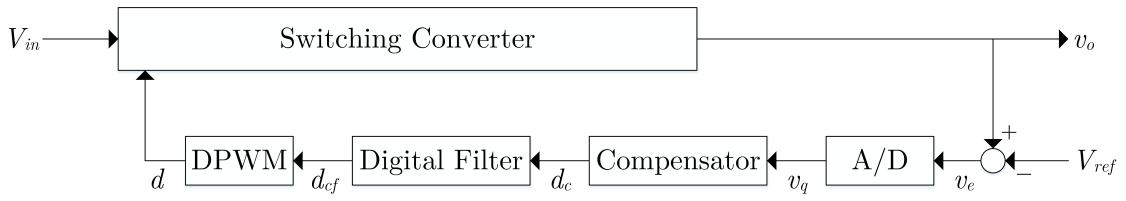

Figure 6.5: Digital control loop inclusive of digital filter.

on the K_P/K_I ratio and therefore, has a fixed frequency, assuming that the control parameters are fixed. If the frequency of the limit-cycle is known, then a simple filter can be used to eliminate it. Figure 6.5 shows the proposed control loop. Placing a digital filter directly after the compensator and filtering the duty-cycle command creates a new signal, d_{cf}, the filtered duty-cycle command. The function of the digital filter is to remove oscillations at the limit-cycle frequency. The rest of the control loop works as described in Section 6.3. The simplest type of filter to first consider is the notch filter.

6.6.1 Implementation of a notch filter

A band-stop filter is a filter that allows most frequencies to pass and attenuates those in a specific range to very low levels, this range is known as the stop-band [84]. A notch filter is a specific type of band-stop filter where the stop-band is narrow. The function of the notch filter is to create a null in the frequency domain at the limit-cycle frequency to effect its elimination while allowing other frequencies to pass. The transfer function of the notch filter is

$$H(z) = \alpha \left(1 - 2\cos\left(\omega_{LC} T\right) z^{-1} + z^{-2}\right) \tag{6.8}$$

where the coefficient α is set so that the transfer function has a unity magnitude at $0\,(Hz)$ and ω_{LC} is the frequency of the limit-cycle in radians. The filter has a zero magnitude response at ω_{LC}. Figure 6.6 (a) shows the magnitude response of the filter described by (6.8). It is clear that the filter has unity magnitude at $0\,(Hz)$ and zero magnitude at $16\,(kHz)$, which is the frequency of the limit-cycle presented in Figure 6.3 (b).

This filter is an example of a finite impulse response (FIR) filter. An FIR filter is one whose impulse response is of finite duration as it settles to zero in finite time. In contrast, the infinite impulse response (IIR) filter may continue to respond indefinitely to an impulse. The main advantage of an FIR filter compared to an IIR filter is that FIR filters have intrinsically stable implementations [85].

Figure 6.6 (b) demonstrates the effectiveness of placing the notch filter in the feedback path of the control loop. Using the initial conditions from Figure 6.1 (a), the system starts with limit-cycle oscillations on the output. However, the notch filter

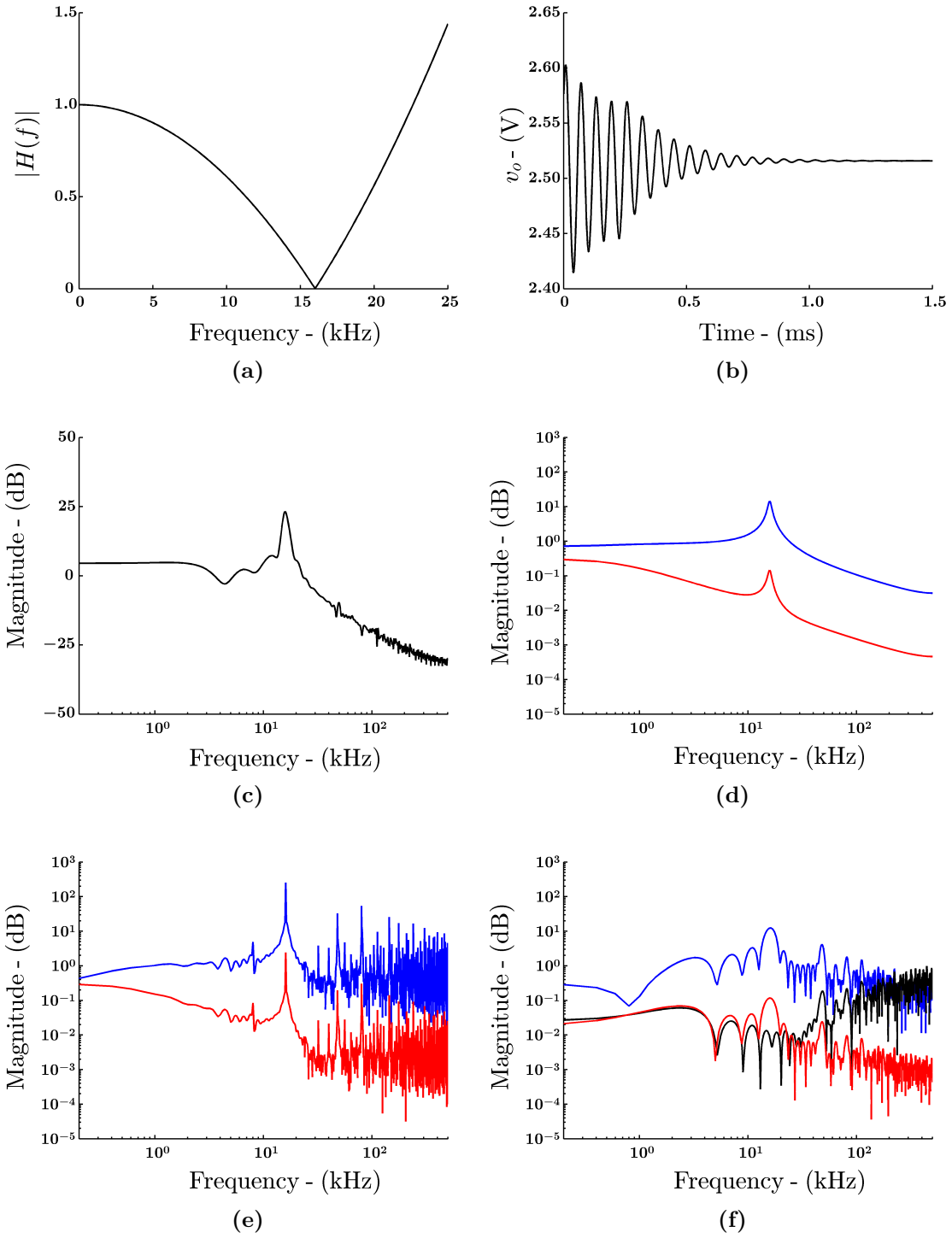

Figure 6.6: (a) Magnitude response of the notch filter (b) Transient response of the system (c) Frequency response of the system (d) Frequency spectra of v_e (blue) and d_c (red) with quantization removed and no filter (e) Frequency spectra of v_q (blue) and d_c (red) when no filter is used and (f) Frequency spectra of v_q (blue), d_c (red) and d_{cf} (black) when the notch filter is used.

dampens the oscillations and the system settles to the desired period-1 orbit. A similar picture is shown in (c), where previously a large spur was shown at $16\,(kHz)$ in the frequency response in Figure 6.3 (d), while the notch filter does not completely remove the spur, its amplitude is greatly reduced.

In (d), the frequency spectra of several signals in the control loop with the effects of quantization removed is plotted. In (e), the frequency spectra with the effects of quantization included but without the digital filter is shown. It is evident that the quantization introduces a lot of high frequency content. In (f), the frequency spectra with the effects of quantization included and with a digital filter is considered. The notch filter is successful in reducing the magnitude at higher frequencies, it is seen that the notch filter actually increases the magnitude of the response when d_c and d_{cf} are compared. In some applications, this may not be acceptable. Thus, the aim of the filter now is to improve dampening at high frequencies. For this reason, a comb filter is considered as this creates a null in the frequency domain at the limit-cycle frequency and at higher frequencies.

It is important to note that the digital filter has an indirect effect on signals in the feedback loop. Since it filters d_c, this has an effect on the duty cycle and thus, the output voltage which is the input to the feedback path. For this reason, d_c in (e) and (f) are different.

6.6.2 Comb filter implementation

A comb filter creates a null in the frequency domain at evenly spaced intervals spread across the frequency domain [86] as illustrated in Figure 6.7 (a) where a null can be seen at the limit-cycle frequency of $16\,(kHz)$ and at evenly spaced intervals. The first null can be used to eliminate oscillations at the limit-cycle frequency. In addition, the filter eliminates higher frequencies and thus, should reduce the effect of the high-frequency content induced by quantization. Figure 6.7 (b) shows the phase response of the filter. It is evident that the comb filter introduces a significant phase lag which would have to be considered in designs and related stability issues. However, if the frequency to be eliminated is close to the resonant frequency of the system, the increased phase lag may not be as important as the loop gain falls before it rises again. The filter is made up of a direct signal and a delayed version. Its transfer function is given as

$$H(z) = 1 - \alpha\left(2 - z^{-N}\right)(1 - g) \tag{6.9}$$

g is the gain parameter where $0 \leq g \leq 1$. It affects the magnitude of the response at the null frequency. Similar to the notch filter, α and g are selected to give unity around the null frequency. The N value determines where the first null in the

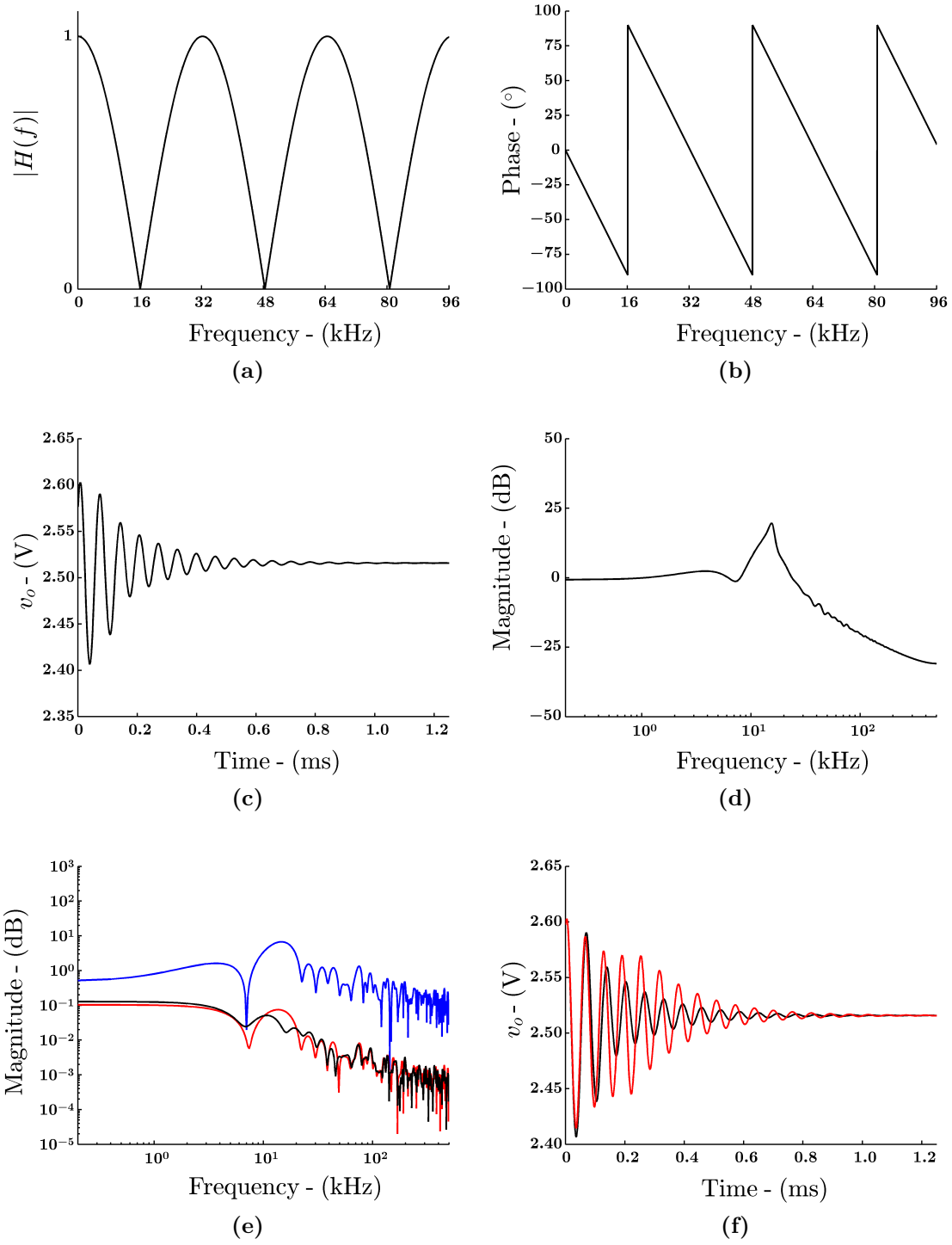

Figure 6.7: (a) Magnitude response of the comb filter (b) Phase response of the filter (c) Transient response of the system (d) Frequency response of the system (e) Frequency spectra of v_q (blue), d_c (red) and d_{cf} (black) and (f) Transient response of both comb filter (black) and notch filter (red).

frequency gain occurs. For this application, the appropriate values are $\alpha = 0.5$, $g = 0$ and $N = 31$. This gives unity at $0\,(Hz)$ and a null at $16\,(kHz)$.

From Figure 6.7 (c), it is clear that limit-cycle oscillations are effectively removed by the comb filter. After an initial oscillation, the system settles to the desired period-1 orbit. This is further illustrated in (d), where the frequency response of the output voltage can be seen. There is a large reduction in the amplitude of the spur at the limit-cycle frequency. Furthermore, the high-frequency content introduced by quantization is greatly reduced compared to Figure 6.6 (c).

Figure 6.7 (e) shows the frequency response of some of the control signals. For the v_q frequency spectrum, the comb filter performs at a similar level to the notch filter. However, when comparing both filters with respect to the d_c and d frequency spectra, it is clear that the comb filter outperforms the notch filter in this regard. After passing through the filter, the notch filter causes the magnitude of the response to increase at high frequencies while the comb filter maintains the response below $10^{-1}\,(dB)$. Furthermore, in (f), the transient response of both the notch filter and comb filter are plotted. It is clear that while both are effective in removing limit-cycle oscillations, the settling time with the comb filter is superior to that when the notch filter is employed. It is clear from this analysis, that the comb filter is more suited for this application.

6.7 Conclusion

A model of a digitally controlled buck converter was derived. It included both capacitor and inductor ESR. The steady-state behaviour of the system, the occurrence of fixed points and limit-cycles were investigated. The issue of quantization-induced limit-cycles and how they manifest themselves in digitally controlled systems was described in detail. Two types of filters were considered to effect their elimination; a notch filter and a comb filter. While the notch filter was effective in dampening the limit-cycle oscillations, it was shown that the quantization effects introduced a lot of high-frequency content. The notch filter was not adept at removing or dampening these effects. In contrast, the comb filter was both effective at removing limit-cycle oscillations and dampening the high-frequency content. Furthermore, the comb filter had a better transient response. Thus, the comb filter is more suited to removing limit-cycle oscillations. However, the comb filter creates a null in the frequency domain at evenly spaced intervals spread across the frequency domain. If the buck converter is required to operate close to once of these frequencies, the comb filter may not be suitable. In this case, a notch filter is recommended.

7 Conclusions

The conclusions arrived at from the research carried out to investigate the occurrence of bifurcations in dc-dc converters and methods to effect their elimination are presented below. Extensive mathematical analyses has been carried out to determine the critical value at which bifurcations occur and simulations verify the validity of the analyses using MATLAB® [65].

Chapter 2 presented a general introduction to the area of nonlinear dynamics. The different types of bifurcations were categorised as well as the common modes of operation exhibited by power electronic converters. The mathematical tools employed to analyse both linear and nonlinear systems were presented along with a derivation of the Filippov method.

Chapter 3 considered the area of dc-dc converters in power electronics. The buck converter was introduced as it forms the basis for the majority of the work in this thesis. Common control techniques used in power electronic converters were discussed as well as the various modelling techniques used in previous works. A survey of previous works concerned with nonlinear analysis of converters was presented, as well as, techniques for controlling the nonlinear behaviours which occur in these circuits.

In Chapter 4, a buck converter with a PID controller was considered. The D-term has been traditionally avoided as it can cause the amplification of noise or inject significant noise into the closed-loop system. On the other hand, the requirement for a fast transient response means the D-term is required. However, little or no work exists on design procedures for PID controller to take into consideration fast-scale instabilities. First, the behaviour found in the system was characterised and the system model was presented. The types of steady-state behaviour exhibited by the system were observed as various parameters were varied, such as the PID control terms and the ramp characteristics, and the system underwent fast-scale bifurcations. It was shown that the inclusion of the D-term not only improves the transient response but also increases the stability margin of the system. However, it is important to note that the inclusion of the D-term must be done with great caution due to the aforementioned problems associated with it.

The research then proceeded to introduce the main framework of how a PID controlled buck converter can be designed to include the consideration of fast-scale in-

stabilities. Specifically, the Filippov method was applied to derive stability bounds to ensure stable period-1 operation which enables designers to select control parameters that will ensure stable behaviour without using high gains the can cause noise problems. This work enabled the development of an adaptive PID controller whereby the D-term is updated at the end of every switching cycle as the load and other characteristics vary. By simulating a step change in the load resistance, the system without the adaptive controller was shown to undergo a period-doubling bifurcation. However, when the adaptive controller was employed, the system maintained stable operation.

The Filippov method requires a smooth scalar function for the manifold that describes the switching action. However, when the D-term is employed, the resulting functions may be non-smooth. Therefore, it is not straightforward to apply this method for such converters and a modification to the Filippov method is required. This work presented a technique for this modification and verified its validity through simulations. How the Filippov method can be used to derive the saltation matrix with a non-smooth switching manifold was detailed.

However, the work in chapter 4 assumes ideal operating conditions and ideal sources. In practical applications, these cannot be guaranteed. Noise signals may arise because of finite input capacitances, ESR of the input capacitor or stray inductance and stray capacitance in a circuit. Thus, Chapter 5 considered a buck converter with a digital state-feedback controller where the input voltage is perturbed by a sinusoidal signal. Since the frequency of the noise signal is unpredictable, all values must be considered. Three categories for the ratio of the noise frequency to the switching frequency were established:

1. When the noise frequency is an integer multiple of the switching frequency.
2. When the noise frequency is an irrational multiple of the switching frequency.
3. When the noise frequency is a rational multiple of the noise frequency but close to one of the integer multiples.

For integer multiples, the system operated with the desired period-1 orbit. For irrational multiples, the system operated with quasi-periodic behaviour. For rational multiples close to integer multiples, intermittent operation was observed on the output. The intermittent operation was shown through the use of time-bifurcation diagrams. However, conventional bifurcation analysis cannot be carried out on these. Instead, a transformation was performed to relate changes in time to changes in another variable. This enabled parameter bifurcation diagrams to be used and thus, conventional bifurcation analysis. Mathematical analysis was performed to identify the critical value at which intermittent operation occurred using Filippov's method. Designers are able to select the controller parameters to avoid intermittent operation and an adaptive controller was proposed. The adaptive controller was

shown to eliminate intermittency.

While digital control was considered in Chapter 5, in order to distinguish between the effects of noise and the effect of the digital implementation, the resolution of the quantizer was assumed to be infinitely small. The effect of quantization on the nonlinear dynamics of the converters was investigated in Chapter 6. A buck converter controlled by a digital PID controller was considered. The types of steady-state behaviour seen in the system was described and compared to the analog implementation. It was shown that quantization can induce limit-cycle oscillations. However, the occurrence of limit cycles is dependent on the initial conditions. An analysis of limit cycles on two duty cycle levels was presented as well as a thorough explanation of how limit cycles manifest themselves in digital controllers.

Unlike the previous chapters, limit-cycles cannot be prevented in the system by simply reducing the gain parameters. Instead, filtering was considered as a method to effect their elimination. Two filters were considered; a notch filter and a comb filter. Placing the filter in the feedback path, it was shown that the notch filter was effective at dampening limit-cycle oscillations. However, quantization introduces a lot of high-frequency content. The notch filter was not effective at dampening the high-frequency content as it only creates one null in the frequency domain at the limit-cycle frequency. Therefore, a comb filter was employed as it creates a null at evenly spaced intervals spread across the frequency domain. The comb filter was effective at dampening limit-cycle oscillations as well as dampening the high-frequency content. The transient response when the comb filter and when the notch filter were used were compared. The comb filter had a faster settling time and is the recommended filter for removing limit-cycle oscillations. However, since the comb filter creates a null in the frequency domain at evenly spread intervals, if the buck converter is required to operate close to one of these frequency, the comb filter may not be suitable. In this case, the notch filter is recommended.

7.1 Scope for future work

With advances in technology, digital control has become a potentially advantageous alternative to analog control. Some of the potential advantages include low power, immunity to analog component variations, compatibility with digital systems and a faster design process [1]. However, digital control of power electronic systems is a field that requires intensive study to completely understand the nonlinear dynamics so as to enable accurate and economic designs. The following areas require further investigation:

- One of the main advantages of digital control is the ability to design more sophisticated control strategies to enable high performance dc-dc converters

to be designed. Digital state-feedback controllers are frequently used in dc-dc converters when high/optimal performance is required. However, little work exists on the nonlinear dynamics of such systems, particularly the effect of quantization. Quantization can induce limit-cycles which greatly reduce the efficiency of the converter. Thus, knowledge of when they occur and techniques for their elimination are required.

- In the work of [49], Bradley derives conditions for a buck converter with a PI digital controller to ensure no limit-cycle oscillations. These conditions are a function of the resolution of the A/D converter, the D/A converter and other system parameters. At present, high resolution DPWMs are used to reduce the effect of limit-cycle oscillations [74]. However, the implementation of these high-resolution DPWMs is highly challenging. One potential method to increase their effective resolution is through the use of non-uniform quantizers. In a uniform quantizer, the input bin sizes and the output quantization levels are all the same. In a non-uniform quantizer, the size of the input bin increases the further the system moves away from the desired value. This can effectively increase the resolution of the quantizer. By selecting bin sizes in order to satisfy the no limit-cycle conditions established by Bradley, non-uniform quantization is a possible technique that may be employed to reduce the effect of quantization induced limit-cycles. This research would obviate the need for the high-resolution DPWMs.
- One drawback of digital control is the phase-lag introduced. Multiple-sampling is a method where the state vector is sampled more than once per switching cycle. This method can be used to extend the control bandwidth of the system. However, it injects high-frequency disturbances into the feedback path of the system [87]. Bradley investigates the effect of multiple-sampling on the nonlinear dynamics of a buck converter with a digital PI controller [49]. Owing to the application of digital state-feedback controllers in high performance applications, a thorough investigation into the effect of multiple sampling on the nonlinear dynamics of a digital state-feedback controller when multiple sampling is used is required.

Design guidelines for the avoidance/elimination of undesired operation typically assume ideal operating conditions. However, in real life applications, dc-dc converters operate in noisy environments leading to the intrusion of spurious signals. While the work in this thesis and other research, detailed in chapter 5, has been carried out, further work is required in order to develop design guidelines that characterise the behaviour of systems operating in noisy environments. The work of [42] and [45], utilize discrete-time iterative maps in order to derive the eigenvalues of dc-dc converters with analog controllers injected with spurious signals with a sinusoidal, triangular and sawtooth wave shape. However, this method is algebraically complex

and not suited to deriving conditions for the elimination of the undesired behaviour. Similar to the approach taken in chapter 5, further investigations into the effect of noise when digital control is employed is required. Initially, by considering noise with waveforms that are triangular and sawtooth in nature, design guidelines can be developed in order to ensure stable operation. The work then needs to consider waveforms of arbitrary shapes before considering random noise signals.

Bibliography

[1] A. Peterchev and S. Sanders, "Quantization resolution and limit cycling in digitally controlled pwm converters," *IEEE Trans. Power Electron.*, vol. 18, no. 1, pp. 301–308, Jan. 2003.

[2] E. N. Lorenz, "Deterministic nonperiodic flow," *Journal of Atmospheric Sciences*, vol. 20, no. 2, pp. 130–141, 1963.

[3] R. M. May, "Simple mathematical models with very complicated dynamics," *Nature*, vol. 261, pp. 459–467, 1976.

[4] S. H. Strogatz, *Nonlinear Dynamics And Chaos: With Applications To Physics, Biology, Chemistry, And Engineering.*, 2nd ed. Westview Press, 2015.

[5] N. Nise, *Control Systems Engineering*, 4th ed. Wiley, 2003.

[6] R. C. Hilborn, *Chaos and Nonlinear Dynamics: An Introduction for Scientists and Engineers.* Oxford University Press, 1994.

[7] R. Leine and H. Nijmeijer, *Dynamics and Bifurcations of Non-Smooth Mechanical Systems.* Springer Berlin Heidelberg, 2004.

[8] A. Filippov, *Differential Equations with Discontinuous Righthand Sides*, 1st ed. Springer Netherlands, 1988.

[9] R. W. Erickson and D. Maksimovic, *Fundamentals of Power Electronics*, 2nd ed. Kluwer Academics Publishers Group, 2001.

[10] H. C. Foong, Y. Zheng, Y. K. Tan, and M. T. Tan, "Fast-transient integrated digital dc-dc converter with predictive and feedforward control," *IEEE Trans. Circuits Syst. I*, vol. 59, no. 7, pp. 1567–1576, Jan. 2012.

[11] Y. Liu and X. Liu, "Recent developments in digital control strategies for dc/dc switching power converters," *IEEE Trans. Power Electron.*, vol. 24, no. 11, pp. 2567–2577, Aug. 2009.

[12] C. K. Tse, *Complex Behavior of Switching Power Converters*, 1st ed. CRC Press, 2003.

[13] R. D. Middlebrook and S. Ćuk, "A general unified approach to modelling switching-converter power stages," in *Proc. Power Electron. Specialists Conf.*, 1976, pp. 18–34.

[14] M. Kennedy and L. Chua, "Van der pol and chaos," *IEEE Trans. Circuits Syst. I*, vol. 33, no. 10, pp. 974–980, Oct. 1986.

[15] J. Baillieul., R. Brockett, and R. Washburn, "Chaotic motion in nonlinear feedback systems," *IEEE Trans. Circuits Syst.*, vol. 27, no. 11, pp. 990–997, Nov. 1980.

[16] P. S. Linsay, "Period doubling and chaotic behavior in a driven anharmonic oscillator," *Phys. Rev. Lett.*, vol. 47, no. 19, pp. 1349–1352, Nov. 1981.

[17] D. Hamill and D. Jeffries, "Subharmonics and chaos in a controlled switched-mode power converter," *IEEE Trans. Circuits Syst. I*, vol. 35, no. 8, pp. 1059–1061, Aug. 1988.

[18] J. R. Wood, "Chaos: A real phenomenon in power electronics," in *Proc. IEEE Appl. Power Electron. Conf. and Exposition*, Baltimore, (APEC), Mar. 1989, pp. 115-124.

[19] J. Deane and D. Hamill, "Instability, subharmonics, and chaos in power electronic systems," *IEEE Trans. Power Electron.*, vol. 5, no. 3, pp. 260–268, Jul. 1990.

[20] J. Deane and D. Hamill, "Analysis, simulation and experimental study of chaos in the buck converter," in *Proc. IEEE Power Electron. Specialists Conf.*, Texas, (PESC), Jun. 1990, pp. 491-498.

[21] J. Deane, "Chaotic behavior in current-mode controlled dc-dc converter," *Electronic Letters*, vol. 27, no. 13, pp. 1172–1173, Jun. 1991.

[22] J. Deane, "Chaos in a current-mode controlled boost dc-dc converters," *IEEE Trans. Circuits Syst. I*, vol. 39, no. 8, pp. 680–683, Aug. 1992.

[23] S. Banerjee and G. C. Verghese, *Nonlinear Phenomena in Power Electronics:Bifurcations, Chaos, Control, and Applications*, 1st ed. Wiley-IEEE Press, 2001.

[24] A. R. Brown and R. D. Middlebrook, "Sampled-data modeling of switching regulators," in *Proc. IEEE Power Electron. Specialists Conf.*, Colorado, (PESC), Jul. 1981, pp. 349-369.

[25] D. Hamill, J. Deane, and D. Jefferies, "Modeling of chaotic dc-dc converters by iterated nonlinear mappings," *IEEE Trans. Circuits Syst. I*, vol. 7, no. 1, pp. 25–36, Jan. 1992.

[26] S. Banerjee and K. Chakrabarty, "Nonlinear modeling and bifurcations in thc boost converter," *IEEE Trans. Power Electron.*, vol. 13, no. 2, pp. 252–260, Mar. 1998.

[27] S. Banerjee, E. Ott, J. A. Yorke, and G. H. Yuan, "Anomalous bifurcations in dc-dc converters: borderline collisions in piecewise smooth maps," in *Proc. of*

IEEE Power Electron. Specialists Conf., Missouri, (PESC), Jun. 1997, 1337-1344.

[28] K. Chakrabarty, G. Poddar, and S. Banerjee, "Bifurcation behavior of the buck converter," *IEEE Trans. Power Electron.*, vol. 11, no. 3, pp. 439–447, May 1996.

[29] E. Fossas and G. Olivar, "Study of chaos in the buck converter," *IEEE Trans. Circuits Syst. I*, vol. 43, no. 1, pp. 13–25, Jan. 1996.

[30] G. Olivar and E. Fossas, "Multiple pulsing in the buck converter," *J. Appl. Math. Mech.*, vol. 86, no. 5, pp. 367–368, Dec. 1996.

[31] G. Yuan, S. Banerjee, E. Ott, and J. A. Yorke, "Border-collision bifurcations in the buck converter," *IEEE Trans. Circuits Syst. I*, vol. 45, no. 7, pp. 707–716, Jul. 1998.

[32] S. Banerjee and C. Grebogi, "Border-collision bifurcations in two-dimentional piecewise smooth maps," *Physical Review E*, vol. 59, pp. 4052–4061, Apr. 1999.

[33] S. Banerjee, M. S. Karthik, G. Yuan, and J. A. Yorke, "Bifurcations in one-dimensional piecewise smooth maps - theory and applications in switching circuits," *IEEE Trans. Circuits Syst. I*, vol. 47, no. 3, pp. 389–394, Mar. 2000.

[34] M. di Bernardo, C. Budd, and A. Champneys, "Grazing, skipping and sliding: analysis of non-smooth dynamics of the dc-dc buck converter," *Nonlinearity*, vol. 11, no. 4, pp. 858–890, Mar. 1998.

[35] M. di Bernardo, M. I. Feigin, S. J. Hogan, and M. E. Homer, "Local analysis of c-bifurcations in n-dimensional piecewise-smooth dynamical systems," *Chaos, solitons and fractals*, vol. 10, no. 11, pp. 1881–1908, Nov. 1999.

[36] Z. T. Zhusubaliyev, E. A. Soukhoterin, and E. Mosekilde, "Quasi-periodicity and border-collision bifurcations in a dc-dc converter with pulsewidth modulation," *IEEE Trans. Circuits Syst. I*, vol. 50, no. 8, pp. 1047–1057, Aug. 2003.

[37] A. el Aroudi, L. Benadero, E. Toribio, and G. Olivar, "Hopf bifurcation and chaos from torus breakdown in a PWM voltage-controlled dc-dc boost converter," *IEEE Transactions on Circuits and Systems I: Fundamental Theory and Applications*, vol. 46, no. 11, pp. 1374–1382, Nov. 1999.

[38] A. el Aroudi, M. Debbat, R. Giral, , and L. Martinez-Salamero, "Quasiperiodic route to chaos in dc-dc switching regulators," in *Proc. IEEE Intl. Symp. Ind. Electron.*, Pusan, (ISIE), Jun. 2001, pp. 2130-2135.

[39] A. el Aroudi and R. Leyva, "Quasi-periodic route to chaos in a PWM voltage-controlled dc-dc boost converter," *IEEE Trans. Circuits Syst. I*, vol. 48, no. 8, pp. 967–978, Aug. 2001.

[40] M. di Bernardo, F. Garofalo, L. Glielmo, and F. Vasca, "Quasi-periodic behaviors in dc-dc converters," in *Proc. IEEE Power Electron. Specialists Conf.*, Baveno, (PESC), Jun. 1996, 1376-1381.

[41] P. Manneville and Y. Pomeau, "Intermittency and the lorenz model," *Physics Letters*, vol. 75, no. 1-2, pp. 1–2, Dec. 1979.

[42] Y. Zhou, J. Chen, C. Iu, and C. K. Tse, "Complex intermittency in switching converters," *International Journal of Bifurcation and Chaos*, vol. 18, no. 1, pp. 121–140, Jan. 2008.

[43] S. Wong, C. Tse, and K. C. Tam, "Intermittent chaotic operation in switching power converters," *International Journal of Bifurcation and Chaos*, vol. 14, no. 8, pp. 2971–2978, May 2004.

[44] C. Tse, Y. Zhou, F. Lau, and S. Qiu, "Intermittent chaos in switching power supplies due to unintented coupling of spurious signals," in *Proc. IEEE Power Electron. Specialists Conf.*, Germany, (PESC), Jun. 2003, pp. 642-647.

[45] P. Deivasundari and G. Uma, "Chaotic dynamics of voltage-mode controlled buck converter with periodic interference signals," *International Journal of Bifurcation and Chaos*, vol. 23, no. 6, pp. 1–32, Oct. 2012.

[46] O. Dranga, B. Buti, I. Nagy, and H. Funato, "Stability analysis of nonlinear power electronic systems utilizing periodicity and introducing auxiliary state vector," *IEEE Trans. Circuits Syst. I*, vol. 52, no. 1, pp. 168–178, Jan. 2005.

[47] I. A. Hiskens and M. A. Pai, "Trajectory sensitivity analysis of hybrid systems," *IEEE Trans. Circuits Syst. I*, vol. 47, no. 2, pp. 204–220, Feb. 2000.

[48] D. Giaouris, S. Banerjee, B. Zahawi, and V. Pickert, "Stability analysis of the continuous-conduction-mode buck converter via Filippov's method," *IEEE Trans. Circuits Syst. I*, vol. 55, no. 4, pp. 1084–1096, May 2008.

[49] M. Bradley, "Nonlinear dynamics of digitally-controlled buck converters," Ph.D. dissertation, University College Dublin, 2013.

[50] L. Yang, J. Park, and A. Q. Huang, "An adaptive external ramp control of the peak current controlled buck converters for high control bandwidth and wide operation range," in *Proc. IEEE Appl. Power Electron. Conf. and Exposition*, California, (APEC), Feb. 2010, pp. 2181-2188.

[51] N. Kondrath and M. K. Kazimierczuk, "Control current and relative stability of peak current-mode controlled pulse-width modulated dc-dc converters without slope compensation," *IET Power Electronics*, vol. 3, no. 6, pp. 936–946, Nov. 2010.

[52] C. Batlle, E. Fossas, and G. Olivar, "Stabilization of periodic orbits of the buck converter by time-delayed feedback," *International Journal of Circuit Theory and Applications*, vol. 27, no. 6, pp. 617–631, Nov. 1999.

[53] K. Kaoubaa, J. Pelaez-Restrepo, M. Feki, B. Robert, and A. el Aroudi, "Improved static and dynamic performances of a two-cell dc-dc buck converter

using a digital dynamic time-delayed control," *International Journal of Circuit Theory and Applications*, vol. 40, no. 4, pp. 395–407, Apr. 2010.

[54] W. Lu, F. Jing, L. Zhou, H. H. C. Iu, and T. Fernando, "Control of subharmonic oscillation in peak current mode buck converter with dynamic resonant perturbation," *International Journal of Circuit Theory and Applications*, vol. 43, no. 10, pp. 1399–1411, Oct. 2015.

[55] C. Fang, "Sampled-data poles, zeros, and modeling for current-mode control," *International Journal of Circuit Theory and Applications*, vol. 41, no. 2, pp. 111–127, Feb. 2013.

[56] J. Stahl, A. Bucher, C. Oeder, and T. Duerbaum, "Sampled-data modeling applied to output impedance reveals missing term in state-space averaging model," in *12th Workshop on Control and Modeling for Power Electronics*, Colorado, (COMPEL), Jun. 2010, pp. 1-8.

[57] E. Rodriguez, A. el Aroudi, F. Guinjoan, and E. Alarcon, "A ripple-based design-orientated approach for predicting fast-scale instability in dc-dc switching power supplies," *IEEE Trans. Circuits Syst. I*, vol. 59, no. 1, pp. 215–227, Aug. 2011.

[58] Y. Song and B. Wang, "Survey on reliability of power electronic systems," *IEEE Trans. Power Electron.*, vol. 28, no. 1, pp. 591–604, 2012.

[59] S. Kapat and P. T. Krein, "Formulation of PID control for dc-dc converters based on capacitor current: A geometric context," in *IEEE 12th Workshop on Control and Modeling for Power Electronics*, Colorado, (COMPEL), Jun. 2010, pp. 1-6.

[60] D. Giaouris, S. Maity, S. Banerjee, V. Pickert, and B. Zahawi, "Application of filippov method for the analysis of sub-harmonic instability in dc-dc converters," *International Journal of Circuit Theory and Applications*, vol. 37, no. 8, pp. 899–919, Oct. 2009.

[61] P. Deivasundari, R. Geetha, G. Uma, and K. Murali, "Chaos, bifurcation and intermittent phenomena in dc-dc converters under resonant parametric perturbation," *Eur. Phys. J. Special Topics*, vol. 222, no. 3, pp. 689–697, Jul. 2013.

[62] C. Olalla, R. Leyva, I. Queinnec, and D. Maksimovic, "Robust gain-scheduled control of switched-mode dc-dc converters," *IEEE Trans. Power Electron.*, vol. 27, no. 6, pp. 3006–3019, Jan. 2012.

[63] G. C. Verghese, M. E. Elbuluk, and J. G. Kassakian, "A genearl approach to sampled-date modeling for power electronic circuits," *IEEE Trans. Power Electron.*, vol. 1, no. 2, pp. 76–89, Apr. 1986.

[64] E. Weisstein, "Characteristic polynomial." [Online]. Available: http://mathworld.wolfram.com/CharacteristicPolynomial.html

[65] MATLAB, *version 8.1.0.604 (R2013a)*, Natick, Massachusetts, Ed. The Mathworks Inc., 2013.

[66] L. Corradini, P. Mattavelli, and D. Maksimovic, "Robust relay-feedback based autotuning for dc-dc converters," in *Proc. Power Electron. Specialists Conf.*, Florida, (PESC), Jun. 2007, pp. 2196-2202.

[67] A. Kelly and K. Rinne, "A self-compensating adaptive digital regulator for switching converters based on linear prediction," in *Proc. IEEE Appl. Power Electron. Conf. and Exposition*, Texas, (APEC), Mar. 2006, pp.712-718.

[68] W. Stefanutti, P. Mattavelli, S. Saggini, and M. Ghioni, "Autotuning of digitally controllled buck convertes based on relay feedback," in *Proc. Power Electron. Specialists Conf. and Exposition*, Brasil, (APEC), Jun. 2005, pp. 2140-2145.

[69] D. Giaouris, C. Yfoulis, F. Stergiopoulos, C. Ziogou, S. Voutetakis, and S. Papadopoulou, "Border collisions and chattering in state feedback controlled boost converters," in *Proc. Intl. Symp. Nonlinear Theory and Applicat.*, Switzerland, (NOLTA), 2014.

[70] D. Giaouris, C. Yfoulis, S. Voutetakis, and S. Papadopoulou, "Stability analysis of digital state feedback controlled boost converters," in *Proc. IEEE Ind. Electron. Soc.*, Austria, (IECON), 2013, pp. 8391-8396.

[71] P. Deivasundari, G. Uma, and C. Vincent, "Non-linear intermittent instabilities and their control in an interleave dc/dc converter," *IET Power Electron.*, vol. 7, no. 5, pp. 1235–1245, May 2014.

[72] Texas Instruments, "Basic calculation of a buck converter's power stage." [Online]. Available: http://www.ti.com/lit/an/slva477b/slva477b.pdf

[73] Maxim Integrated, "Input and output noise in buck converters explained." [Online]. Available: http://pdfserv.maximintegrated.com/en/an/AN986.pdf

[74] A. Syed, E. Ahmed, and D. Maksimovic, "Digital pulse width modulator architectures," in *Proc. IEEE Power Electron. Conf. and Exposition*, California, (PESC), Jun. 2004, pp. 4689-4695.

[75] A. Kelly and K. Rinne, "High resolution DPWM in dc-dc converter application using digital sigma-delta techniques," in *Proc. IEEE Power Electron. Specialists Conf.*, Brasil, (PESC), Jun. 2005, pp. 1458-1463.

[76] Z. Lukic, K. Wang, and A. Prodic, "High-frequency digital controller for dc-dc converters based on multi-bit sigma-dela pulse-width modulation," in *Proc. IEEE Appl. Power Electron. Conf. and Exposition*, Texas, (APEC), Mar. 2005, pp. 6-10.

[77] H. Hu, V. Yousefzadeh, and D. Maksimovic, "Nonuniform A/D quantization for improved dynamic responses of digitally controlled dc-dc converters," *IEEE Trans. Power Electron.*, vol. 23, no. 4, pp. 1998–2005, Jul. 2008.

[78] Z. Zhao and A. Prodic, "Non-zero error method for improving output voltage regulation of low-resolution digital controllers for SMPS," in *Proc. IEEE Power Electron. Conf. and Exposition*, Texas, (APEC), Feb. 2008, pp. 1106-1110.

[79] S. Hashimoto, S. Naka, U. Sosorhang, and N. Honjo, "Generation of optimal voltage reference for limit cycle oscillation in digital control-based switching power supply," *Journal of Energy and Power Engineering*, vol. 6, pp. 623–628, 2012.

[80] D. Burbano and F. Angulo, "Decreasing quantization effects in a buck converer controlled by gzad strategy," in *Proc. of IEEE IX Latin American Robotics Symp. and IEEE Colombian Conf. on Automat. Control and Ind. Applicat.*, Bogota, (LARC), Oct. 2011, pp. 1-6.

[81] W. Stefanutti, E. D. Monica, E. Tedeschi, P. Mattavelli, and S. Saggini, "Reduction of quantization effects in digitally controlled dc-dc converters using inductor current estimation," in *Proc. IEEE Power Electron. Specialists Conf. and Exposition*, Jeju, (PESC), Jun. 2006, pp. 1-7.

[82] M. Bradley, O. Feely, and E. Teplinsky, "Limit cycles in a digitally controlled buck converter," in *Proc. European Conference on Circuit Theory and Design*, Linkoping, (ECCTD), Aug. 2011, pp. 246-249.

[83] M. Bradley, E. Alarcon, and O. Feely, "Analysis of limit cycles in a pi digitally controlled buck converter," in *IEEE Intl. Symp. on Circuits and Syst.*, Seoul, May 2012, pp. 628-631.

[84] U. Zolzer and X. Amatriain, *DAFX: digital Audio Effect*. John Wiley & Sons Ltd., 2002.

[85] P. Dinz, E. da Silva, and S. Netto, *Digital Signal Processing: System Analysis and Design*. Cambridge University Press, 2010.

[86] J. Smith, *Introduction to Digital Filter with Audio Applications*. W3K Publishing, 2007.

[87] L. Corradini, P. Mattavelli, E. Tedeschi, and D. Trevisan, "High-bandwidth multisampled digitally controlled dc-dc converters using ripple compensation," *IEEE Trans. Ind. Electron.*, vol. 55, no. 4, pp. 1501–1508, Apr. 2008.

Publications

Journals

B. Hayes and M. Condon and D. Giaouris, "Design of PID controllers using Filippov's method for stable operation of DC-DC converters," International Journal of Circuit Theory and Applications, vol. 62, no. 11, pp. 7073-7078, 2015.

M. Condon and B. Hayes, "Control of Limit Cycles in Buck Converters," *The International Journal for Computation and Mathematics in Electrical and Electronic Engineering*, vol. 33, no. 4, pp. 1448-1461, 2014.

Conferences

B. Hayes and M. Condon, "Application of the Real-Time Hilbert Huang Transform to a Noise Perturbed Buck Converter," in *The 10th International Conference on Circuits, Systems and Telecommunications*, Feb. 2016, Barcelona, Spain..

B. Hayes and M. Condon, "Nonlinear Dynamics of Digitally Controlled Buck Converters," in *The 17th Research Colloquium on Communications and Radio Science into the 21st Century,* May 2014, Dublin, Ireland.

Funding Acknowledgement

This material is based upon works supported by Dublin City University under the Daniel O'Hare Research Scholarship scheme.